Czech Technical University in Prague
Faculty of Mechanical Engineering

Dissertation

Development and Calibration of Elasto-Plasticity Models with Directional Distortional Hardening

Slavomír Parma

Prague 2018

Czech Technical University in Prague
Faculty of Mechanical Engineering

Dissertation

Development and Calibration of Elasto-Plasticity Models with Directional Distortional Hardening

Ing. Slavomír Parma

Supervisor
Ing. Jiří Plešek, CSc.

Study Programme
Mechanical Engineering

Field of Study
Mechanics of Solids, Deformable Bodies and Continua

Prague, January 2018

Acknowledgements

I would like to express my gratitude to my supervisor, Dr. Jiří Plešek, who provided me with a very supportive environment, who was anytime opened to new ideas and research topics, and whose deep experience in the research field of phenomenological plasticity, among others, allowed me to meet the objectives of our research.

I would like to thank my colleague, René Marek, with whom I worked with on several projects, written several papers, and spent several years of Ph.D. study together.

I am deeply grateful to Dr. Heidi P. Feigenbaum, Prof. Yannis F. Dafalias, and Dr. Constantin Ciocanel for their support, numerous consultations, proof-reading, and warm welcome during my visits in their research groups. Besides the scientific benefits of collaboration, these visits allowed me to recognize why *E Pluribus Unum.*

Also, I would like to thank my wife Vendula and my mother Dagmar, whose patience, tolerance, and enthusiasm are the very essence of the following pages.

My deepest gratitude belongs to my teacher, Dr. Jiří Steckbauer, who has never ceased to show me how to *watch the world by different eyes.*

This work was supported by the Ministry of Education, Youth and Sports of the Czech Republic under grants CeNDYNMAT CZ.02.1.01/0.0/0.0/15_003/0000493 and KONTAKT II LH14018, by the Czech Science Foundation under grant GAČR 15-20666, and by the Czech Academy of Sciences with institutional support RVO: 61388998.

Slavomír Parma

Annotation

Tittle:	Development and Calibration of Elasto-Plasticity Models with Directional Distortional Hardening
Thesis:	Dissertation
Author:	Ing. Slavomír Parma
Email:	`parma@it.cas.cz, origon@seznam.cz`
University:	Czech Technical University in Prague
Faculty:	Faculty of Mechanical Engineering
Department:	Department of Mechanics, Biomechanics and Mechatronics
Address:	Technicka 4, 166 07 Prague 6, Czech Republic
Supervisor:	Ing. Jiří Plešek, CSc. Institute of Thermomechanics of the Czech Academy of Sciences, v. v. i. Dolejškova 1402/5, 182 00 Praha 8, Czech Republic
Email:	`plesek@it.cas.cz`
Submitted:	January 30, 2018
Study Programme:	P2301 Mechanical Engineering
Field of Study:	3901V024 Mechanics of Solids, Deformable Bodies and Continua
Key Words:	plasticity, strain hardening, integration, calibration, finite element method

Abstract: This thesis deals with the phenomenological modeling of the directional distortional hardening and the metal plasticity in general. A particular plasticity model is analytically integrated for the proportional multiaxial loading case. The integrated model is used to model the stress–strain curves, the hysteresis loops, and the cyclic stress–strain curves. Based on these curves, two calibration algorithms are developed. In the end, a sensitivity analysis of both calibration algorithms is done. A general aim of this thesis is to develop the procedures that would support an industrial application of advanced models with directional distortional hardening.

Anotace

Název práce:	Vývoj a kalibrace modelů elasto-plasticity se směrovým deformačním zpevněním
Druh práce:	dizertační práce
Autor:	Ing. Slavomír Parma
Email:	`parma@it.cas.cz, origon@seznam.cz`
Univerzita:	České vysoké učení technické v Praze
Fakulta:	Fakulta strojní
Ústav:	Ústav mechaniky, biomechaniky a mechatroniky
Adresa:	Technická 4, 166 07 Praha 6
Školitel:	Ing. Jiří Plešek, CSc. Ústav termomechaniky Akademie věd České republiky, v. v. i. Dolejškova 1402/5, 182 00 Praha 8
Email:	`plesek@it.cas.cz`

Datum odevzdání:	30. leden 2018
Studijní program:	P2301 Strojní inženýrství
Studijní obor:	3901V024 Mechanika tuhých a poddajných těles a prostředí
Klíčová slova:	plasticita, deformační zpevnění, integrace, kalibrace, metoda konečných prvků

Abstrakt: Práce se zabývá fenomenologickým modelováním směrového deformačního zpevnění a obecně plasticity kovů. Konkrétní model je analyticky integrován pro případ víceosého proporcionálního zatěžování. Výsledná křivka je použita k modelování tahového diagramu, a dále k modelování hysterezních smyček a cyklických deformačních křivek. Na základě těchto analytických modelů jsou navrženy dva zcela nové algoritmy pro kalibraci parametrů modelu. V závěru je provedena citlivostní analýza obou kalibračních algoritmů. Obecným cílem práce je vývoj procedur pro průmyslovou aplikaci pokročilých modelů plasticity se směrovým deformačním zpevněním.

Declaration

I hereby declare that my dissertation entitled *Development and Calibration of Elasto-Plasticity Models with Directional Distortional Hardening* is the result of my own work and includes nothing which is the outcome of work done in collaboration except as specified in the text.

Slavomír Parma
January 2018
Prague

Contents

Chapter 1

Introduction

Continuum models of plasticity are considered to be one of the most successful phenomenological constitutive models of solids [123]. Although comprehensive theories that describe the mechanical behavior of materials at the microscale have been developed, it is still not common to employ these theories to predict a behavior of materials at the macroscale. Instead, phenomenological models of plasticity are used, and, for now, seem to keep their essential role in engineering design. There are several reasons the phenomenological models are successful at competing the microscale approach: less computational complexity, straightforward interpretation of internal variables and parameters, easier calibration, *etc.*

In general, the phenomenological modeling can be characterized as a predicting behavior based on correlations between physical quantities, where the empirical relationship is based on experimental observation, but not necessarily supported by any theory. It should be emphasized that the phenomenological approach is not limited to the constitutive modeling of materials, but it comprises numerous branches of science as well, including astronomy [138], biology [139], metallurgy [141], and others. Below is a brief historical overview of experimental and theoretical research in metal plasticity.

A Historical Overview of Experiments in Plasticity

As inherent to phenomenological modeling in general, an experimental research has played a fundamental role in the evolution of the phenomenological theory of plasticity. Early attempts at experimental research in plasticity can be traced back to the turn of the 18^{th} and 19^{th} century [38, 128]. In 1784, Coulomb published his paper on experiments of a torsional loading of an iron wire [1]. In these experiments, he recognized an increasing plastic strain manifested by an increasing

total strain. In 1831, Gerstner published his work on a piano wire loading [2, 3]. He has observed increasing plastic strain due to increasing load and presented his results in form of stress–strain curves. Some of his results are shown in Tab. 1.1 and plotted in Fig. 1.1. Starting in 1864, Tresca published several papers on experiments of metal forming [5]. In these papers, he tested punching, extrusion and compression of various metals and focused on metal flow, rather than yielding. An important experimental observation was published in 1885 by Bauschinger, who employed a 100-ton axial load capacity testing machine and a highly precise mirror extensometer of his own construction, which allowed him to carry out highly precise strain measurement of the order of 10^{-6} [9,11,38]. Bauschinger experimentally studied the change of the yield point under reversal uniaxial loading, *i.e.*, when the specimen is first loaded in tension and subsequently loaded in compression, or *vice versa*. He observed that yielding in one direction decreases a yield strength in the opposite direction and this behavior is now referred to as the *Bauschinger effect*. Further, experimental results under more complex test conditions were published in 1900 by Guest [12]. He carried out experiments under multiaxial stress states achieved with a combination of axial and torsional load, and internal pressure applied to thin-walled tubular specimens.

Without a doubt, the 20^{th} century is a golden age of experimental research of metal plasticity [71, 72, 87]. This period is characterized by rapid development of experimental techniques, testing devices, and an increasing number of research groups. In addition, the 20^{th} century can be divided into several eras according to the research topics typical for each era.

During the time period 1900–1925, investigators mainly concentrated on validation of initial yield criteria [15, 16, 18, 19]. This research was motivated by the design of structures, as the region of elastic behavior needed to be determined for constructions. From 1925 to 1940, however, research went beyond the elastic domain boundary and into the plastic range. Thus, yield curves of different materials were investigated and researchers studied the plastic flow of materials [21, 23, 24]. As uniform stress states were necessary for the experiments to correlate with the behavior at a material point, two different experimental techniques became prevalent. The first one uses thin-walled tubular specimens simultaneously loaded by axial stress and internal pressure, *e.g.*, the work of Lode published in 1926 [21]. The second also uses thin-walled tubular specimens, however, the specimens are loaded by combined axial load and torque, *e.g.*, the work of Taylor and Quinney published in 1932 [23]. It should be noted that, later on, many researchers combined both methods in order to achieve more general stress states. In the years between 1940 and 1950, as the industry grew, so did demand for experimental data, and the number of materials being investigated increased. In this time, a proof stress definition based on the 0.2 % offset strain threshold was adopted as a standard [72].

From 1950, an enormous effort in experimental research was devoted to validation of the slip theory of plasticity. This theory predicted an existence of the corner

on subsequent yield surfaces. In 1972 Hecker published a paper on experimental investigation of these corners [62]. In the summary, he refers to 7 papers that supported the existence of corners, and to 7 papers that rejected the existence of corners. Hence, a complexity of experimental investigation revealed by ambivalence in results may be seen. While experimental proofs for a size change and translation of subsequent yield surfaces can be traced back to Bauschinger [11], observations from the late 1950s indicate that subsequent yield surfaces become even distorted due to plastic prestraining [42]. This behavior is now referred to as the *Directional Distortional Hardening (DDH)*.

Over the last several decades, experiments in plasticity mainly concern yield surfaces detection with results being used to develop new phenomenological descriptions. Further, a brief overview of some outstanding experimental papers is given. In all these papers, the yield surface detection was aimed, and the distortion was observed. Phillips *et al.* in 1972 studied distortion of yield surfaces at elevated temperatures and used the proportional limit to define yielding [63]. Phillips and Lu in 1984 used both the stress and the strain paths to detect distorted yield surfaces [82]. Again, they used a proportional limit to define yielding. Wu and Yeh in 1991 discussed factors affecting yield surfaces detection, *e.g.*, the elastic moduli variation, the zero offset strain, and the strain rate of probing [96]. They used the offset strain of $5\,\mu\varepsilon$ as the yield definition ($1\,\mu\varepsilon = 10^{-6}\,\mathrm{m/m}$). Wu *et al.* in 1995 addressed large prestrains reaching up to $20\,\%$ [100]. To define yielding, they used a strain offset of $5\,\mu\varepsilon$. Ishikawa in 1997 applied radial loading paths to detect yield surfaces [104]. The offset strain used for the yielding definition was $50\,\mu\varepsilon$. In the yield surfaces detection experiment, Sung *et al.* in 2011 employed an autonomous testing system controlled by a script instead of a dedicated GUI-designed application with limited functionalities [132]. Moreover, they described an advanced method used to suppress the data scattering.

A Historical Overview of Plasticity Theories

As experimental methods in plasticity evolved, so did plasticity theories and models. However, the phenomenological approach does not necessarily imply that the theory and models strictly follow the experiments. Rather, there are numerous examples of the opposite, *i.e.*, when theoretical predictions precede and are validated by experiments.

At first, theoretical plasticity was part of the study of the strength of materials and focused on developing criteria to avoid a failure of constructed structures. Later, these criteria evolved in a general relation referred to as the *yield condition*, which is an essential component of most of the modern theories of plasticity. Beginning in 1864, Tresca published several papers on experiments of metal forming [5]. Although he addressed the flow of material rather than the condition of when the flow initiates, he concluded that the material flows under a constant maximum shear

Tab. 1.1: *An experimental data of stress–strain curve of a piano wire with unloading sequences published by von Gerstner in 1831 [2, 3].* 1 Line ≈ 2.195 mm, 1 Austrian Pfund ≈ 0.56 kg.

Test No.	Residual Elongation	Loading Weight (Austrian Pfund)												
		4	8	12	16	20	24	28	32	36	40	44	48	52
	(1/54 Line)	Actual Elongation (1/54 Line)												
0	0													
1	0	14												
2	1	14	28											
3	2	15	29	43										
4	3	17	30	44	58									
5	6	20	33	47	60	74								
6	9	23	37	50	63	77	90.5							
7	13	26	40	54	67	81	94	108						
8	18	32	45	59	72	86	100	113	127					
9	24	38	51	65	78	92	105	119	133	146				
10	32	45	59	72	86	100	113	126	140	154	167			
11	41	54	68	82	95	108	122	136	150	163	177	190		
12	52	66	79	93	107	120	133	147	161	175	188	202	215	
13	67	81	94	108	121	135	148	162	176	189	203	216	230	244

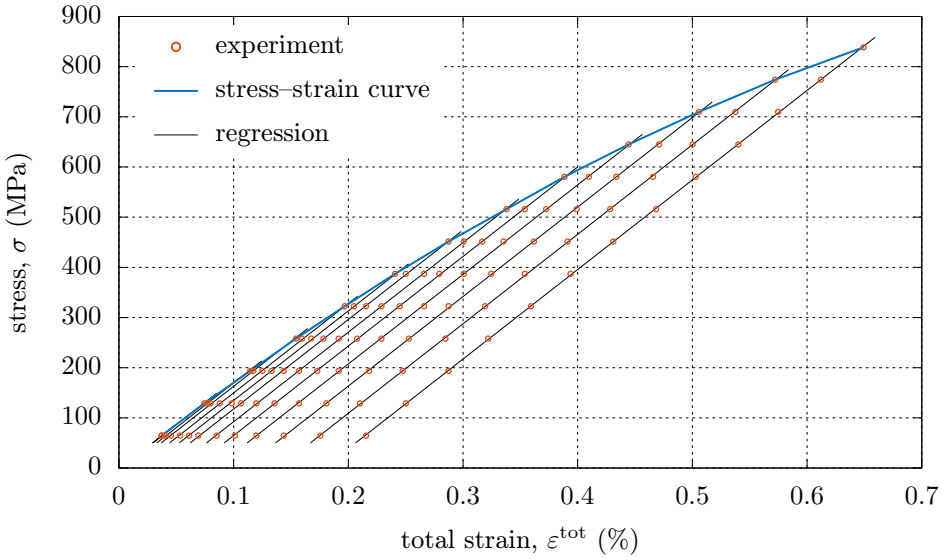

Fig. 1.1: *The stress–strain curve plotted from data given in Tab. 1.1.*

stress and listed particular values for several materials. A fundamental breakthrough in theoretical plasticity was contributed by Saint-Venant, who followed up Tresca's research and in 1871 published a paper with three postulates founding the theoretical plasticity [8]. The postulates are as follows: (*i*) the plastic strain is isovolumetric, (*ii*) the directions of principal strains coincide with the directions of principal stresses, and (*iii*) the maximum shear stress remains fixed during the plastic deformation. Despite the fact that two last postulates are no longer considered valid, Saint-Venant's contribution to the concept of the theory of plasticity is doubtless. Moreover, the third postulate evolved in a condition now referred to as *Tresca yield criterion*. In 1882, Mohr published a graphical representation of the stress at a material point [10]. He considered a two-dimensional stress state given by principal stresses σ_1 and σ_2, a cut through the point by a plain given by the angle ϕ, and the normal and shear stress components σ and τ, respectively. He found out that the stress components σ and τ form a circle parameterized by the angle 2ϕ and described some basic properties of this circle. Further, based on his graphical representation, he proposed a fracture criterion later on referred by plasticity theories to as *Mohr–Coulomb yield criterion*.

The most influential yield condition developed thus far is that based on maximum distortion energy. Named after scientists contributed to its development, this criterion is referred to as *Maxwell–Huber–Hencky–von Mises yield condition*. In his letter to Kelvin from 1856, Maxwell has resolved the strain energy density into volumetric and deviatoric parts, and consequently strongly suspected that when the later one reaches a certain limit, then "the element will begin to give way" [4]. Unfortunately, he has never come back to this topic nor published it. In 1904, Huber published the same criterion, however, his work did not become broadly known because it was written in the Polish language [13, 14, 116]. In 1913, von Mises published the very same criterion [17], and finally, Hencky obtained the same result independently from his predecessors publishing it in 1924 and citing Huber and von Mises [20].

Subsequently, the yield condition usually referred to as *Drucker–Prager yield criterion* was published in 1952 [37]. This criterion encloses the group of four conservative yield criteria described in here, namely, Tresca, Mohr–Coulomb, Maxwell–Huber–Hencky–von Mises, and Drucker–Prager yield criteria [123]. In addition, there have been other yield criteria developed, some of which are reported in [112].

Besides the question of yielding initiation, a rule to relate the stress and the strain under plastic deformation was needed. The coincidence of directions of principal stresses with those of principal strains postulated by Saint-Venant in 1871 is now known as the *total strain theory* [8]. As soon as 1872, however, Lévy, Saint-Venant's student, published his work where the increments of plastic strain components are pronounced to be proportional to deviatoric stress components [6, 7]. Once again, von Mises formulates the same relation in 1913 [17]. The relation is now referred to as the *Lévy–Mises equation* and later on evolved in the *flow plasticity*

theory. We know today that co-axiality (same eigenvectors) between the stress and plastic strain increment tensors is not satisfied in general at the presence of anisotropy and its expression by means of tensor-valued internal variables; these variables contribute together with the stress in defining the plastic strain increment direction based on experiments and modern representation theorems of tensor-valued functions.

Experimental results showed that initial yield surfaces given by initial yield criteria evolve due to plastic straining. This phenomenon known as the *strain hardening* has motivated authors to establish internal variables responsible for particular hardening effects. The most simple effect manifested by an expansion of yield surfaces is referred to as the *isotropic hardening* and first theories aiming to model this phenomenon can be traced back to Nádai and Prager in 1937 [29, 30]. Further, Bauschinger's observation [9] was generalized as a translation of yield surfaces and referred to as the *kinematic hardening*. The first models of kinematic hardening were proposed by Melan in 1938 [31], Ishlinskii in 1954 [39], and Prager in 1955 and 1956 [40, 41]. Prager's hardening rule was modified by Ziegler in 1959 [43].

Following the aforementioned first proposition, there have been many hardening rules suggested. The overview provided here is a very basic and does not aim to cover all proposed hardening rules and developments in plasticity theory. Some other important findings and improvements in phenomenological plasticity that are relevant to this thesis or historically important are briefly described.

In 1926, Schmid did some early attempts on crystal plasticity [22]. In 1934, the dislocation theory of slip was initiated by works of Orowan, Polanyi, and Taylor [25, 26, 27]. Hill in 1950 published models of the plasticity of anisotropic materials [35]. Armstrong and Frederick in 1966 proposed a nonlinear kinematic hardening rule [52]. Mróz in 1967 suggested using a multi-yield-surface model capable to capture both the isotropic and kinematic hardening [54]. Valanis in 1971 developed a theory of viscoplasticity without a yield surface [59, 60]. Dafalias and Popov between 1975 and 1977 and Krieg in 1975 proposed a two-surface theory that according to the first authors was called *bounding surface plasticity theory*, and included a model of zero elastic range, *i.e.*, model with no yield surface [68, 69, 70, 73]. Lemaitre and Chaboche in 1990 generalized the Armstrong–Frederick model of kinematic hardening by superposition of several independent kinematic variables [93]. In regards to numerical implementation, Simo and Taylor in 1985 and Runesson *et al.* in 1986 proposed a concept of the *consistent tangent operator* [85, 88].

Structure of the Thesis

The dissertation is organized as follows. After the introduction in Chapter 1, a state of the art of distortional hardening is placed in Chapter 2, where a detailed overview of last achievements and actual problems in modeling of distortional hardening is stated, including experimental evidence, early attempts, and advanced models of

distortional hardening. The aims of the thesis are listed in Chapter 3. Chapter 4 presents the methods used to achieve the specified aims of the thesis. Chapters 5 and 6 are the essential parts of the thesis, where the results for monotonic and cyclic loading, respectively, are presented, including analytical integration of a particular directional distortional hardening model, equations for the stabilized hysteresis loops and the cyclic stress–strain curves inherent to the model, two calibration algorithms for model's parameters, and sensitivity analysis of these algorithms. Finally, Chapter 7 presents conclusions from the results achieved.

Chapter 2

State of the Art of Distortional Hardening

DISTORTION of yield surfaces due to strain hardening has been observed in numerous experiments on various types of metals, including but not limited to [42, 44, 67, 96, 98, 104, 105]. In stress space, the subsequent yield surfaces exhibit distorted ellipses, being highly curved in the direction of loading—often with a sharp apex—and flattened in the opposite direction. Some examples of experimental data of distorted yield surfaces are given in Figs. 2.1–2.8. Although the terminology has been evolving and may vary among the authors, nowadays, this phenomenon is commonly referred to as the *Directional Distortional Hardening (DDH)*. The word "directional" was added to distinguish from cases of simple *distortional hardening*, where distortion changes only the ratio of elliptical axes while maintaining the elliptical shape. The term DDH was firstly coined in Feigenbaum and Dafalias [118]. Several complex mathematical models of DDH were introduced in the last decades, some of which are reported in [79, 81, 90, 94, 101, 109, 114, 131]. Basically DDH expresses a form of deformation induced anisotropy, and often in this thesis the word anisotropy will be used in this context. In this chapter, the state of the art of DDH is given, covering an experimental evidence of DDH, development of experimental methods for investigation of DDH, early attempts in modeling, models involving higher-order tensors, and some advanced models of DDH.

2.1 Experimental Evidence

Directional distortional hardening is inherent to various types metals, *e.g.*, steels, aluminum and its alloys, copper, brass, titanium and its alloys, and nickel alloys. Thus, it covers materials with various crystal stuctures, *e.g.*, body-centered cubic

(bcc), face-centered cubic (fcc), and hexagonal close-packed (hcp). Besides metals, there has been observed some anisotropy in plastic behavior of polymers and soils as well. Although this anisotropy does not strictly match and/or correspond to the definition of DDH, it has some key features in common, namely, complex or distorted shapes of yield surfaces.

Wu & Yeh (1991) carried out experiments on specimens made of type 304 stainless steel [96]. They probed the yield surface of a virgin material and found out, that results are in good agreement with von Mises theory, *i.e.*, that the initial yield surface in σ–$\sqrt{3}\tau$ space is circular. Further, they subjected the same specimen to axial total strain of $0.2\,\%$, which gave rise the axial plastic strain of $540\,\mu\varepsilon$. After this prestrain, they used the same method to detected the yield surface as in case of the virgin material. Unlike the test on virgin material, the test on strained steel revealed distortion of the circular shape of the yield surface. They went on the testing on the same specimen with increasing prestrains. The higher prestrain applied, the higher distortion observed. In Fig. 2.1, the second subsequent yield surface is shown. Lissenden *et al.* (1997) investigated specimens made of type 316 stainless steel [105]. They used a biaxial stress loading trajectory to prestrain a virgin material. The distortion observed is shown in Fig. 2.2. Hu *et al.* (1997) observed distortion in type 45 steel in normalized condition [134], as shown in Fig. 2.3. Some other results for various types of steels may be seen in [66, 78, 80, 100, 104].

Also, DDH occurs in pure aluminum and its alloys. Phillips and Tang (1972) studied an effect of loading path on the yield surface of pure aluminum at elevated temperatures [64]. They concluded that increasing temperature shrinks the size of yield surafces, while the distortion is not essentially affected by temperature rise. An example of the distorted yield surface determined at room temperature is given in Fig. 2.4. Khan *et al.* (2009) investigated Al6061-T6511 aluminum alloy [125]. They prestrained specimens by biaxial stress in σ–$\sqrt{3}\tau$ space, which caused distorion shown in Fig. 2.5. More results from investigation on aluminum alloys may be seen in [63, 82, 86, 113, 115].

Besides the investigations on steels and aluminum alloys, DDH was reported by Helling *et al.* (1986) in experiments on 70:30 brass [87]. In Fig. 2.6, a yield surface obtained in this testing and distorted by shear prestraining is depicted. Dietrich and Kowalewski (1997) detected distortion of yield surfaces in experiments on pure copper [103]. An example of their results is given in Fig. 2.7. Nixon *et al.* (2010) carried out experiments on pure α-titanium [127]. Although they used a different method to detect yield surface than other authors mentioned above, they observed distortion too, as shown in Fig. 2.8. Some experiments on nickel-base superalloy Inconel 718 are reported in [107]. Some more experiments on other metals except steel and aluminum may be seen in [65, 84, 97, 120, 135, 136]. Also, distorted yield surfaces and yield surfaces with complex shapes, not necessarily evolved due to strain hardening, may be seen in polymers [117] and soils [108, 124, 137].

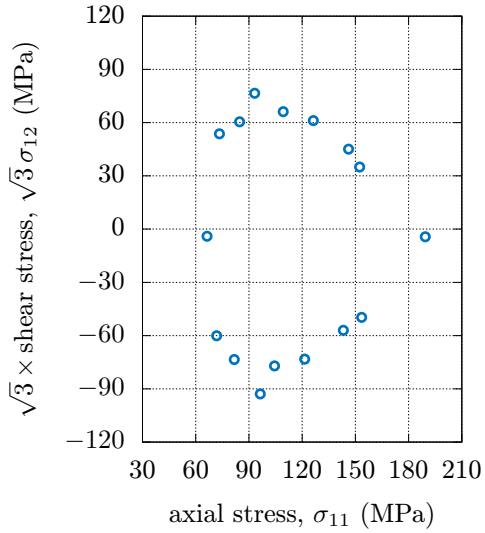

Fig. 2.1: *DDH in experiments on type 304 stainless steel by Wu & Yeh (1991) [96].*

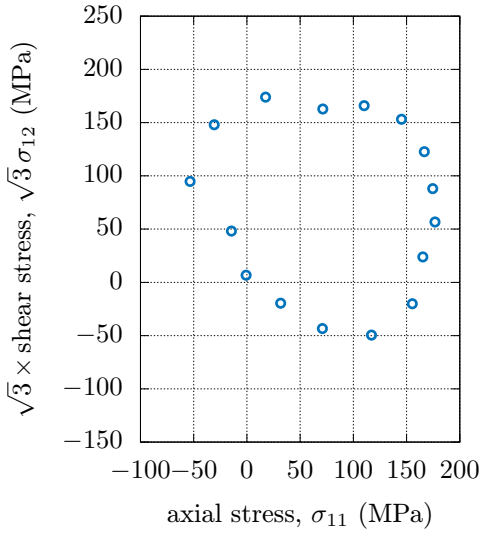

Fig. 2.2: *DDH in experiments on type 316 stainless steel by Lissenden et al. (1997) [105].*

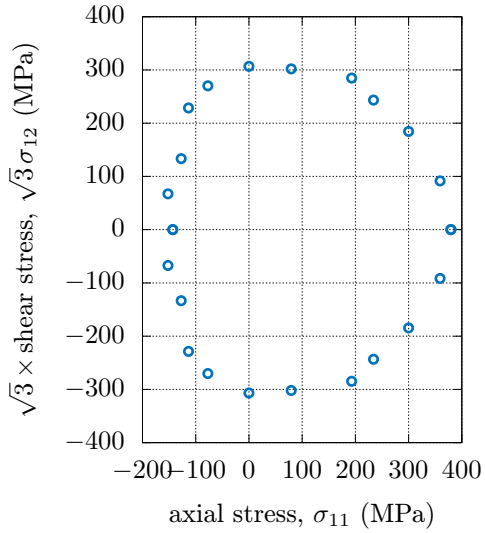

Fig. 2.3: *DDH in experiments on type 45 steel by Hu et al. (2012) [134].*

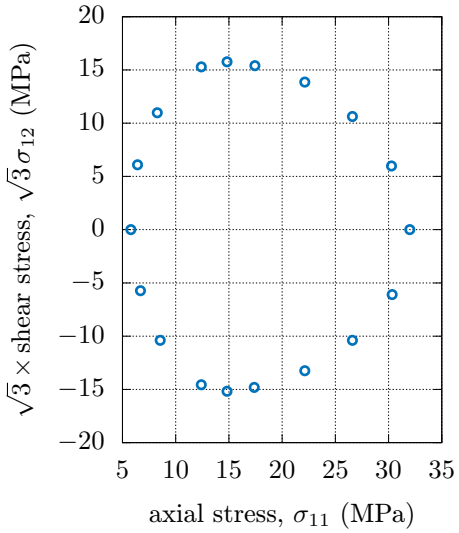

Fig. 2.4: *DDH in experiments on pure aluminum by Phillips & Tang (1972) [64].*

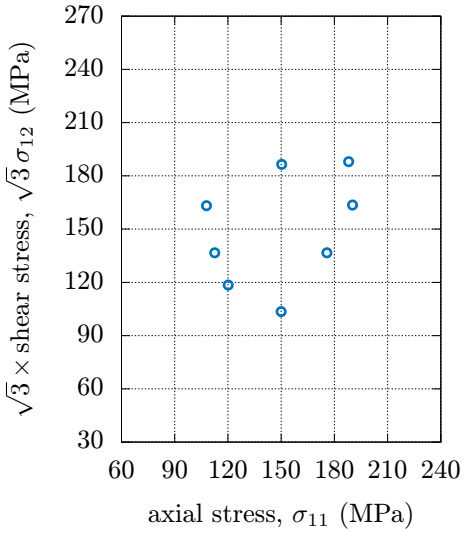

Fig. 2.5: *DDH in experiments on Al6061-T6511 aluminum alloy by Khan et al. (2009) [125].*

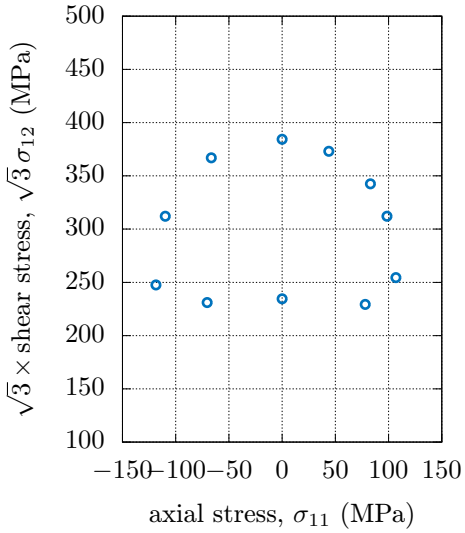

Fig. 2.6: *DDH in experiments on 70:30 brass by Helling et al. (1986) [87].*

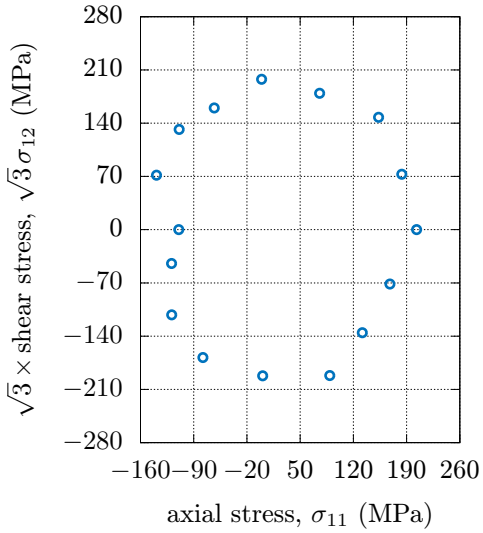

Fig. 2.7: *DDH in experiments on copper by Dietrich & Kowalewski (1997) [103].*

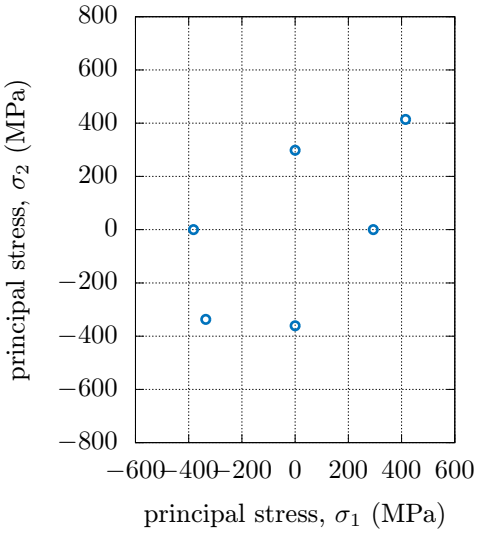

Fig. 2.8: *DDH in experiments on pure α-titanium by Nixon et al. (2010) [127].*

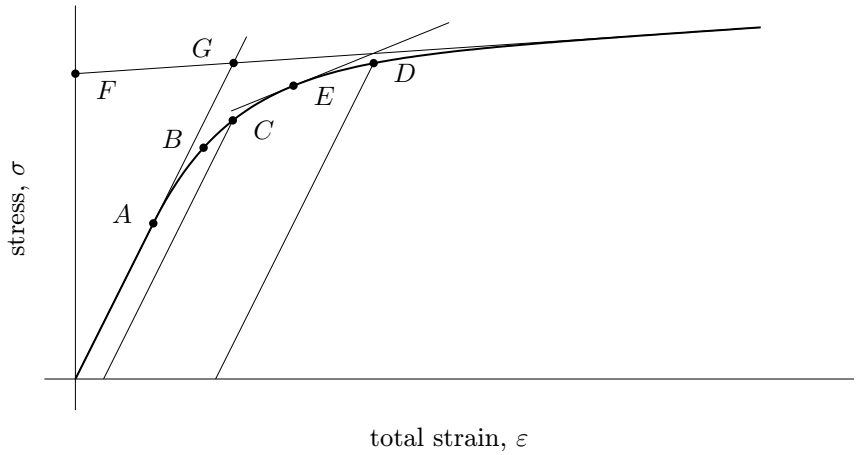

Fig. 2.9: *Various definitions of the yield point [71, 77].*

2.2 Yield Point Definition

In plasticity theories, yielding is defined when plastic strain increment is induced either as a result of a stress increment in rate independent plasticity or under the existing stress in rate dependent viscoplasticity. The current stress at yielding lies on the yield surface in stress space. In experimental plasticity, however, the yielding definition is not so straight-forward, because of the difficulty to identify an appropriate plastic strain increment (not too small, not too large). There are several definitions that, in general, vary in particular assumptions. Moreover, these definitions together with their assumptions are often affected by plasticity theories or enforced by testing methods. In particular many definitions of the yield point rely on linear behavior of material in elastic domain [78, 89, 96]. Further, there are some definitions that adopt von Mises effective strain formula to evaluate multiaxial strain states [92, 95, 97]. Also, there are some definitions based on assumptions imposed by particular testing methods [47, 51, 76]. An overview of various methods of how to define the yield point in experimental plasticity may be seen in [71, 77]. Here, only the definitions suitable for monotonically hardening stress–strain curves, *i.e.*, curves with no plateau effect at the yielding, are discussed.

In their experiments, many researchers defined yielding by the *proportionality limit* A, as shown in Fig. 2.9 [45, 63, 64]. Although this method seems to be quite simple and has an explicit physical interpretation, there are two main drawbacks related. At first, the method assumes linear elastic behavior, which may disqualify this definition for materials with nonlinear behavior in the elastic domain [71]. Further, no universal definition is given of when the proportionality is corrupted, which led authors to adopt the lowest deviation from linearity distinguished by their

experimental setup. Due to this, the yield point strongly depends on the sensitivity of the measurement and the method does not provide consistent results [71].

Because some materials may undergo pure elastic deformation of non-linear type beyond the proportionality limit, it is reasonable to define the yield point by the *elastic limit* B shown in Fig. 2.9. The elastic limit B is the highest stress that does not cause any permanent deformation when the specimen completely unloaded. With no doubts, this definition fits best an intuitive understanding of the plastic deformation as the permanent deformation. Despite its clear physical interpretation, this definition brings two substantial problems. The first is in common with the proportional definition given above. Namely, no universal threshold is given by this method to distinguish between the neglectable residual strain and the permanent plastic strain. Further, it is quite cumbersome to keep switching between the loaded and unloaded configuration in order to determine the permanent strain.

In experiments of yield surfaces detection, the most frequently used definition of the yield point is that of the *proof stress* [47, 87, 96]. In Fig. 2.9, the particular yield point that represents this method is denoted by C. During loading, the offset stress is given by the difference of the total strain measured from the experiment and the elastic strain computed from the Hooke's law. If this offset strain reaches prescribed threshold, yielding is consiered to have occured. The threshold offset strains vary among authors, usually lying in the range of 10–200 $\mu\varepsilon$. For recent papers, the lower values are typical. Note that the proof stress definition of the yield point in engineering is standardized and adopts the threshold of 0.2 % of total strain. This point is denoted by D in Fig. 2.9.

Several other definitions of the yield point may be found in literature. Some authors used the *elastic modulus fraction* to define the yield point [71]. This is represented by the point E in Fig. 2.9. Another way is to project the slope of the stress–strain curve to the zero plastic strain, as shown in Fig. 2.9 and denoted by F [49]. Also, some authors projected the slope of the stress–strain curve to the zero total strain, which is represented by the point G in Fig. 2.9 [23, 48].

2.3 Experimental Methods in Distortional Hardening

Some early experiments that revealed the distortion of yield surfaces due to plastic straining induced on purpose during these experiments may be traced back to late 1950s [42, 44, 45, 47, 48]. Note, the distortion of yield surfaces of metals due to manufacture process was observed even in late 1930s [28, 34]. There have been developed several experimental techniques suitable to detect yield surfaces distorted by straining, of which the most frequently employed ones are described below.

In general, there are two main challenges concerning capabilities of experimental techniques. The first challenge is to achieve uniform stress states in the material.

This is crucial since the uniform stress states induce uniform strain effects in the bulk, which makes these effects easier to be observed. The second main challenge is to achieve probing in the general direction relatively to the loading direction of prestraining, *i.e.*, relatively to the loading that induced distortion of the yield surface. This requirement is fundamental to detect distortion.

The simplest method to detect the distortion of yield surfaces is based on the uniaxial testing of the specimens cut off from a single plate or sheet of prestrained material. This method was used by a few authors, *e.g.*, Klingler and Sachs in 1948 [34], Szczepiński in 1963 [47], Ascione *et al.* in 1982 [76], and Nixon *et al.* in 2010 [127], and it brings several adventages. In particular, it is sufficient to test the specimens in uniaxial loading mode, which permits to design a simple geometry of specimens, and keeps the testing methodology quite simple too. On the other hand, this method requires a high-capacity device to prestrain the plates. Moreover, it is necessary to unload the plates completly before the specimens are cut off. This may bring some discrepancy, because, when compared to the other testing methods, several authors reported the plastic straining even during unloading [64, 96, 125]. Thus, this method disqualifies to observe such an effect.

Theocaris and Hazell in 1965 used a moiré method to detect yield surfaces [51]. This method is based on the measurement of deflexions of square and rhomboid plates. The plates are illuminated by a collimated light beam, which causes an oblique moiré pattern on the surface of plates. From the moiré pattern, the relative deflection of plates is computed. To relate the stress and displacement fields in loaded specimens, Theocaris and Hazell used the theory of plates. The main challange in experiments was to induce various stress ratios in specimens so that the distorted surfaces would be determined in all quadrants of the respective space. For this an advanced experimental method was developed, employing several sofisticated techniques. In particular, square- and rhomboid-shaped specimens were used, several loading and supporting configurations were exploited, and some stress states were even achieved virtually using a superposition of two real states. The major advantage of this method is that any stress ratio may be addressed. Note, some other experimental methods described here may suffer from the loss of structural stability of specimens when particular loading modes are to be achieved. The main disadvantage of this method is that distorted yield surfaceses are plotted in the two-dimensional bending moment space. Thus, this method does not provide absolute values of yield stresses of tested material, but rather a relative shape of yield surfaces is obtained.

Lode in 1926 [21], Hecker in 1972 [62], and Khan *et al.* in 2010 [126], among the other authors, used thin-walled tubular specimens loaded by a combined axial load and internal pressure. As the specimens are thin-walled, internal pressurizing induce neglectable radial stress and substantial hoop stress. Thus, using this type of loading, the biaxial membrane stress state in specimens is well approximated. The major advantage of this method is that principal directions are fixed and aligned

with axial, radial, and tangential directions of specimens' geometry. The major disadvantage is in lower structural stability of specimens in compressive loading cases.

Taylor and Quinney in 1931 [23], Naghdi *et al.* in 1958 [42], and Wu and Yeh in 1991 [96], among the other authors, used thin-walled specimens loaded by a combined axial load and torque. This testing method requires more sofisticated biaxial testing machine. As the specimens are thin-walled, torque induce quite uniform shear stress in specimens' wall. Again, the biaxial stress state is achieved, however, the principal directions do not remain fixed nor aligned with any directions within the testing, but rather they depend on particular ratios of torque and axial load. This is the major difference with the method of combined axial load and internal pressurizing described above. The variation of principal directions may bring some discrepancies when the specimens show high plastic anisotropy [57]. Another disadvantage—lower structural stability of specimens in compressive testing cases—is in common with the method of combined axial load and internal pressurizing described above.

The most advanced testing method developed thus far combines the both methods that make use of thin-walled specimens and are described above. Thus, the specimens are loaded by a combination of axial load, torque, and internal pressure. This method was emloyed by several authors, *e.g.*, Shiratori *et al.* in 1973 [65], Phillips and Das in 1985 [84], and Sung *et al.* in 2011 [132], and allows to achieve biaxial stress states by a variation of components of the stress tensor in three-dimensional space of axial, shear, and hoop stress. In general, the methods of yield surfaces detection emloying thin-walled tubular specimens are quite time consuming, since they usually require one probing trajectory to determine particular point located on the yiled surface. To make the methodology consistent and effective, Sung *et al.* [132] developed a computer code to control the testing machine, which allows to make the testing fully automated. Moreover, from their results they concluded that initial yield surfaces determined in three-dimensional stress space do not fully match von Mises criterion. Also, they have observed some more complex strain hardening effects manifested by yield surfaces rotation.

2.4 Early Attempts in Modeling

The early attempts to model the distortion of yield surfaces may be traced back to Hill in 1948 [33]. Motivated by observation of plastic anisotropy in components manufactured by forming process, he has extended von Mises criterion to the orthotropic plasticity case. The proposed yield function is given by

$$2f = F(\sigma_y-\sigma_z)^2+G(\sigma_z-\sigma_x)^2+H(\sigma_x-\sigma_y)^2+2L\tau_{yz}^2+2M\tau_{zx}^2+2N\tau_{xy}^2-1, \quad (2.1)$$

where σ_α and $\tau_{\alpha\beta}$ are the stress tensor components, and F, G, H, L, M, and N are material parameters. Note, the model inherits pressure insensitivity after von Mises criterion. Later on, Hill proposed hardening laws for model's parameters [35].

Williams and Svensson in 1971 [61] and Lee and Zaverl in 1978 and 1979 [74, 75] developed a model based on the yield function given by

$$3f = M_{ij}\,(s_i - \alpha_i)\,(s_j - \alpha_j) - k^2, \tag{2.2}$$

where M_{ij} are the components of the distortional tensor, s_i and α_i are the deviatoric stress and back-stress components, respectively, and k is the isotropic hardening variable. The model extends Hill's criterion [33], and incorporates the isotropic, kinematic, and distortional hardening. The strain rate equation was formulated in terms of the equivalent plastic strain rate, the equivalent stress, and the plastic strain potential. The equivalent plastic strain rate was expressed in terms of an equivalent stress, a scalar-valued plastic shear resistance, and temperature. In general, it was formulated so that it is capable to model different micromechanical processes of deformation.

Ortiz and Popov in 1983 [79] proposed a model of the yield surface distortion that involves a scalar-valued multiplier expressed in terms of a Fourier series. The yield function is given by

$$f = \sqrt{(s_{ij} - \alpha_{ij})\,(s_{ij} - \alpha_{ij})} - k\left(1 + \sum_{2}^{+\infty} \rho_n \cos n\theta_n\right), \tag{2.3}$$

where s_{ij} and α_{ij} are the deviatoric stress and back-stress tensor components, respectively, k is the isotropic hardening variable, and ρ_n and θ_n, $n = 2, 3, \ldots$, are scalar-valued parameters. Thus, the multiplier of isotropic hardening variable k is responsible for the distortion in this model. This is quite a unique concept, since the yield surface distortion is often modeled via a general quadratic form in variable $(s_\beta - \alpha_\beta)$, *e.g.*, Eqs. (2.2), (2.4), and (2.12), where s_β and α_β stands for the stress and backstress components, respectively.

Kurtyka and Życzkowski in 1996 [101] published a general model capable to capture proportional expansion, translation, affine deformation, rotation, and distortion of the yield surface. The yield criterion emloyed in this model is given by

$$f = (\sigma_i - a_i)\,Q_{ji} D_{jk} Q_{kl}\,(\sigma_l - a_l) - 1, \tag{2.4}$$

where σ_i are the deviatoric stress vector elements, a_i are the back-stress vector elements, Q_{ij} are the rotation matrix elements, D_{jk} are the diagonal functional matrix elements, and $i, j, k, l = 1, \ldots, 5$; the elements of vectors are expressed in terms of Ilyushin's five-dimensional stress space. The authors used purely geometric description of transformations of the yield surface, and, later on, they proposed the evolution equations for model's internal variables.

François in 2001 [109] proposed a model with the yield criterion given by

$$f = \sqrt{\left(S^{\mathrm{d}}_{ij} - X_{ij}\right)\left(S^{\mathrm{d}}_{ij} - X_{ij}\right)} - R - \sigma_{\mathrm{y}}, \tag{2.5}$$

where S_{ij}^{d} are the distorted stress tensor components, X_{ij} are the back-stress tensor components, R is the isotropic hardening function, and σ_{y} is the initial yield stress. The distorted stress tensor components are given by $S_{ij}^{\mathrm{d}} = S_{ij} + X_{ij}\left(S_{kl}^{\mathrm{o}} S_{kl}^{\mathrm{o}}\right) / \left(2X_1(R+\sigma_{\mathrm{y}})\right)$, where (S_{kl}^{o}) is an orthogonal part of the deviatoric stress tensor (S_{ij}) given by $S_{ij}^{\mathrm{o}} = S_{ij} - S_{ij}^{X}$, and where $\left(S_{ij}^{X}\right)$ is the collinear part of the deviatoric stress tensor (S_{ij}) with respect to the back-stress tensor (X_{ij}) given by $S_{ij}^{X} = X_{ij}(S_{kl}X_{kl})/(X_{mn}X_{mn})$. Thus, this yield criterion implements the yield surface distortion via distorted stress tensor, which is another concept of how to capture DDH effect. Some other plasticity models with the yield criterion capable to capture the distortion of yield surfaces may be seen in [50, 89, 99, 102, 114].

2.5 Higher Order Evolving Tensor Approach

The early attempts to employ the higher order tensors in constitutive modeling of mechanical behavior of materials may be traced back to Mālmeisters in 1966 [53,55]. Mālmeisters has proposed the strength criterion in the form

$$f = \Pi_{ij}\sigma_{ij} + \Pi_{ijkl}\sigma_{ij}\sigma_{kl} + \Pi_{ijklmn}\sigma_{ij}\sigma_{kl}\sigma_{mn} + \ldots - 1, \tag{2.6}$$

where σ_{ij} are the stress tensor components, and $\Pi_{ij\ldots}$ are components of the even order tensor-valued parameters that represent material properties.

Rees in 1984 [83] developed a plasticity model with the yield criterion given by

$$f = f_{\mathrm{s}}\left(F_1, F_2, F_3\right) - 1, \tag{2.7}$$

where

$$F_1 = \left(C_{ij} - A_{ij}\right)\left(s_{ij} - \alpha_{ij}\right), \tag{2.8}$$

$$F_2 = \frac{1}{2}\left(C_{ijkl} - A_{ijkl}\right)\left(s_{ij} - \alpha_{ij}\right)\left(s_{kl} - \alpha_{kl}\right), \tag{2.9}$$

$$F_3 = \frac{1}{3}\left(C_{ijklmn} - A_{ijklmn}\right)\left(s_{ij} - \alpha_{ij}\right)\left(s_{kl} - \alpha_{kl}\right)\left(s_{mn} - \alpha_{mn}\right), \tag{2.10}$$

and where $C_{ij\ldots}$ are the components of isotropic tensors, $A_{ij\ldots}$ are the components of tensors responsible for the plastic anisotropy, s_{ij} are the deviatoric stress components, α_{ij} are the back-stress components, and where three different expressions for f_{s} were used, namely, $f_{\mathrm{s}} = F_1 + F_2$, $f_{\mathrm{s}} = F_2 + F_3$, and $f_{\mathrm{s}} = F_1 + F_2 + F_3$.

Following the work by Mālmeisters in 1966 [53] and by Goľdenblat and Kopnov in 1968 [55], Grewolls and Kreißig in 2001 [110,131] truncated the general polynomial expression after the cubic degree, which gives the yield criterion in the form

$$f = K_0\left(\varepsilon_{\mathrm{eq}}^{\mathrm{p}}\right) + K_{ij}\sigma_{ij} + K_{ijkl}\sigma_{ij}\sigma_{kl} + K_{ijklmn}\sigma_{ij}\sigma_{kl}\sigma_{mn}, \tag{2.11}$$

where $K_{ij\ldots}$ are components of material tensors of 2^{nd}, 4^{th}, and 6^{th} degree, and K_0 is a scalar-valued material parameter that depends on the equivalent plastic strain $\varepsilon_{\mathrm{eq}}^{\mathrm{p}}$. They used an approach by Danilov [58] to formulate evolution equations.

2.6 Advanced Directional Distortional Models

Feigenbaum and Dafalias in 2007 [118,121,122] proposed a family of four different DDH models referred to as the *A-model*, the *r-model*, the *alpha-model*, and the *alpha-model with fixed distortional parameter*. These models have several distinguishing features, which make them suitable for engineering application.

In particular, the yield criteria of these models extend von Mises yield criterion via a distortional variable. This variable is tensor-valued in case of the A-model and the r-model, and it is scalar-valued in case of α-models. Moreover, this extension is as simple as possible since just a single variable was added to capture the distorion.

Next, the evolution laws for models' internal variables are proposed so that the plastic straining would preserve the second law of thermodynamics equivalently expressed via the Clausius–Duhem inequality. Henceforth, this property is referred to as the *thermodynamical consistency*, and allows to keep the model consistent from the physical point of view.

For the stability of the numerical integration algorithms, the convexity of yield functions is crucial. Plešek *et al.* in 2010 [129] addressed this topic and discussed the convexity of yield functions of models from Feigenbaum–Dafalias' family. Although the convexity of yield functions is not inherent to these models, some necessary and sufficient conditions imposed on models' parameters were found, so that the yield function convexity would be preserved.

In this thesis, the simplest model from the family reffered to as the α-model with fixed distortional parameter will be employed. Its yield function f is based on the J_2-invariant, which is subsequently modified by a directional multiplier as

$$f(\boldsymbol{\sigma}) = \frac{3}{2}\left[1 - c\,(\boldsymbol{n}_{\mathrm{r}}{:}\boldsymbol{\alpha})\right](\boldsymbol{s}-\boldsymbol{\alpha}){:}(\boldsymbol{s}-\boldsymbol{\alpha}) - k^2 = 0, \tag{2.12}$$

where $\boldsymbol{\sigma}$ is the stress tensor, $\boldsymbol{s}$ is the deviatoric stress tensor, $\boldsymbol{\alpha}$ is the deviatoric backstress tensor acting as the "center" of the yield surface, c is a positive distortional parameter, and k is a scalar internal variable responsible for the isotropic hardening. The double dot symbol represents the inner product of two tensors as in $\boldsymbol{a}{:}\boldsymbol{b} = a_{ij}\,b_{ij}$, and $\|\cdot\|$ denotes the Euclidean norm of a second order tensor. Further,

$$\boldsymbol{n}_{\mathrm{r}} = \frac{\boldsymbol{s}-\boldsymbol{\alpha}}{\|\boldsymbol{s}-\boldsymbol{\alpha}\|} \tag{2.13}$$

is the deviatoric unit norm tensor along the radius $(\boldsymbol{s}-\boldsymbol{\alpha})$. Hence, it is the inner product $\boldsymbol{n}_{\mathrm{r}}{:}\boldsymbol{\alpha}$ which is responsible for the directional distorsion of the yield surface.

The model's internal variables are governed by standard evanescent memory type equations. The kinematic hardening rule is Armstrong–Frederick's type defined according to

$$\dot{\boldsymbol{\alpha}} = a_1\left(\dot{\boldsymbol{\varepsilon}}^{\mathrm{p}} - a_2\,\|\dot{\boldsymbol{\varepsilon}}^{\mathrm{p}}\|\,\boldsymbol{\alpha}\right), \tag{2.14}$$

and the isotropic hardening is defined by

$$\dot{k} = \lambda \kappa_1 k \left(1 - \kappa_2 k\right), \tag{2.15}$$

where λ is the loading index or plastic multiplier defined as usual in terms of stress or strain rate. Both of these evolution equations can be shown [121] to be sufficient to satisfy the second law of thermodynamics. Plastic strain rate is obtained by an associated flow rule

$$\dot{\boldsymbol{\varepsilon}}^{\mathrm{p}} = \lambda \frac{\partial f}{\partial \boldsymbol{\sigma}} \ . \tag{2.16}$$

The initial values are defined for unstrained material as $\boldsymbol{\varepsilon}^{\mathrm{p}} = \mathbf{0}$, $\boldsymbol{\alpha} = \mathbf{0}$ and $k = k_0$, that is, k_0 is the initial yield stress. Thus the model features six positive parameters a_1, a_2, κ_1, κ_2, k_0, and c. Details of this constitutive model are explained in [121].

In order to simplify governing equations, one can explicitly calculate the yield function gradient

$$\frac{\partial f}{\partial \boldsymbol{\sigma}} = \frac{3}{2} \left\| \boldsymbol{s} - \boldsymbol{\alpha} \right\| \left[2\boldsymbol{n}_{\mathrm{r}} - c \left(\boldsymbol{n}_{\mathrm{r}} : \boldsymbol{\alpha} \right) \boldsymbol{n}_{\mathrm{r}} - c\boldsymbol{\alpha} \right] \tag{2.17}$$

and its magnitude as

$$\left\| \frac{\partial f}{\partial \boldsymbol{\sigma}} \right\| = \frac{3}{2} \left\| \boldsymbol{s} - \boldsymbol{\alpha} \right\| \sqrt{\left[2 - c \left(\boldsymbol{n}_{\mathrm{r}} : \boldsymbol{\alpha} \right) \right] \left[2 - 3c \left(\boldsymbol{n}_{\mathrm{r}} : \boldsymbol{\alpha} \right) \right] + c^2 \boldsymbol{\alpha} : \boldsymbol{\alpha}}. \tag{2.18}$$

It was proved in [121] and [129] that the necessary and sufficient condition, which keeps dissipation positive and simultaneously preserves strict convexity for all times, yields

$$\left\| c\boldsymbol{\alpha} \right\| < 1. \tag{2.19}$$

Substitution of Eq. (2.14) into Eq. (2.15) yields

$$\dot{\boldsymbol{\alpha}} = a_1 \lambda \left\| \frac{\partial f}{\partial \boldsymbol{\sigma}} \right\| \left(\boldsymbol{n} - a_2 \boldsymbol{\alpha} \right). \tag{2.20}$$

For monotonic loading the saturated state is reached when $\dot{\boldsymbol{\alpha}} = \mathbf{0}$, thus, Eq. (2.20) yields

$$\boldsymbol{n} - a_2 \boldsymbol{\alpha} = \mathbf{0}. \tag{2.21}$$

Since $\boldsymbol{\alpha}$ starts from zero and the magnitude of the limit backstress, $1/a_2$, is independent of the loading direction, one may write

$$\left\| \boldsymbol{\alpha} \right\| \leq 1/a_2. \tag{2.22}$$

Hence the left-hand side of inequality (2.19) may be bounded by c/a_2, which yields

$$c < a_2. \tag{2.23}$$

This is the only constraint to be observed in the present constitutive modeling.

To illustrate the behavior of the discussed model, material parameters after [121], and given in Tab. 2.1 were used. Yield surfaces of the model are shown in Figs. 2.10, 2.11, and 2.12. The evolution of subsequent yield surfaces under uniaxial tension is shown in two stress subspaces in Fig. 2.13. Observe that all three kinds of hardening, namely isotropic, kinematic and directional distortional, contribute to the plotted shapes of the yield surface. The stress–strain curves and the evolution of other internal variables are plotted in Fig. 2.14.

Tab. 2.1: *Model's parameters k_0, κ_1, κ_2, a_1, a_2 and c taken from [121]. Initial condition for α_{11} represents a virgin material. The plastic prestrain $\varepsilon_{11}^{\mathrm{p}}$ was set up to be sufficient to develop distortion. Values from this table are used to plot Figs. 2.10–2.14.*

k_0 (MPa)	κ_1 (MPa)	κ_2 (MPa^{-1})	a_1 (MPa)	a_2 (MPa^{-1})	c (MPa^{-1})	$\alpha_{11,0}$ (MPa)	$\varepsilon_{11}^{\mathrm{p}}$ (%)
128	6 000	0.006	10 500	0.02	0.019	0	1.0

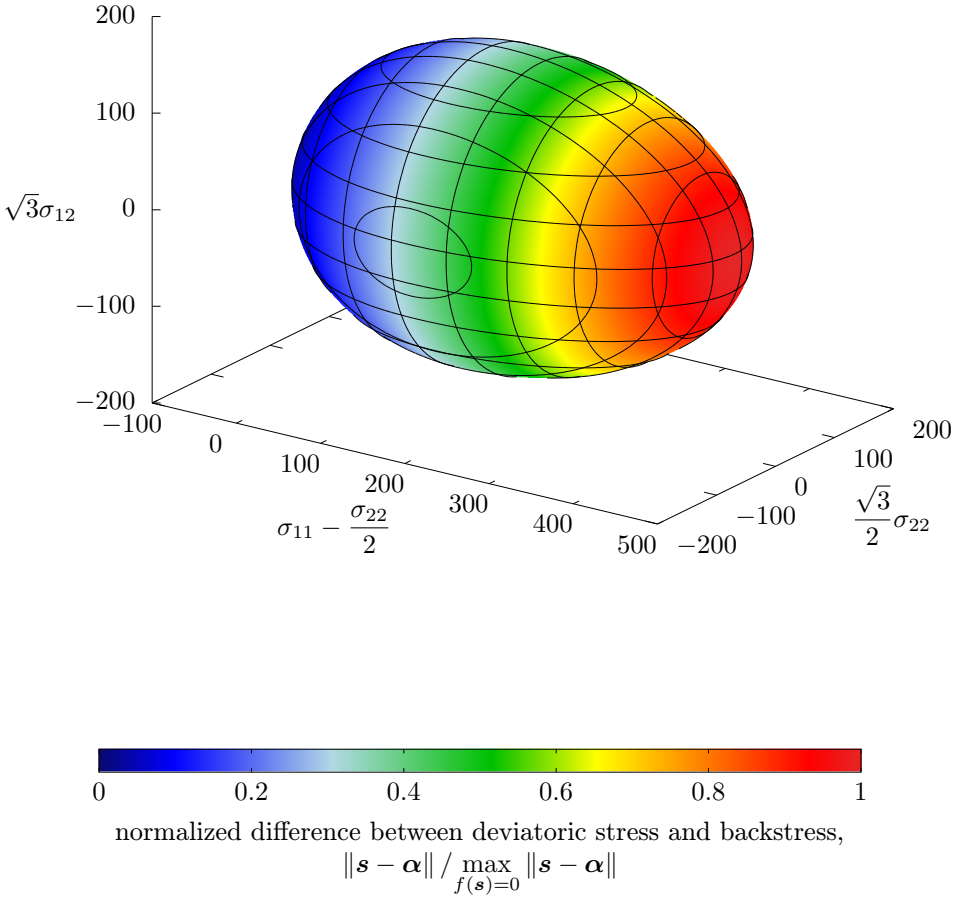

Fig. 2.10: *Directional distortion of the yield surface of α-model with fixed c parameter by Feigenbaum and Dafalias [121] plotted in $(\sigma_{11} - \sigma_{22}/2)$—$\left(\sqrt{3}\sigma_{22}/2\right)$—$\left(\sqrt{3}\sigma_{12}\right)$ space. Parameters of the model, initial conditions and plastic prestrain to plot this example are taken from Tab. 2.1.*

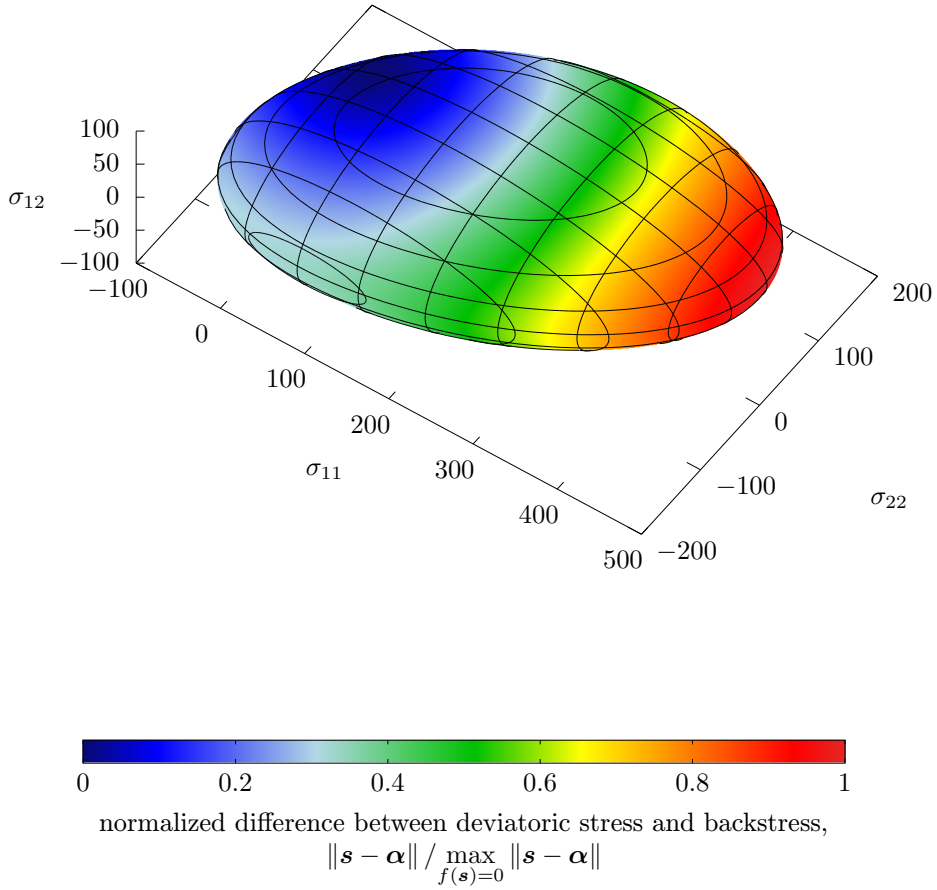

Fig. 2.11: *Directional distortion of the yield surface of α-model with fixed c parameter by Feigenbaum and Dafalias [121] plotted in σ_{11}—σ_{22}—σ_{12} space. Parameters of the model, initial conditions and plastic prestrain to plot this example are taken from Tab. 2.1.*

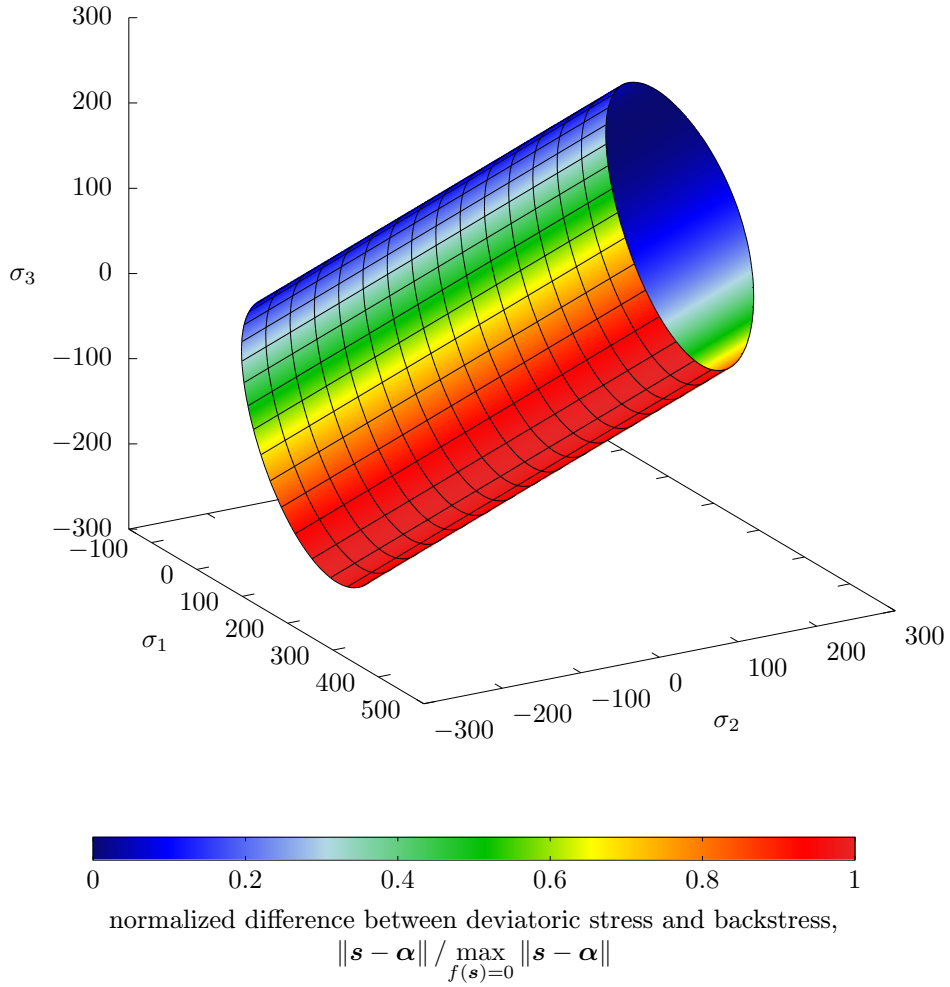

Fig. 2.12: *Directional distortion of the yield surface of α-model with fixed c parameter by Feigenbaum and Dafalias [121] plotted in principal stresses space σ_1—σ_2—σ_3. Parameters of the model, initial conditions and plastic prestrain to plot this example are taken from Tab. 2.1. The surface is not limited in the first octant axis direction.*

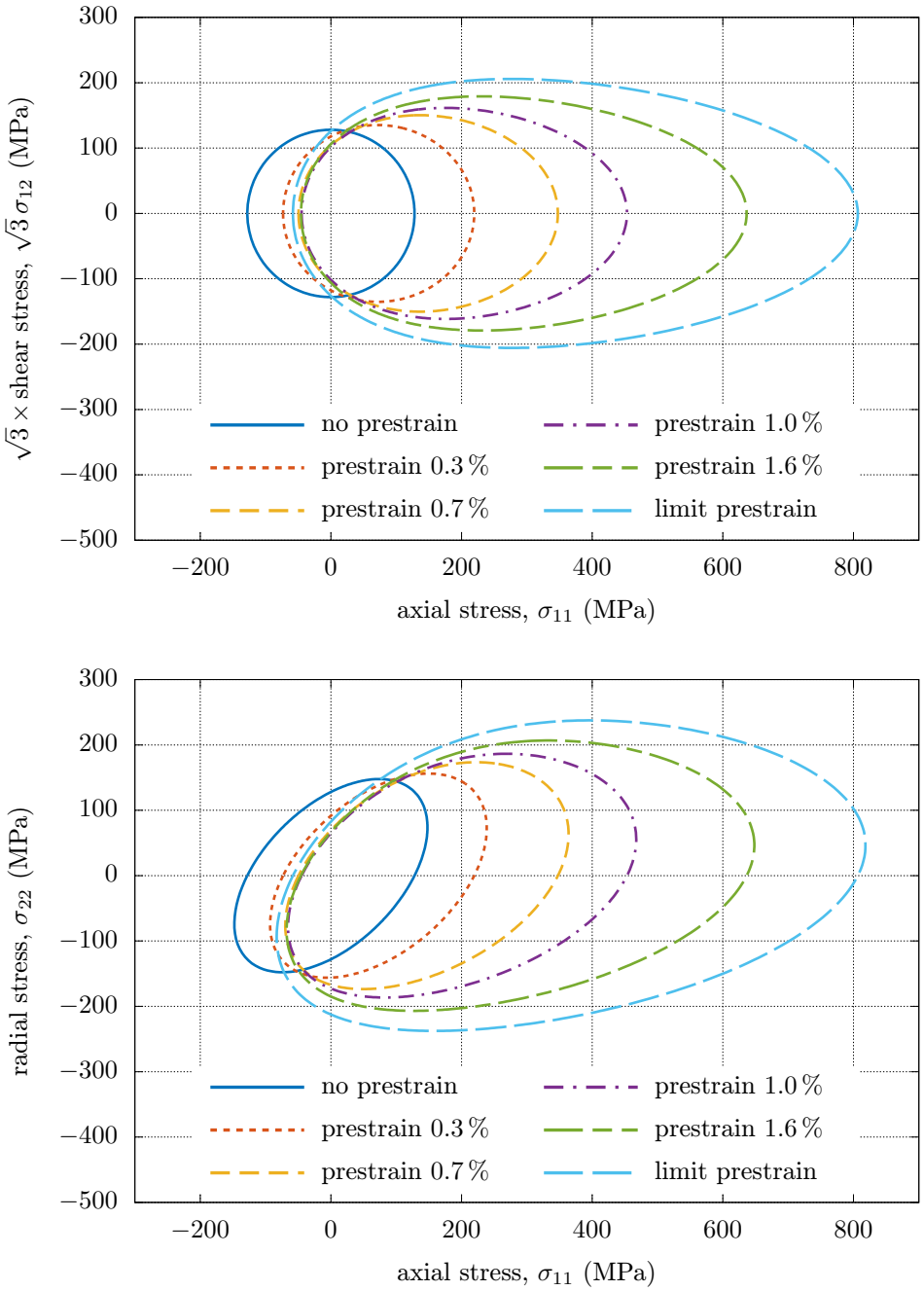

Fig. 2.13: *Yield loci evolution for stress driven loading.*

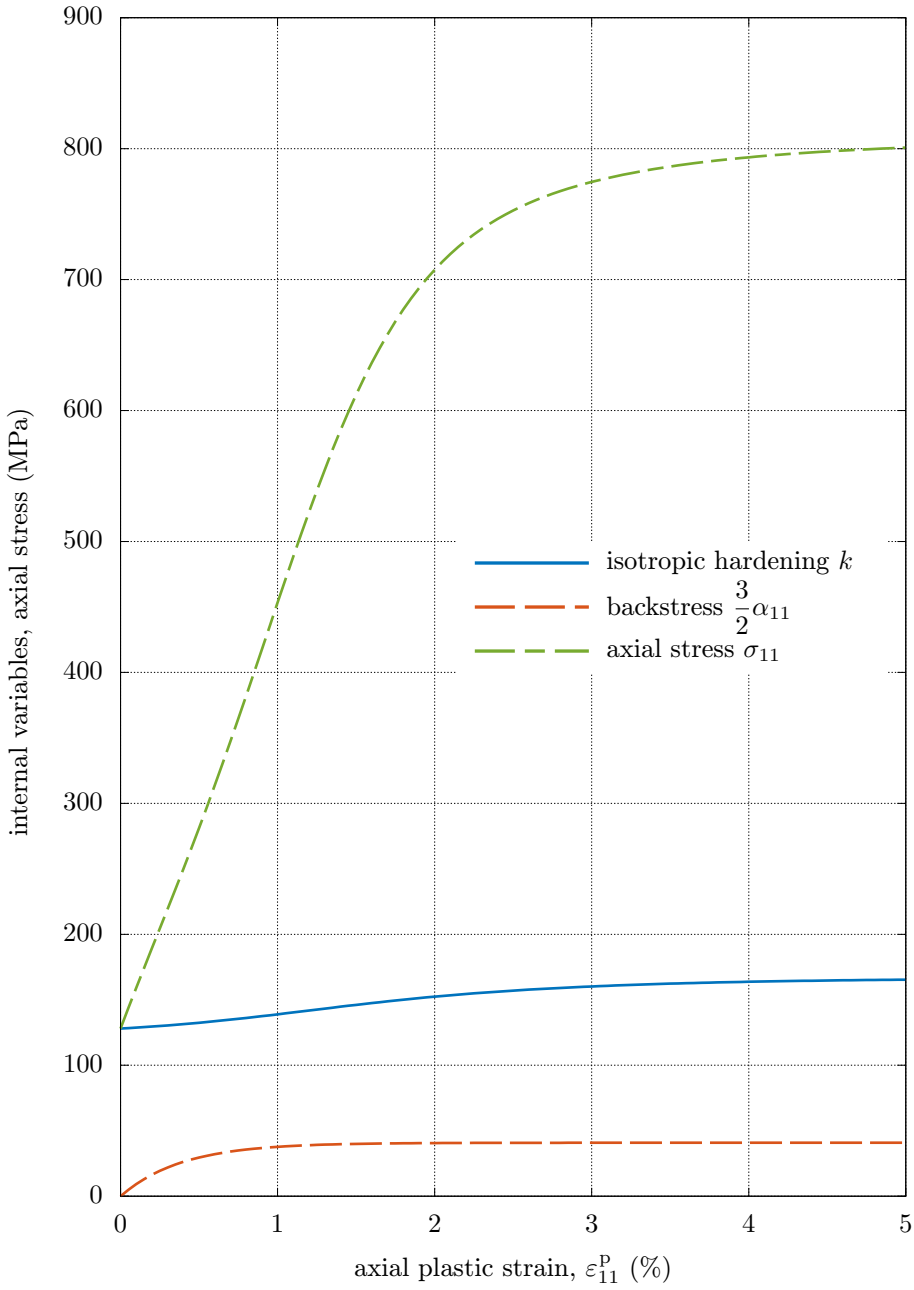

Fig. 2.14: *Evolution of stress and internal variables for parameters from Tab. 2.1. The σ_{11} curve represents a stress–strain curve in σ_{11}–$\varepsilon_{11}^{\mathrm{p}}$ variables.*

Chapter 3

Aims of the Thesis

The directional distortional hardening (DDH) phenomenon, *i.e.*, the asymmetric distortion of yield surfaces due to plastic straining, has been experimentally proved on a wide variety of metals, and nowadays might be considered a common feature in experimental plasticity of metals. Despite this, there seems to be no preferred model for DDH nor paradigm being employed and widespread in industrial applications. Thus, DDH models might be considered occupying a *death valley* from an engineering application point of view.

The general aim of this thesis is to *identify* problems preventing the application of DDH models and to bring *answers*, *solutions*, and *explanations* of these problems via analysis of distinguishing features of DDH models. Thereby bridging the death valley and making engineering use of DDH possible.

In general, there may be several reasons why DDH models are rarely utilized and not widespread in engineering application. First, these models are most useful in multiaxial stress states with non-proportional loading trajectories, which is an experimental challenge. Although multiaxial stress states can be easily reached, the commercial testing systems do not provide nor support any standard operating procedures suitable for advanced multiaxial testing. In fact, because control systems for multiaxial test equipment still rely on GUI forms instead of script based architecture, it is still quite hard to assemble a testing setup for calibration experiments with well-arranged modular and parametrized control.

In addition to the issues with experiments for calibration, it should be emphasized that there is little systematic theoretical effort to introduce calibration algorithms. Such calibration algorithms ideally would exploit the closed-form solutions and available experimental methodologies. Thus, this thesis suggests schemes and algorithms for calibration of a particular DDH model. While the focus is on a particular model, the algorithms can be generalized for any similar model.

In order to keep the thesis consistent, the general aim is split into four particular aims that have solidified during the analysis of the problem. Each of four aims defines a compact problem and each of these compact problems is solved separately, though some may exploit results of others. To meet a general aim of the thesis, a DDH model by Feigenbaum and Dafalias referred to as *alpha-model with fixed distortional parameter* is used as a representative of DDH models [121, 122].

3.1 Aim #1—Finding Closed Form Solutions for Monotonic Loading

In general, stress fields seen in structural applications are too complicated and therefore are beyond the possibility of an analytical solution. Since the stress field is an essential ingredient in plasticity theories, the same holds for plasticity problems. However, there are often individual problems when quite uniform stress field occurs and when the exact or analytical solution might be possible and useful. This uniform stress fields may occur in applications due to the symmetry of the loading and structure, *e.g.*, tubes, trusses, membranes; or in the laboratory due to testing for model calibration, *e.g.*, uniaxial tensile testing, axial load–torque testing, membranes pressurizing; or in simulations, *e.g.*, debugging FE solvers.

Aim #1 of this thesis is to find a closed form analytical solution for general monotonic proportional loading case of Feigenbaum–Dafalias α-model with fixed distortional parameter. This aim requires simplifying equations used to describe a particular loading case, integrating all internal variables of the plasticity model, and expressing the stress field according to the plastic strain field, or *vice versa*.

3.2 Aim #2—Locating Limit Envelope for Cyclic Loading

There are two well-known curves suitable to capture and analyze the plastic behavior of a material under cyclic loading—a *stabilized hysteresis loop* and a *cyclic stress–strain curve*. While both these curves are commonly determined experimentally, an analytical representation inherent to a particular DDH model would be desired as well. The reason is that analytical expressions of both these curves can be used to relate experimental data with internal parameters of particular DDH model and therefore can be employed to calibrate model's parameters. Moreover, due to the cyclic character of loading, some of the internal variables of the model may saturate which may simplify expressions and reduce the number of active parameters.

Thus, *Aim #2* of this thesis is to find those analytical expressions of a stabilized hysteresis loop and a cyclic stress–strain curve, that are inherent to Feigenbaum–

Dafalias α-model with fixed distortional parameter in case of general proportional cyclic loading. This aim requires to derive an expression for monotonic stress–strain curve described in aim #1, to express a limit state for a series of concatenated monotonic curves, and to express the stress amplitudes according to the plastic strain amplitudes, or *vice versa*.

3.3 Aim #3—Developement of Analytical Calibration Algorithms

For successful engineering application of any model, a robust calibration algorithm is needed. This crucial point is often omitted and limits the application of many models. Modern DDH theories are usually designed to reflect several different phenomena, *e.g.*, yield surface convexity, thermodynamic consistency, and isotropic and kinematic hardening. This trend means that modern models involve a higher number of parameters and become highly nonlinear. The higher number of parameters, the higher dimension of the calibration problem, which imposes higher demands on calibration procedures and increases numerical complexity. The higher nonlinearity, the higher sensitivity of the calibration algorithm to the initial estimation of parameters.

Aim #3 of this thesis is to propose calibration algorithms of Feigenbaum–Dafalias α-model with fixed distortional parameter. The algorithms will be based on results obtained from the aims #1 and #2, *i.e.*, on analytical solutions for the stress–strain curve, the stabilized hysteresis loop, and the cyclic stress–strain curve. These algorithms should be suitable for initial estimation of parameters in a numerical calibration scheme or to fully identify parameters analytically. Moreover, the calibration algorithms should match the curves of monotonic and cyclic loading cases with the monotonic and cyclic experimental data, respectively.

3.4 Aim #4—Sensitivity Analysis of Calibration Algorithms

In general, the sensitivity of nonlinear systems with respect to their parameters varies among the parameters and the states of the system, *i.e.*, the values of these parameters. This variation may reach even several orders, which often brings some inconveniences in numerical procedures used for modeling. The calibration algorithms announced in the aim #3 relate internal parameters of DDH model to experimental data. As these algorithms are expected to be highly nonlinear, there is a call for sensitivity analysis.

Aim #4 of this thesis is to carry out and evaluate a sensitivity analysis of calibration algorithms developed within the aim #3. At first, this aim requires to

express internal parameters of the Feigenbaum–Dafalias α-model with fixed distortional parameter with respect to the experimental data. Then, derivatives of these internal parameters with respect to the experimental parameters need to be expressed. Next, some suitable set of parameters is required and will be chosen in order to present the sensitivity for particular material and experiment. Finally, some general conclusions based on the analysis will be given in order to localize potentially problematic relations between particular parameters. This analysis is crucial to formulate limitations of the calibration algorithms as well as the model.

Chapter 4

Methods Used

In this thesis, several classical methods and theoretical concepts are employed to develop the methodology and procedures to support an application and development of DDH models, *i.e.*, to meet the aims of the thesis. In particular, the developed methodology comprises the analytical integration of particular DDH model, the verification of integrated model by the numerical integration, the development of analytical and numerical calibration procedures, *etc.* Therefore, this chapter summaries the theory related to the methods as follows: the integration by substitution, the numerical integration of ordinary differential equations, the cubic equation solving, and the least squares method fitting. For the sake of clarity, the topics are briefly outlined and only reflect aspects needed later in the thesis.

4.1 Integration by Substitution

The *integration by substitution* is a method of finding integrals [36]. It is an important tool in calculus, and like the *integration by parts*, it is crucial to find integrals and solve differential equations. While the integration by parts is related to the *product rule of differentiation,* the integration by substitution is related to the *chain rule.* The method is based on the theorem that follows.

Theorem (Integration by Substitution). *Let $a < b$. For $a < x < b$, let*

$$\int f(x)\,\mathrm{d}x$$

exist. Let

$$x = g(z)$$

be continuous in the z-interval $[\alpha, \beta]$, let $g'(z)$ always be > 0 or always < 0, for $\alpha < z < \beta$, and let

$$g(\alpha) = a, \quad g(\beta) = b, \quad g(\alpha) = b, \quad g(\beta) = a,$$

respectively. Then

$$\int f\big(g(z)\big)\, g'(z)\, \mathrm{d}z$$

exists for $\alpha < z < \beta$, and

$$\int f(x)\, \mathrm{d}x = \int f\big(g(z)\big)\, g'(z)\, \mathrm{d}z.$$

The integration by substitution is employed in Section 5.1 to solve Eq. (5.11).

4.2 Numerical Integration of ODEs

There are numerous methods for numerical solving of *ordinary differential equations* (ODEs), from which the *methods of Runge–Kutta* family are the most widely known ones. This family belongs to the class of iterative methods and includes both the implicit and explicit methods. Later in this thesis, the *Bogacki–Shampine method* [91] from the Runge–Kutta family is employed and, therefore, it is described in detail here. Suppose that the initial value problem is given by

$$y'(t) = \varphi\big(t, y(t)\big), \tag{4.1}$$

and

$$y_0 = y(t_0), \tag{4.2}$$

where y is an unknown function of time t, and y_0 is the value of y at the initial time t_0. Suppose that y_n is the numerical solution at time t_n, and h_n is the step size given by $h_n = t_{n+1} - t_n$. Then, in general, the step of the Bogacki–Shampine method is given by

$$k_1 = \varphi(t_n, y_n), \tag{4.3}$$

$$k_2 = \varphi(t_n + \tfrac{1}{2}h_n, y_n + \tfrac{1}{2}h_n k_1), \tag{4.4}$$

$$k_3 = \varphi(t_n + \tfrac{3}{4}h_n, y_n + \tfrac{3}{4}h_n k_2), \tag{4.5}$$

$$y_{n+1}^{(3)} = y_n + \tfrac{2}{9}h_n k_1 + \tfrac{1}{3}h_n k_2 + \tfrac{4}{9}h_n k_3, \tag{4.6}$$

$$k_4 = \varphi(t_n + h_n, y_{n+1}^{(3)}), \tag{4.7}$$

$$y_{n+1}^{(2)} = y_n + \tfrac{7}{24}h_n k_1 + \tfrac{1}{4}h_n k_2 + \tfrac{1}{3}h_n k_3 + \tfrac{1}{8}h_n k_4, \tag{4.8}$$

where $y_{n+1}^{(3)}$ and $y_{n+1}^{(2)}$ are the third and the second order approximations, respectively. Note that this pair may be used to adapt the step size. Furthermore, due

to "first same as last" property, the k_4 parameter in one step equals the k_1 parameter in the next step, and, therefore, only three function evaluations are necessary per one step. This explicit method is implemented in several software products, *e.g.*, Matlab [106], GNU Octave [140]. Some details on stability, accuracy, and step adaptibility of the method may be seen in [91,106]. The Bogacki–Shampine method of numerical integration is employed in Section 5.1 to solve Eqs. (5.10) and (5.11).

4.3 Solving Cubic Equation

A general form of the *cubic equation* with real coefficients reads

$$ax^3 + bx^2 + cx + d = 0, \tag{4.9}$$

where a, b, c, and d are real numbers, $a \neq 0$, and x is the unknown [56]. This equation has at least one real root. In general, this is true for all odd degree polynomial equations. The numbers of real and complex roots are determined by the *discriminant* of Eq. (4.9), which reads

$$\Delta = 18abcd - 4b^3d + b^2c^2 - 4ac^3 - 27a^2d^2. \tag{4.10}$$

If $\Delta > 0$, then Eq. (4.9) has three distinct real roots. If $\Delta = 0$, then Eq. (4.9) has a multiple root and all the roots are real. If $\Delta < 0$, then Eq. (4.9) has one real root and two non-real complex conjugate roots [56].

All of the roots of Eq. (4.9) can be found algebraically. There are numerous methods for finding roots of Eq. (4.9), *e.g.*, Cardano's method, Vieta's substitution, trigonometric method. Note that different methods for solving cubic equation are suitable for different cases of cubic equations. In particular, these cases may be distinguished by the sign of the discriminant Δ. For example, the Cardano's method is not suitable for the cases with $\Delta \geq 0$, which is typical for the eigenvalues problem of the second order tensors.

Later in this thesis, the cubic equation with negative discriminant is solved, and, therefore, this case is discussed in detail. If $\Delta < 0$, then the only real root of Eq. (4.9) may be expressed in the closed form by

$$\begin{aligned} x_1 = -\frac{b}{3a} &- \frac{1}{3a}\sqrt[3]{\frac{1}{2}\left[2b^3 - 9abc + 27a^2d + \sqrt{-27a^2\Delta}\right]} \\ &- \frac{1}{3a}\sqrt[3]{\frac{1}{2}\left[2b^3 - 9abc + 27a^2d - \sqrt{-27a^2\Delta}\right]}. \end{aligned} \tag{4.11}$$

As can be seen from Eq. (4.11), if $\Delta < 0$, the term "$-27a^2\Delta$" is positive, all operations in Eq. (4.11) can be done, and the root may be expressed by a single real number. To the contrary, if $\Delta > 0$, the term "$\sqrt{-27a^2\Delta}$" is an imaginary number which cannot be eliminated from the formula. Such a case is referred to as the *casus irreducibilis* [56]. The theory of solving cubic equations is employed in Section 5.2 to solve Eq. (5.39).

4.4 Nonlinear Least Squares Method

Many models involve parameters that make the models nonlinear with respect to these parameters. Then, the *least square analysis* used to fit the models to experimental data yields a system of nonlinear equations. The sum of squares of the deviations may be expressed in the form

$$S(\boldsymbol{\beta}) = \sum_{i=1}^{n} \big[y_i - f(x_i, \boldsymbol{\beta})\big]^2, \tag{4.12}$$

where (x_i, y_i), $i = 1, \ldots, n$, is a set of pairs of experimental data, $\boldsymbol{\beta}$ denotes model's parameters, and f is the model to be fitted [46]. The problem of fitting of the model f may be now formulated in terms of minimization of the sum S given by Eq. (4.12).

In this thesis, the *Levenberg–Marquardt algorithm* (LMA) is used to minimize Eq. (4.12) [32,46]. The LMA is an iterative minimization algorithm with a dumping parameter. It finds only a local minimum, which, in general, may differ from the global one. The LMA requires an initial estimation of the parameter $\boldsymbol{\beta}$. Within one step, a new estimation $\boldsymbol{\beta} + \boldsymbol{\delta}$ is assigned from the current estimation $\boldsymbol{\beta}$. Assuming the linearization of the model f with respect to the parameter $\boldsymbol{\beta}$, one obtains

$$f(x_i, \boldsymbol{\beta} + \boldsymbol{\delta}) \approx f(x_i, \boldsymbol{\beta}) + \boldsymbol{J}_i \boldsymbol{\delta}, \tag{4.13}$$

where

$$\boldsymbol{J}_i = \frac{\partial f(x_i, \boldsymbol{\beta})}{\partial \boldsymbol{\beta}}. \tag{4.14}$$

By substituting Eq. (4.13) into Eq. (4.12), one obtains

$$S(\boldsymbol{\beta} + \boldsymbol{\delta}) \approx \big\|\boldsymbol{y} - \boldsymbol{f}(\boldsymbol{\beta}) - \boldsymbol{J}\boldsymbol{\delta}\big\|^2, \tag{4.15}$$

which, taking the derivative with respect to $\boldsymbol{\delta}$ and setting the result to zero, yields

$$(\boldsymbol{J}^\intercal \boldsymbol{J})\boldsymbol{\delta} = \boldsymbol{J}^\intercal \big[\boldsymbol{y} - \boldsymbol{f}(\boldsymbol{\beta})\big]. \tag{4.16}$$

Finally, Levenberg [32] added a damping factor to Eq. (4.17), which yields a system of linear equations in the form

$$(\boldsymbol{J}^\intercal \boldsymbol{J} + \lambda \boldsymbol{I})\boldsymbol{\delta} = \boldsymbol{J}^\intercal \big[\boldsymbol{y} - \boldsymbol{f}(\boldsymbol{\beta})\big], \tag{4.17}$$

where $\boldsymbol{J}$ is the Jacobian matrix, whose i-th row equals $\boldsymbol{J}_i$, λ is the dumping factor, $\boldsymbol{\delta}$ is the unknown, and $\boldsymbol{y}$ and $\boldsymbol{f}$ are vectors with i-th component y_i and $f(x_i, \boldsymbol{\beta})$, respectively. Further details, *e.g.*, the choise of damping parameter λ, may be seen in [46]. This method is implemented in several software products, *e.g.*, Matlab [106], GNU Octave [140], and is employed in Chapter 6 to fit the cyclic stress–strain curve model given by Eq. (6.8).

Chapter 5

Results for Monotonic Loading

THERE have been developed many models suitable to describe plasticity of metals and capable to capture the directional distortional hardening (DDH) phenomenon, some of which were referred to in previous chapters. Although many of these models employ advanced theoretical concepts—*e.g.*, the yield surface convexity, thermodynamical consistency, combined hardening—their industrial application is still limited, namely due to the lack of analysis and understanding of models' properties and behavior from an application point of view.

In this chapter, the DDH model proposed by Feigenbaum and Dafalias [121, 122] and referred to as the *alpha-model with fixed distorional parameter* is choosen as a representative one. For this particular model, a set of tools for its analysis and application is developed. Although these tools are related to this particular model, they may be extended for other DDH models as well. Note that this extension is not straightforward, but in can be done for any model that can be integrated analytically for some simple loading modes as the uniaxial or proportional loading.

At first, the Feigenbaum–Dafalias α-model with fixed distorional parameter is integrated in the case of proportional monotonic loading. This integration results in the closed form solutions for the isotropic hardening variable and the kinematic hardening variable, the later one known as the *back-stress*. The distortional hardening variable remains fixed and stands as the parameter of the model. The solutions are expressed in terms of the norm of the plastic strain tensor, which is proportional to the von Mises effective plastic strain. As the norm of the deviatoric stress can be expressed from the yield condition in terms of hardening variables, and as it is proportional to the von Mises effective stress, a closed form equation for the effective stress–effective strain curve is obtained.

Based on this result, the calibration algorithm employing the data of the monotonic loading experiments is proposed. The algorithm makes use of the experimental data of the stress–strain curve, the distorted yield surface, and two reversals in tensile testing. Some experimental techniques may be seen in [A17]. Comparison of the experimental data with the parametrized models of particular curves yields a system of nonlinear equations for unknown parameters. This system is analytically solved, by which means the model's parameters are calibrated. Next, some calibration examples are given in order to test the robustness of the algorithm. Finally, the sensitivity of the algorithm is analyzed in particular point given by a set of parameters. Note that, besides the calibration algorithm development, the analytical solutions obtained in this section may be used to verify and analyze FE implementation of α-model with fixed distortional parameter [A2, A3, A4, A8, A9].

5.1 Solution for Proportional Loading/Unloading

The tensile testing of materials is one of the most widely used testing methods in engineering. In the six-dimensional stress space, this testing can be represented by a linear one-dimensional loading trajectory along the 11-axis. Here, more general loading case referred to as the *proportional loading* is adopted to integrate the model and develop the methodology. Like the tensile loading, the proportional loading is also represented by a linear one-dimensional trajectory which passes through the origin of the coordinate system of the same space. However, unlike the tensile loading, its trajectory has a general direction given by the second order tensor. In this section, the α-model with fixed distortional parameter by Feigenbaum and Dafalias is analytically integrated along the proportional trajectory. In general, the integrated model represents the effective stress–effective strain curve and includes the uniaxial stress–strain curve as a special case [A5, A7].

5.1.1 Integration of Model

The α-model with fixed distortional parameter is defined by Eqs. (2.12)–(2.16) in Section 2.6. Assuming the proportional loading mode in the six-dimensional stress space, the loading trajectory can be written in the form

$$\boldsymbol{\sigma} = \sigma \boldsymbol{d}, \tag{5.1}$$

where $\boldsymbol{\sigma}$ is the stress tensor, σ is the norm of the stress tensor $\boldsymbol{\sigma}$, and $\boldsymbol{d}$ is the unit norm tensor that defines the direction of proportional loading and remains fixed during the loading. In the five-dimensional deviatoric stress space, the same loading trajectory reads

$$\boldsymbol{s} = s \boldsymbol{d}^{\mathrm{d}}, \tag{5.2}$$

where $\boldsymbol{s}$ is the deviatoric stress tensor, s is the norm of the deviatoric stress tensor $\boldsymbol{s}$, and $\boldsymbol{d}^{\mathrm{d}}$ is the deviatoric unit norm tensor that defines the direction of proportional loading and remains fixed during the loading. From the definition of the deviatoric stress tensor by $s_{ij} = \sigma_{ij} - \delta_{ij}\sigma_{kk}/3$, one can express the relation between the trajectories in the form

$$sd_{ij}^{\mathrm{d}} = \sigma\Big(d_{ij} - \frac{d_{kk}}{3}\delta_{ij}\Big), \tag{5.3}$$

which yields the relation between the norms σ and s in the form

$$s = \sigma\sqrt{1 - \frac{1}{3}\left(d_{kk}\right)^2}. \tag{5.4}$$

As can be seen from Eqs. (2.13), (2.14), (2.16), and (2.17), during the plastic straining, all the tensors $\boldsymbol{\alpha}$, $\boldsymbol{n}$, $\boldsymbol{n}_{\mathrm{r}}$, and $\boldsymbol{\varepsilon}^{\mathrm{p}}$ remain in the linear span of the directional deviatoric tensor $\boldsymbol{d}^{\mathrm{d}}$. Therefore, one can set

$$\boldsymbol{\alpha} = \alpha\boldsymbol{d}^{\mathrm{d}}, \tag{5.5}$$

$$\boldsymbol{\varepsilon}^{\mathrm{p}} = \varepsilon^{\mathrm{p}}\boldsymbol{d}^{\mathrm{d}}, \tag{5.6}$$

where α is the norm of the deviatoric back-stress tensor $\boldsymbol{\alpha}$, and ε^{p} is the norm of the plastic strain tensor $\boldsymbol{\varepsilon}^{\mathrm{p}}$. Note that in the case of proportional monotonic loading, one can write $\varepsilon^{\mathrm{p}}_{\mathrm{ef}} = \sqrt{2/3}\,\varepsilon^{\mathrm{p}}$, *i.e.*, the von Mises effective plastic strain is proportional to the plastic strain tensor norm. Similarly, one can write $\sigma_{\mathrm{ef}} = \sqrt{3/2}\,s$, *i.e.*, the von Mises effective stress is proportional to the deviatoric stress tensor norm. Making use of Eqs. (2.12), (2.13), (2.16), and (2.17), Eqs. (2.14) and (2.15) for evolution of internal variables $\boldsymbol{\alpha}$ and k, respectively, may be rewritten [133, A5, A6, A7, A28] as

$$\dot{\alpha} = a_1\dot{\varepsilon}^{\mathrm{p}}\left(1 - a_2\alpha\,\mathrm{sgn}\left(s - \alpha\right)\right), \tag{5.7}$$

$$\dot{k} = \frac{1}{2}\kappa_1\left(1 - \kappa_2 k\right)\frac{\dot{\varepsilon}^{\mathrm{p}}\,\mathrm{sgn}\left(s - \alpha\right)}{\sqrt{1 - c\alpha\,\mathrm{sgn}\left(s - \alpha\right)}}. \tag{5.8}$$

Henceforth, the term $\mathrm{sgn}\left(s - \alpha\right)$ will be denoted as m. Using the transformation

$$\frac{\mathrm{d}g}{\mathrm{d}t} = \frac{\mathrm{d}g}{\mathrm{d}\varepsilon^{\mathrm{p}}}\frac{\mathrm{d}\varepsilon^{\mathrm{p}}}{\mathrm{d}t}, \tag{5.9}$$

Eqs. (5.7) and (5.8) emerge to their final form as

$$\alpha' = a_1\left(1 - ma_2\alpha\right), \tag{5.10}$$

$$k' = \frac{1}{2}\frac{m\kappa_1\left(1 - \kappa_2 k\right)}{\sqrt{1 - mc\alpha}}, \tag{5.11}$$

where $(.)'$ operator is defined by $(.)' \equiv \mathrm{d}(.)/\mathrm{d}\varepsilon^{\mathrm{p}}$. A general initial condition for Eq. (5.10) can be written as

$$\alpha(\varepsilon_0^{\mathrm{p}}) = \alpha_0 \tag{5.12}$$

and for Eq. (5.11) as

$$k(\varepsilon_0^{\mathrm{p}}) = k_0. \tag{5.13}$$

It should be emphasized that not every initial condition $\{\varepsilon_0^{\mathrm{p}}, \alpha_0, k_0\}$ is admissible [A28]. An initial condition for the variable α should fulfill inequality (2.22), and for the variable k similar restriction can be established.

The differential equation (5.10) and the initial condition (5.12) yield a *Cauchy problem* in the variable α. The solution can be obtained [A14, A19, A28] in the form

$$\alpha = \frac{1}{ma_2}\left[1 - (1 - ma_2\alpha_0)\cdot\exp\left(-ma_1a_2\left(\varepsilon^{\mathrm{p}} - \varepsilon_0^{\mathrm{p}}\right)\right)\right]. \tag{5.14}$$

The differential equation (5.11) and the initial condition (5.13) yield a Cauchy problem in the variable k. Making use the *method of separation of variables* to solve this problem, one obtains the integral

$$\int \frac{m\,\mathrm{d}\varepsilon^{\mathrm{p}}}{\sqrt{1 - mc\alpha}}. \tag{5.15}$$

To find this integral, substitutions $mc\alpha = \varphi$, $\sqrt{1-\varphi} = p$, and $\sqrt{\frac{a_2}{a_2 - c}}p = q$ may be used. Finaly, the solution can be obtained [A14, A19, A28] in the form

$$k = \frac{1}{\kappa_2}\left[1 - (1 - \kappa_2 k_0)\exp\xi\right], \tag{5.16}$$

where

$$\xi = -\frac{\kappa_1\kappa_2}{a_1\sqrt{a_2(a_2 - c)}}\left(\operatorname{artanh}(1/p) - \operatorname{artanh}(1/p_0)\right),$$

$$p(\varepsilon^{\mathrm{p}}) = \sqrt{1 + \frac{c}{a_2 - c}(1 - ma_2\alpha_0)\exp\left(-ma_1a_2\left(\varepsilon^{\mathrm{p}} - \varepsilon_0^{\mathrm{p}}\right)\right)},$$

$$p_0 = p(\varepsilon_0^{\mathrm{p}}) = \sqrt{1 + \frac{c}{a_2 - c}(1 - ma_2\alpha_0)}.$$

Note the artanh function is defined as

$$\operatorname{artanh} x = \frac{1}{2}\ln\left(\frac{1+x}{1-x}\right). \tag{5.17}$$

Thus, relations (5.14) and (5.16) express the evolution of α and k respectively. The norm of the deviatoric stress tensor s can be expressed from Eqs. (2.12) and (5.3) in the form

$$s = \frac{mk}{\sqrt{\frac{3}{2}\left(1 - mc\alpha\right)}} + \alpha, \tag{5.18}$$

where α and k are given by Eqs. (5.14) and (5.16), respectively. Finally, making use Eqs. (5.1), (5.4), and (5.6), one obtains relation between the stress and the plastic strain tensors for the general monotonic proportional loading.

5.1.2 Summary of Uniaxial Loading/Unloading

The most routinely used method of testing of materials is the tensile testing, which is characterized by the uniaxial stress state. Since the closed form solution for the uniaxial stress state is exploited later in this thesis, a relation for uniaxial loading curve is derived from the general relation given by Eq. (5.18). For the uniaxial stress loading, the directional tensor $\boldsymbol{d}$ is given by

$$\boldsymbol{d} = \begin{bmatrix} 1 & 0 & 0 \\ 0 & 0 & 0 \\ 0 & 0 & 0 \end{bmatrix}, \tag{5.19}$$

and the directional deviatoric tensor $\boldsymbol{d}^{\mathrm{d}}$ is given by

$$\boldsymbol{d}^{\mathrm{d}} = \sqrt{\frac{2}{3}} \begin{bmatrix} 1 & 0 & 0 \\ 0 & -1/2 & 0 \\ 0 & 0 & -1/2 \end{bmatrix}. \tag{5.20}$$

From Eq. (5.14), the evoluton equation for the axial component of kinematic hardening variable $\boldsymbol{\alpha}$ may be rewritten as

$$\alpha_{11} = \sqrt{\frac{2}{3}} \frac{1}{ma_2} \left[1 - \left(1 - m\sqrt{\frac{3}{2}} a_2 \alpha_{11,0} \right) \cdot \exp\left(-m\sqrt{\frac{3}{2}} a_1 a_2 \left(\varepsilon^{\mathrm{p}}_{11} - \varepsilon^{\mathrm{p}}_{11,0} \right) \right) \right], \tag{5.21}$$

where the index "11" denotes the axial component of respective tensor-valued variables, and the initial condition reads

$$\alpha_{11,0} = \alpha_{11}\left(\varepsilon^{\mathrm{p}}_{11,0} \right). \tag{5.22}$$

From Eq. (5.16), the evoluton equation for the isotropic hardening variable k may be rewritten as

$$k = \frac{1}{\kappa_2} \left[\, 1 - (1 - \kappa_2 k_0) \exp \xi \, \right], \tag{5.23}$$

where

$$\xi = -\sqrt{\frac{2}{3}}\frac{\kappa_1\kappa_2}{a_1\sqrt{a_2\,(a_2-c)}}\left(\operatorname{artanh}(1/p) - \operatorname{artanh}(1/p_0)\right),$$

$$p\left(\varepsilon^{\mathrm{p}}_{11}\right) = \sqrt{1 + \frac{c}{a_2-c}\left(1 - m\sqrt{\frac{3}{2}}a_2\alpha_{11,0}\right)\exp\left(-m\sqrt{\frac{3}{2}}a_1a_2\left(\varepsilon^{\mathrm{p}}_{11} - \varepsilon^{\mathrm{p}}_{11,0}\right)\right)},$$

$$p_0 = p\left(\varepsilon^{\mathrm{p}}_{11,0}\right) = \sqrt{1 + \frac{c}{a_2-c}\left(1 - m\sqrt{\frac{3}{2}}a_2\alpha_{11,0}\right)},$$

where the index "11" denotes the axial component of respective tensor-valued variables, and the initial condition reads

$$k_0 = k\left(\varepsilon^{\mathrm{p}}_{11,0}\right). \tag{5.24}$$

Finally, the axial component of the stress tensor $\boldsymbol{\sigma}$ may be rewritten from Eqs. (5.3) and (5.18) as

$$\sigma_{11} = \frac{mk}{\sqrt{1 - m\sqrt{\frac{3}{2}}\,c\,\alpha_{11}}} + \frac{3}{2}\alpha_{11}. \tag{5.25}$$

Thus, the equations above describe any curve that match a general uniaxial loading case, *e.g.*, stress–strain curve, hysteresis loop branches, reversed loading. In particular the uniaxial stress–strain curve may be derived from Eqs. (5.21)–(5.25) by setting the variable $m = 1$ and the initial conditions $\alpha_{11}\left(\varepsilon^{\mathrm{p}}_{11,0}\right) = 0$ and $k\left(\varepsilon^{\mathrm{p}}_{11,0}\right) = k_0$ for $\varepsilon^{\mathrm{p}}_{11,0} = 0$.

In order to verify an analytical solution for internal variables α and k given by Eqs. (5.14) and (5.16), respectively, differential equations (5.10) and (5.11) were integrated numerically by the third-order *Bogacki–Shampine method* [106] described in Chapter 4. The integration step size $h_n = 10^{-6}$ was used, and both equations were integrated on the interval $[0, 0.05]$. The comparison of analytical and numerical solutions for variables α and k may be seen in Figs. 5.1 and 5.2, respectively. To compare the solutions, model's parameters from Tab. 2.1 were used. For the particular model's parameters and on the particular inteval, both the analytical and numerical solutions match exactly.

Once the virgin material is uniaxially prestrained, the yield condition Eq. (2.12) under subsequent biaxial stress loading becomes

$$f(\sigma_{11},\sigma_{12}) = \left[1 - c\frac{3\left(\frac{\sigma_{11}}{3} - \frac{\alpha_{11}}{2}\right)\alpha_{11}}{\sqrt{6\left(\frac{\sigma_{11}}{3} - \frac{\alpha_{11}}{2}\right)^2 + \frac{2}{3}\left(\sqrt{3}\sigma_{12}\right)^2}}\right] \cdot$$

$$\left[6\left(\frac{\sigma_{11}}{3} - \frac{\alpha_{11}}{2}\right)^2 + \frac{2}{3}\left(\sqrt{3}\sigma_{12}\right)^2\right] - \frac{2}{3}k^2 = 0, \quad (5.26)$$

where α_{11} and k are values of internal variables evolved by uniaxial prestraining and given by Eqs. (5.21) and (5.23), respectively, and σ_{11} and σ_{12} are the stress tensor components defining the biaxial stress state [A15, A28].

5.2 Calibration for Monotonic Loading

In Section 5.1, the α-model with fixed distortional parameter by Feigenbaum and Dafalias [121,122] was analytically integrated. As the result, a closed form solution for the stress–strain curve given by Eq. (5.25) and an implicit equation of the distorted yield surface given by Eq. (5.26) were obtained. In this section, the both solutions are exploited to develop an algorithm for the calibration of model's parameters [A6, A14, A19, A20, A28].

5.2.1 Calibration Algorithm Derivation

In general, the proposed calibration procedure requires 10 experimental inputs that are shown in the Figs. 5.3–5.6 and denoted $A_1, \ldots, D_3$ [A6, A14, A19, A20, A28]. These experimental inputs can be expressed as a function of model's parameters in the form $\{A_1, \ldots, D_3\} = \mathcal{F}(k_0, \kappa_1, \kappa_2, a_1, a_2, c)$. A closed form analytical inversion of this system is shown and model's parameters are formally expressed by $\{k_0, \kappa_1, \kappa_2, a_1, a_2, c\} = \mathcal{F}^{-1}(A_1, \ldots, D_3)$.

In particular, the calibration procedure is based on parametric approximation of 4 experimental curves, which serve as inputs [A19,A28]. The first experimental curve is set to be the stress–strain curve as shown in Fig. 5.3. This experimental input is referred to as the A experiment. The second experimental curve is set to be the stress–strain curve with a reversal of loading at some level $\varepsilon^{\mathrm{p}}_{11,B}$ of plastic strain. The curve is shown in Fig. 5.4, and the respective experiment is referred to as the B experiment. The third experimental curve is set to be the stress–strain curve with a reversal of loading at some different level $\varepsilon^{\mathrm{p}}_{11,C}$ of plastic strain. This curve is shown in Fig. 5.5, and the experiment is referred to as the C experiment. The difference between the B and C experiments is in the plastic strain levels. Further in this text, it is shown that strain levels $\varepsilon^{\mathrm{p}}_{11,B}$ and $\varepsilon^{\mathrm{p}}_{11,C}$ denoting the loading reversal

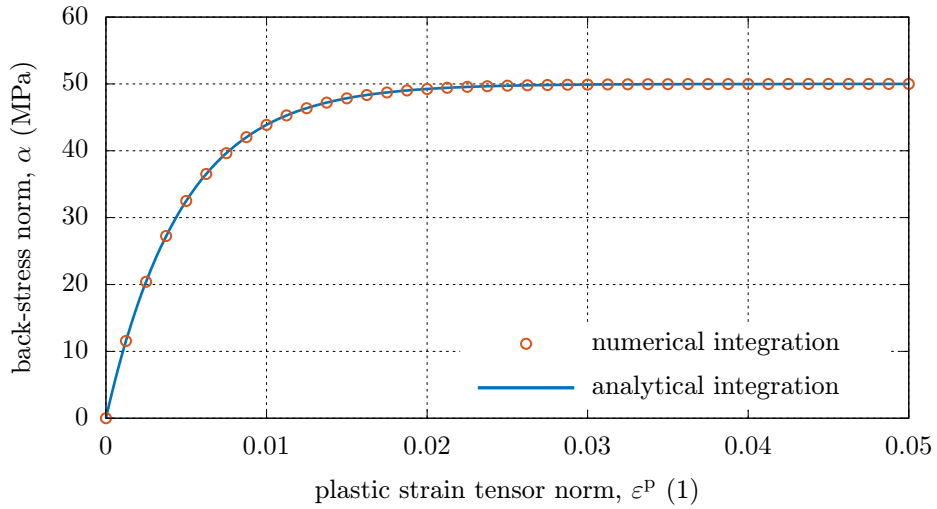

Fig. 5.1: *Comparison of numerical and analytical integration of the differential equation* (5.10) *in variable* α *for parameters from Tab. 2.1.*

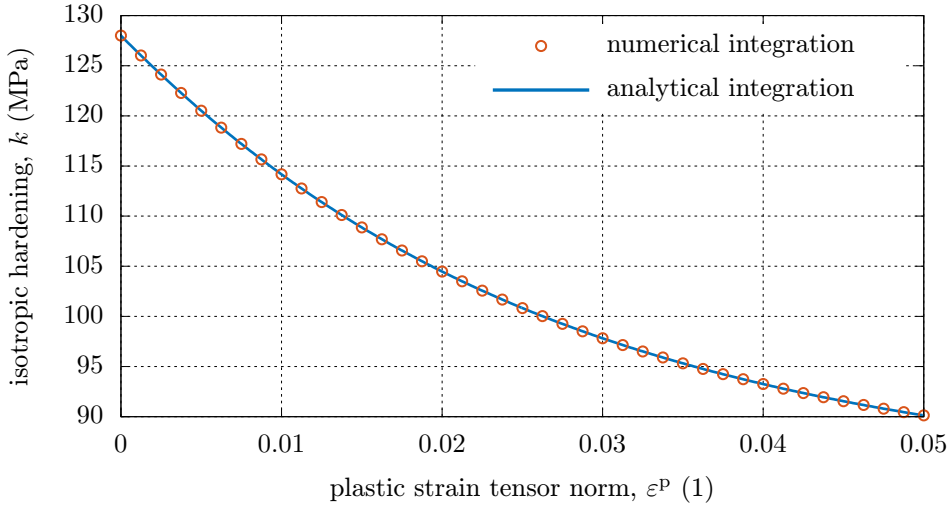

Fig. 5.2: *Comparison of numerical and analytical integration of the differential equation* (5.11) *in variable* k *for parameters from Tab. 2.1.*

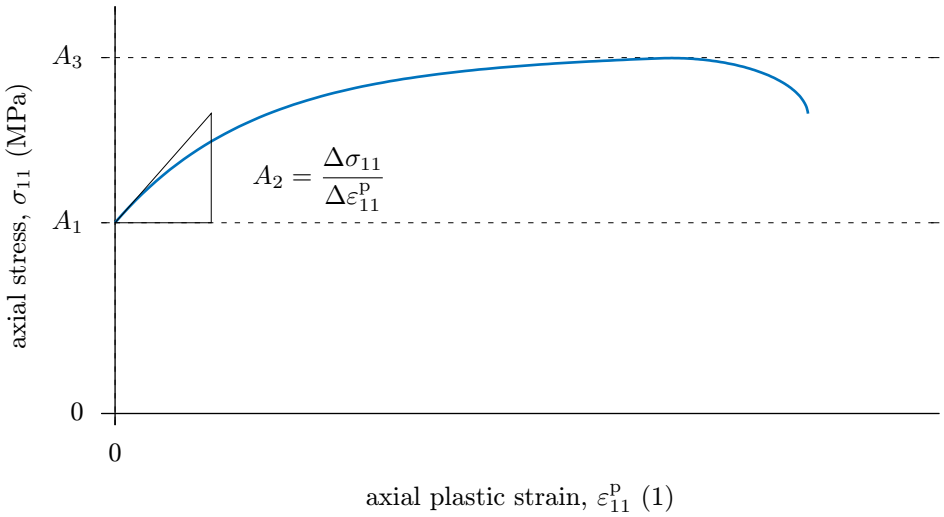

Fig. 5.3: *Stress–strain curve data—the A experiment.*

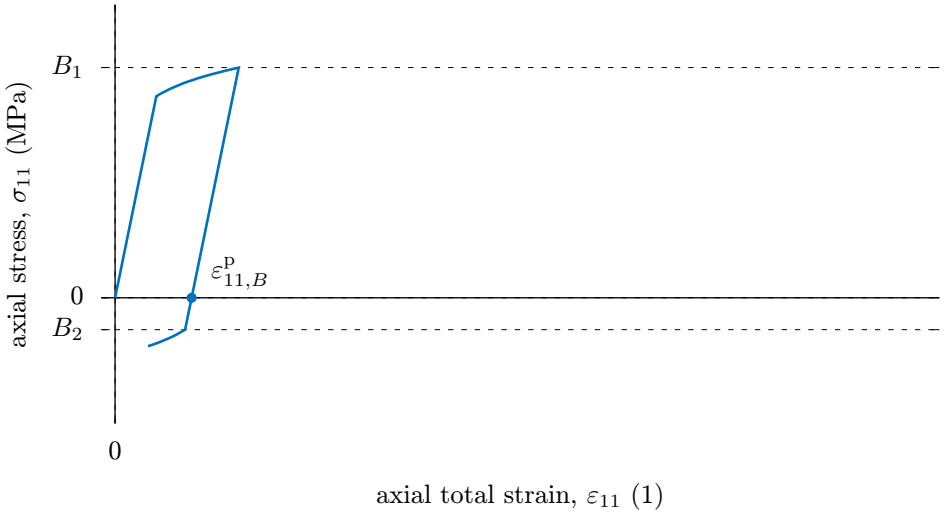

Fig. 5.4: *Reversal loading data—the B experiment.*

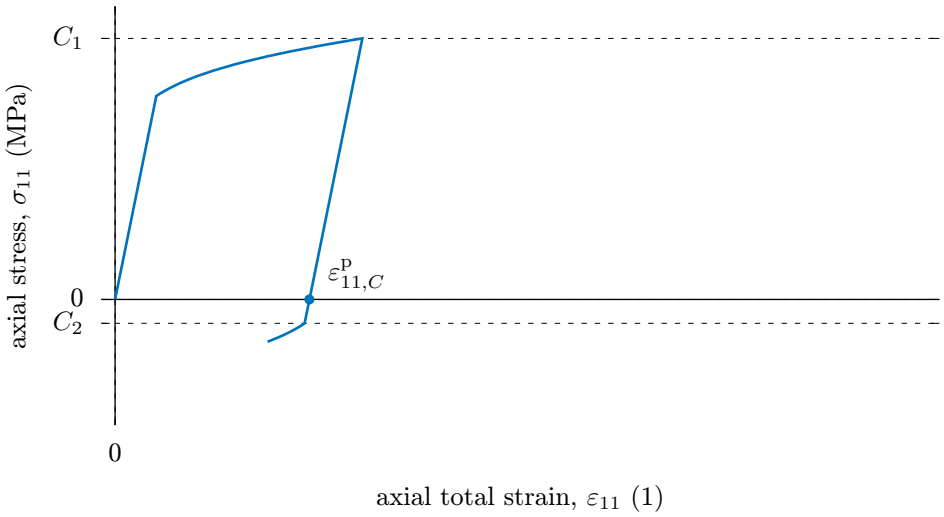

Fig. 5.5: *Reversal loading data—the C experiment.*

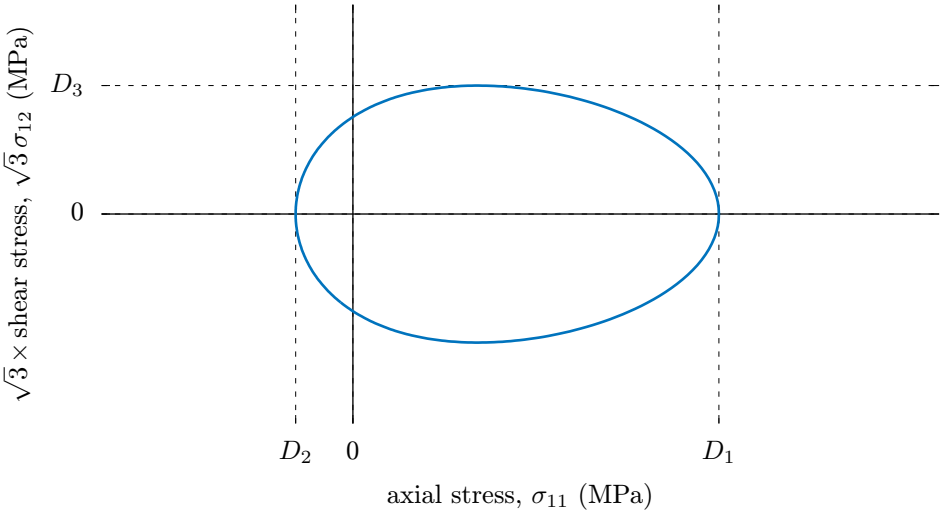

Fig. 5.6: *Shape of the distorted surface—the D experiment.*

have to satisfy the specific condition $\varepsilon^{\mathrm{p}}_{11,C}/\varepsilon^{\mathrm{p}}_{11,B} = 2$ to provide a closed form calibration. The fourth experimental curve is set to be the distorted yield surface in σ_{11}–$\sqrt{3}\sigma_{12}$ subspace obtained for arbitrary uniaxial plastic prestrain. This curve is shown in Fig. 5.6 and is referred to as the D experiment. Although tracing of distorted surfaces is quite complex and rather expensive, it is quite common in experimental research of plasticity as can be seen in [96, 104], among others. Moreover, there are modern testing systems that are able to do this experiment autonomously as reported in [132]. Thus, four experiments denoted A, B, C and D will be used for calibration of aforementioned six parameters $k_0, \kappa_1, \kappa_2, a_1, a_2$, and c. Note that it is possible to cover experiments A, B, C and even D on a single specimen. This can be done if the reversals at plastic strain levels $\varepsilon^{\mathrm{p}}_{11,B}$ and $\varepsilon^{\mathrm{p}}_{11,C}$ in experiments B and C and the probing of the yield surface in experiment D do not cause significant plastic strain or mutually influence the individual experiments.

The starting point of plastic part of stress–strain curve is determined by the relation

$$A_1 = \sigma_{11}\big(\varepsilon^{\mathrm{p}}_{11}\big)\big|_{\varepsilon^{\mathrm{p}}_{11}=0} = \sigma_{\mathrm{y}} = k_0. \tag{5.27}$$

At the start of the plastic part of the stress–strain curve the slope can be expressed as

$$A_2 = \frac{\partial \sigma_{11}}{\partial \varepsilon^{\mathrm{p}}_{11}}\big(\varepsilon^{\mathrm{p}}_{11}\big)\big|_{\varepsilon^{\mathrm{p}}_{11}=0} = \frac{1}{2}\kappa_1\big(1-\kappa_2 k_0\big) + \frac{1}{2}\sqrt{\frac{3}{2}}k_0 a_1 c + \frac{3}{2}a_1. \tag{5.28}$$

If plastic deformation $\varepsilon^{\mathrm{p}}_{11}$ is fully developed, one can suppose that the limit state is reached, *i.e.*,

$$A_3 = \lim_{\varepsilon^{\mathrm{p}}_{11}\to+\infty} \sigma_{11}\big(\varepsilon^{\mathrm{p}}_{11}\big) = \frac{1}{\kappa_2}\frac{1}{\sqrt{1-\dfrac{c}{a_2}}} + \sqrt{\frac{3}{2}}\frac{1}{a_2}. \tag{5.29}$$

From Eq. (5.25), it follows that the yield stress in tensile direction ($\oplus$) at some $\big(\varepsilon^{\mathrm{p}}_{11,B}\big)$ level of plastic deformation can be expressed as

$$B_1 = \sigma_{11}\big(\varepsilon^{\mathrm{p}}_{11,B}\big)^{\oplus} = \frac{k\big(\varepsilon^{\mathrm{p}}_{11,B}\big)}{\sqrt{1-\sqrt{\dfrac{3}{2}}\alpha_{11}\big(\varepsilon^{\mathrm{p}}_{11,B}\big)c}} + \frac{3}{2}\alpha_{11}\big(\varepsilon^{\mathrm{p}}_{11,B}\big). \tag{5.30}$$

The yield stress in opposite direction ($\ominus$) at the same $\big(\varepsilon^{\mathrm{p}}_{11,B}\big)$ level of plastic deformation can be expressed as

$$B_2 = \sigma_{11}\big(\varepsilon^{\mathrm{p}}_{11,B}\big)^{\ominus} = -\frac{k\big(\varepsilon^{\mathrm{p}}_{11,B}\big)}{\sqrt{1+\sqrt{\dfrac{3}{2}}\alpha_{11}\big(\varepsilon^{\mathrm{p}}_{11,B}\big)c}} + \frac{3}{2}\alpha_{11}\big(\varepsilon^{\mathrm{p}}_{11,B}\big). \tag{5.31}$$

The parametric expression of the C experiment is the same as in the previous case,

$$C_1 = \sigma_{11}\big(\varepsilon^{\mathrm{p}}_{11,C}\big)^{\oplus} = \frac{k\big(\varepsilon^{\mathrm{p}}_{11,C}\big)}{\sqrt{1-\sqrt{\frac{3}{2}}\alpha_{11}\big(\varepsilon^{\mathrm{p}}_{11,C}\big)c}} + \frac{3}{2}\alpha_{11}\big(\varepsilon^{\mathrm{p}}_{11,C}\big), \tag{5.32}$$

$$C_2 = \sigma_{11}\big(\varepsilon^{\mathrm{p}}_{11,C}\big)^{\ominus} = -\frac{k\big(\varepsilon^{\mathrm{p}}_{11,C}\big)}{\sqrt{1+\sqrt{\frac{3}{2}}\alpha_{11}\big(\varepsilon^{\mathrm{p}}_{11,C}\big)c}} + \frac{3}{2}\alpha_{11}\big(\varepsilon^{\mathrm{p}}_{11,C}\big). \tag{5.33}$$

Regarding the parametric description of the D experiment, the distorted yield surface in σ_{11}–$\sqrt{3}\sigma_{12}$ space is shown on the Fig. 5.6. As significant points, the left, the right and the upper peak are choosen. This distorted surface is determined by Eq. (5.26). Analysing Eq. (5.26) the left and right peak of the distorted yield surface in σ_{11}–$\sqrt{3}\sigma_{12}$ space can be expressed as

$$D_1 = \frac{k\big(\varepsilon^{\mathrm{p}}_{11,D}\big)}{\sqrt{1-\sqrt{\frac{3}{2}}\alpha_{11}\big(\varepsilon^{\mathrm{p}}_{11,D}\big)c}} + \frac{3}{2}\alpha_{11}\big(\varepsilon^{\mathrm{p}}_{11,D}\big), \tag{5.34}$$

$$D_2 = -\frac{k\big(\varepsilon^{\mathrm{p}}_{11,D}\big)}{\sqrt{1+\sqrt{\frac{3}{2}}\alpha_{11}\big(\varepsilon^{\mathrm{p}}_{11,D}\big)c}} + \frac{3}{2}\alpha_{11}\big(\varepsilon^{\mathrm{p}}_{11,D}\big). \tag{5.35}$$

This expression is possible if one declare $\sqrt{3}\tau = 0$ in Eq. (5.26). Further, the upper peak can be expressed in the form

$$D_3 = \sqrt{2}k\big(\varepsilon^{\mathrm{p}}_{11,D}\big)\frac{\sqrt{1-\sqrt{1-\frac{3}{2}\alpha^2_{11}\big(\varepsilon^{\mathrm{p}}_{11,D}\big)c^2}}}{\sqrt{\frac{3}{2}}\alpha_{11}\big(\varepsilon^{\mathrm{p}}_{11,D}\big)c} \tag{5.36}$$

The identification algorithm needs to determine six parameters of the model that depend on experimentally determined parameters A_1, A_2, A_3, B_1, B_2, B_3, C_1, C_2, C_3, D_1, D_2 and D_3 [A19, A28]. Parameters that must be identified are k_0, a_1, a_2, κ_1, κ_2 and c. The system of equations can be formulated for the determination of these parameters. The identification algorithm may then be summarized as follows.

The k_0 parameter results form Eq. (5.27). One can write

$$k_0 = A_1. \tag{5.37}$$

The c parameter arises form Eqs. (5.34), (5.35), and (5.36). This system can be solved analytically [A28], the solution for the variable c may be expressed as

$$c = \frac{\sqrt{6\,(D_1 - D_2)\,(D_1 - D_2 - 2D_3)}}{(D_1 - D_2 - D_3)\left[D_1 + D_2 - \sqrt{(D_1 - D_2)\,(D_1 - D_2 - 2D_3)}\right]}. \tag{5.38}$$

The a_2 parameter can be determined from the B and the C experiments [A28]. At first, if one knows two values of the backstress α_{11} in Eq. (5.21), *e.g.*, $\alpha_{11}\big(\varepsilon^{\mathrm{p}}_{11,B}\big)$ and $\alpha_{11}\big(\varepsilon^{\mathrm{p}}_{11,C}\big)$, apparently the a_2 parameter can be determined. Two values of the backstress $\alpha_{11}\big(\varepsilon^{\mathrm{p}}_{11,B}\big)$ and $\alpha_{11}\big(\varepsilon^{\mathrm{p}}_{11,C}\big)$ may be expressed from Eqs. (5.30)–(5.33). The system (5.30) and (5.31) yields the cubic equation in the form

$$K\alpha^3_{11,B} + L\alpha^2_{11,B} + M\alpha_{11,B} + N = 0, \tag{5.39}$$

where

$$K = \frac{9}{2}\sqrt{\frac{3}{2}}c\,, \qquad L = -3\sqrt{\frac{3}{2}}c\,(B_1 + B_2)\,, \tag{5.40}$$

$$M = \sqrt{\frac{3}{2}}c\left(B_1^2 + B_2^2\right) + 3\,(B_1 - B_2)\,, \quad N = -\left(B_1^2 - B_2^2\right)\,. \tag{5.41}$$

For this cubic equation, the discriminant can be written in the form

$$\Delta = 18KLMN - 4L^3N + L^2M^2 - 4KM^3 - 27K^2N^2. \tag{5.42}$$

It can be easily shown that for $B_2 < 0$, *i.e.*, when the plastic deformation in reversed direction occurs in the compressive state rather than in the tensile one, $\Delta < 0$, and the cubic equation (5.39) has the one real root and two non-real complex conjugate roots. Furthermore, the real root can be expressed in the form

$$\begin{aligned}\alpha_{11,B} = &-\frac{L}{3K} - \frac{1}{3K}\sqrt[3]{\frac{1}{2}\left[2L^3 - 9KLM + 27K^2N + \sqrt{-27K^2\Delta}\right]} \\ &- \frac{1}{3K}\sqrt[3]{\frac{1}{2}\left[2L^3 - 9KLM + 27K^2N - \sqrt{-27K^2\Delta}\right]},\end{aligned} \tag{5.43}$$

where no negative arguments occour in square roots. The $\alpha_{11,C}$ backstress can be expressed from Eqs. (5.32)–(5.33) in the same way. Now, Eqs. (5.21) with initial condition $\alpha_{11,0} = 0$ may be rewritten in the form

$$a_1 = -\sqrt{\frac{2}{3}}\frac{1}{a_2\varepsilon^{\mathrm{p}}_{11,B}}\ln\left(1 - \sqrt{\frac{3}{2}}\alpha_{11,B}a_2\right) \tag{5.44}$$

for the $\varepsilon^{\mathrm{p}}_{11,B}$ level at reversion, and in the form

$$a_1 = -\sqrt{\frac{2}{3}}\frac{1}{a_2\varepsilon^{\mathrm{p}}_{11,C}}\ln\left(1 - \sqrt{\frac{3}{2}}\alpha_{11,C}a_2\right) \tag{5.45}$$

for the $\varepsilon^{\mathrm{p}}_{11,C}$ level at reversion. These two equations formulate a system that yields

$$\left(1-\sqrt{\frac{3}{2}}\alpha_{11,B}a_2\right)^{\varepsilon^{\mathrm{p}}_{11,C}/\varepsilon^{\mathrm{p}}_{11,B}}+\sqrt{\frac{3}{2}}\alpha_{11,C}a_2-1=0. \tag{5.46}$$

If the $\varepsilon^{\mathrm{p}}_{11,C}/\varepsilon^{\mathrm{p}}_{11,B}$ term equals 2, previous relation is a quadratic equation [A28] and its solution is

$$a_2=\sqrt{\frac{2}{3}}\frac{2\alpha_{11,B}-\alpha_{11,C}}{\alpha^2_{11,B}}. \tag{5.47}$$

Now the a_1 parameter is given by Eq. (5.44) [A28]. The κ_2 parameter may be expressed [A28] from Eq. (5.29) as

$$\kappa_2=\frac{1}{\sqrt{1-\dfrac{c}{a_2}}\left(A_3-\sqrt{\dfrac{3}{2}}\dfrac{1}{a_2}\right)}. \tag{5.48}$$

Finally, the κ_1 parameter can be expressed [A28] form Eq. (5.28) as

$$\kappa_1=\frac{2A_2-\sqrt{\dfrac{3}{2}}k_0a_1c-3a_1}{1-\kappa_2k_0}. \tag{5.49}$$

Thus all parameters are determined.

5.2.2 Calibration Algorithm Summary

The calibration procedure proposed is suited to calibrate parameters based on monotonic loading data for corresponding monotonic loading simulations [A28]. The procedure reflects distortion of the yield surface, stress–strain diagram, and some reversals in loading and uses this experimental data as an input. Moreover, the calibration procedure allows one to determinate model's parameters by analytical solution of a system of several nonlinear equations. Having experimentally determined 10 input parameters A_1, A_2, A_3, B_1, B_2, C_1, C_2, D_1, D_2, and D_3, the parameters of model can be obtained as follows.

The k_0 parameter results form the A experiment and can be expressed as

$$k_0=A_1. \tag{5.50}$$

The c parameter, which is associated with the yield surface distortion arises form the D experiment and may be expressed as

$$c=\frac{\sqrt{6\left(D_1-D_2\right)\left(D_1-D_2-2D_3\right)}}{\left(D_1-D_2-D_3\right)\left[D_1+D_2-\sqrt{\left(D_1-D_2\right)\left(D_1-D_2-2D_3\right)}\right]}. \tag{5.51}$$

As can be seen from Fig. 5.6, the term $D_1 - D_2 - 2D_3$ in Eq. (5.51) represents the difference between the length and the width of the evolved yield surface at the experiment D. Since the term under the square root in Eq. (5.51) must be positive, Eq. (5.51) implies that the length of the yield surface at the D experiment must be larger than the width of this surface. It should be empasized that Eq. (5.51) expresses an inherent property of the DDH model itself and thus has a significant impact on the model properties. In general, the equation implies that for any value of model's parameter c the yield surface elongates in the straining direction and shrinks in the transverse direction, which contradicts various experimental results, *e.g.*, [67], [96], and [104]. Because this property of the model contradicts some experimental findings, it is undesirable, but cannot be eliminated in the current model. Some attempts to suppress this behavior by developing more sophisticated models may be seen in [A22, A23, A24, A26]. Note that some attempts are also motivated by requirements to capture the complex ratcheting behavior [A25, A27]. Furthermore, the square root at the denominator of Eq. (5.51) implies that experimental parameters are also constrained by the relation $D_3 \geq -2D_1D_2/\left(D_1 - D_2\right)$.

The a_2 parameter can be determined on the basis of the B and C experiments. First, the backstress values $\alpha_{11,B}$ and $\alpha_{11,C}$ on two levels of plastic deformation $\varepsilon^{\mathrm{p}}_{11,B}$ and $\varepsilon^{\mathrm{p}}_{11,C}$, respectively, need to be expressed. The backstress $\alpha_{11}\left(\varepsilon^{\mathrm{p}}_{11,B}\right)$ on some level of plastic deformation $\varepsilon^{\mathrm{p}}_{11,B}$ can be expressed as

$$\begin{aligned}\alpha_{11,B} = &-\frac{L}{3K} - \frac{1}{3K}\sqrt[3]{\frac{1}{2}\left[2L^3 - 9KLM + 27K^2N + \sqrt{-27K^2\Delta}\right]} \\ &- \frac{1}{3K}\sqrt[3]{\frac{1}{2}\left[2L^3 - 9KLM + 27K^2N - \sqrt{-27K^2\Delta}\right]},\end{aligned} \tag{5.52}$$

where Δ is defined as

$$\Delta = 18KLMN - 4L^3N + L^2M^2 - 4KM^3 - 27K^2N^2, \tag{5.53}$$

where

$$K = \frac{9}{2}\sqrt{\frac{3}{2}}c\,, \qquad L = -3\sqrt{\frac{3}{2}}c\left(B_1 + B_2\right)\,, \tag{5.54}$$

$$M = \sqrt{\frac{3}{2}}c\left(B_1^2 + B_2^2\right) + 3\left(B_1 - B_2\right)\,, \quad N = -\left(B_1^2 - B_2^2\right)\,. \tag{5.55}$$

It should be noted that Eq. (5.52) is valid if the condition $B_2 < 0$ is satisfied.

The $\alpha_{11,C}$ backstress can be expressed in the same way substituting for the B experiment parameters the C experiment parameters. Finally, the a_2 parameter can be expressed as

$$a_2 = \sqrt{\frac{2}{3}}\frac{2\alpha_{11,B} - \alpha_{11,C}}{\alpha_{11,B}^2}. \tag{5.56}$$

Note that this equation assumes that $\varepsilon^{\mathrm{p}}_{11,C}/\varepsilon^{\mathrm{p}}_{11,B} = 2$.

Having the a_2 parameter, the a_1 parameter can be written in the form

$$a_1 = -\sqrt{\frac{2}{3}}\frac{1}{a_2\varepsilon^{\mathrm{p}}_{11,B}}\ln\left(1-\sqrt{\frac{3}{2}}\alpha_{11,B}a_2\right). \tag{5.57}$$

Further, the κ_2 parameter may be expressed as

$$\kappa_2 = \frac{1}{\sqrt{1-\dfrac{c}{a_2}}\cdot\left(A_3-\sqrt{\dfrac{3}{2}}\dfrac{1}{a_2}\right)}. \tag{5.58}$$

Finally, the κ_1 parameter can be written in the form

$$\kappa_1 = \frac{2A_2-\sqrt{\dfrac{3}{2}}k_0a_1c-3a_1}{1-\kappa_2k_0}. \tag{5.59}$$

Thus, all material parameters are calibrated [A28].

5.3 Examples for Monotonic Loading

In order to present a calibration example, an experimental data is necessary. However, no suitable experimental data is available and data in the literature generally do not include all necessary experiments for calibration. Moreover, experiments in the literature, *e.g.*, [67,96,104], show shortening of the yield surface in the direction of loading, while this model requires elongation in the direction of loading. Thus, the calibration example in this work utilizes data generated by the model itself.

The material parameters from Tab. 5.1 [A28] were used to generate the 4 "experimental" plots similar to that plotted in Figs. 5.3–5.6. From these plots, experimental parameters were read of and summarized in Tab. 5.4. Thus, Tab. 5.4 should be thought of as a simulation of experiments. Then, using the identification algorithm in Eqs. (5.50)–(5.59), the experimental parameters from Tab. 5.4 give the model parameters in Tab. 5.2.

Figs. 5.7–5.20 compare the original stress–strain curves and yield surfaces obtained with the assumed parameters in Tab. 5.1 to those obtained for identified parameters in Tab. 5.2. The original and identified stress–strain curves as well as the original and identified yield surfaces show good agreement. Furthermore, the parameters in Tab. 5.4 and Tab. 5.5 are "close each other," as can be seen from the comparison of parameters given in Tab. 5.6. All of this suggest that the identification algorithm in Eqs. (5.50)–(5.59) provides sufficient accuracy.

In order to test a robustness of the calibration algorithm, some intentional errors in reading from generated experimental data were introduced. Thus, there is about 5 % difference in the data in Tab. 5.4 and exact values gained from parameters in Tab. 5.1. As can be seen in Figs. 5.7–5.20, these intentional errors do not evoke an essential deviation between the original and calibrated model in terms of generated curves. On the other hand, as can be seen from Tabs. 5.1, 5.2, and 5.3, there can be an essential deviation between the original and calibrated internal parameters of the model. This property of the calibration algorithm is supposed to be related to the sensitivity of model's parameters relatively to experimental data. Therefore, the sensitivity analysis of calibration algorithm has been carried out and is described in Section 5.4. If no intentional errors are involved and exact reading is performed, calibration algorithm fully recovers original parameters and graphs match exactly.

5.4 Sensitivity Analysis for Monotonic Loading

In order to understand relations between inputs and outputs of the calibration procedure and to test robustness of the procedure, its sensitivity analysis was carried out. The approach is to consider the derivative $\partial p_{\mathrm{int}}/\partial P_{\mathrm{inp}}$ of a model interal parameter p_{int} with respect to an input data P_{inp}, and pre-multiply it by $P_{\mathrm{inp}}/p_{\mathrm{int}}$ for normalization. In general, since inputs of calibration algorithms are experimentally determined and can be represented as mechanical properties of modeled material, the sensitivity analysis of calibration procedures reveals sensitivity of model's parameters to some basic mechanical properties of modeled material, *e.g.*, the yield strength and the ultimate tensile strength.

For the sensitivity analysis of monotonic calibration algorithm given by Eqs. (5.50)–(5.59), parameters from Tab. 5.1 were used. The sensitivity matrix is given by Eq. (5.60) on Page 61. This analysis reveals higher sensitivity of the internal rate parameter κ_1 to experimental parameters $A_1, \ldots, D_3$, while other internal parameters have rather lower sensitivity [A28].

Tab. 5.1: *Set up model's parameters used to generate the experimental parameters in Tab. 5.4.*

parameters set	k_0 (MPa)	κ_1 (MPa)	κ_2 (MPa^{-1})	a_1 (MPa)	a_2 (MPa^{-1})	c (MPa^{-1})	$\varepsilon^{\mathrm{p}}_{11,B}$ (%)
set #1	128	6 000	0.006	10 500	0.02	0.019	1.0
set #2	400	10 000	0.004	4 000	0.01	0.009	2.5
set #3	400	20 000	0.004	4 000	0.01	0.005	1.0
set #4	400	12 000	0.003 5	5 000	0.007	0.005	2.5
set #5	400	3 000	0.005 5	5 000	0.004	0.003 6	4.0
set #6	400	35 000	0.003 2	7 000	0.006 4	0.005 2	2.5
set #7	400	20 000	0.006	15 000	0.011	0.010 5	1.0

Tab. 5.2: *Calibrated model's parameters used to generate experimental parameters in Tab. 5.5.*

parameters set	k_0 (MPa)	κ_1 (MPa)	κ_2 (MPa^{-1})	a_1 (MPa)	a_2 (MPa^{-1})	c (MPa^{-1})	$\varepsilon^{\mathrm{p}}_{11,B}$ (%)
set #1	129	14 467	0.005 64	11 044	0.017 59	0.016 47	1.0
set #2	389	4 323	0.004 93	3 619	0.010 98	0.010 23	2.5
set #3	413	15 934	0.004 18	3 373	0.011 77	0.006 81	1.0
set #4	403	10 021	0.003 98	4 727	0.007 65	0.005 91	2.5
set #5	414	862	0.012 90	4 588	0.004 10	0.004 04	4.0
set #6	383	55 819	0.003 18	7 914	0.006 14	0.004 82	2.5
set #7	383	14 600	0.007 03	14 379	0.011 42	0.011 02	1.0

Tab. 5.3: *Relative errors in model's parameters from Tabs. 5.1 and 5.2.*

parameters set	Δk_0	$\Delta\kappa_1$	$\Delta\kappa_2$	Δa_1	Δa_2	Δc	$\varepsilon^{\mathrm{p}}_{11,B}$
				(%)			
set #1	0.8	141.1	−6.0	5.2	−12.0	−13.3	–
set #2	−2.8	−56.8	23.3	−9.5	9.8	13.6	–
set #3	3.2	−20.3	4.5	−15.7	17.7	36.2	–
set #4	0.8	−16.5	13.7	−5.5	9.3	18.2	–
set #5	3.5	−71.3	134.5	−8.2	2.5	12.2	–
set #6	−4.2	59.5	−0.6	13.1	−4.1	−7.3	–
set #7	−4.2	−27.0	17.2	−4.1	3.9	4.9	–

Tab. 5.4: *Experimental parameters used to calibrate model's parameters in Tab. 5.2.*

set	A_1	A_2	A_3	B_1	B_2	C_1	C_2	D_1	D_2	D_3	$\varepsilon^{\mathrm{p}}_{11,B}$
					(MPa)						(%)
#1	129	32 903	772	439	−44	681	−49	677	−47	195	1.0
#2	389	12 258	884	621	−169	781	−92	771	−91	299	2.5
#3	413	5 065	472	444	−282	430	−186	448	−195	310	1.0
#4	403	10 965	687	595	−168	679	−88	651	−94	319	2.5
#5	414	9 710	918	672	−69	847	+69	832	+69	276	4.0
#6	383	14 716	878	692	−111	829	−55	791	−59	347	2.5
#7	383	46 379	862	717	−94	854	−18	821	−19	211	1.0

Tab. 5.5: *Experimental parameters obtained from plots generated using model's parameters in Tab. 5.2.*

set	A_1	A_2	A_3	B_1	B_2	C_1	C_2	D_1	D_2	D_3	$\varepsilon^{\mathrm{p}}_{11,B}$
					(MPa)						(%)
#1	129	32 906	772	459	−50	708	−54	708	−54	206	1.0
#2	389	12 260	885	647	−181	815	−102	815	−102	317	2.5
#3	413	5 080	472	450	−286	466	−211	466	−211	327	1.0
#4	403	10 960	687	588	−164	658	−79	658	−79	310	2.5
#5	414	9 708	919	699	−83	835	+73	835	+73	274	4.0
#6	383	14 737	878	663	−97	813	−49	813	−49	345	2.5
#7	383	46 367	861	698	−88	800	−9	800	−9	197	1.0

Tab. 5.6: *Relative errors in experimental parameters from Tabs. 5.4 and 5.5.*

set	ΔA_1	ΔA_2	ΔA_3	ΔB_1	ΔB_2	ΔC_1	ΔC_2	ΔD_1	ΔD_2	ΔD_3	$\varepsilon^{\mathrm{p}}_{11,B}$
						(%)					(%)
#1	0.0	0.0	0.0	4.6	13.6	4.0	10.2	4.6	14.9	5.6	–
#2	0.0	0.0	0.1	4.2	7.1	4.4	10.9	5.7	12.1	6.0	–
#3	0.0	0.3	0.0	1.4	1.4	8.4	13.4	4.0	8.2	5.5	–
#4	0.0	0.0	0.0	−1.2	−2.4	−3.1	−10.2	1.1	−16.0	−2.8	–
#5	0.0	0.0	0.1	4.0	20.3	−1.4	5.8	0.4	5.8	−0.7	–
#6	0.0	0.1	0.0	−4.2	−12.6	−1.9	−10.9	2.8	−16.9	−0.6	–
#7	0.0	0.0	−0.1	−2.6	−6.4	−6.3	−50.0	−2.6	−52.6	−6.6	–

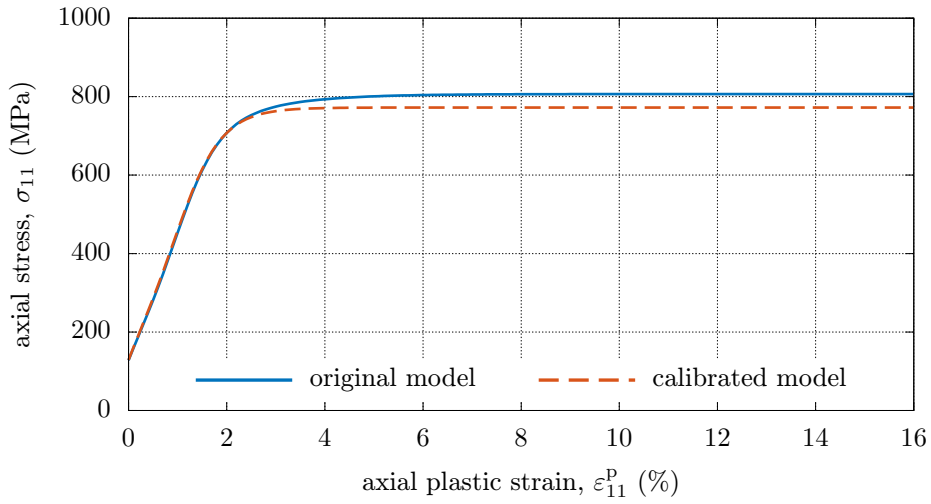

Fig. 5.7: *Original and identified stress–strain curves comparison—set #1.*

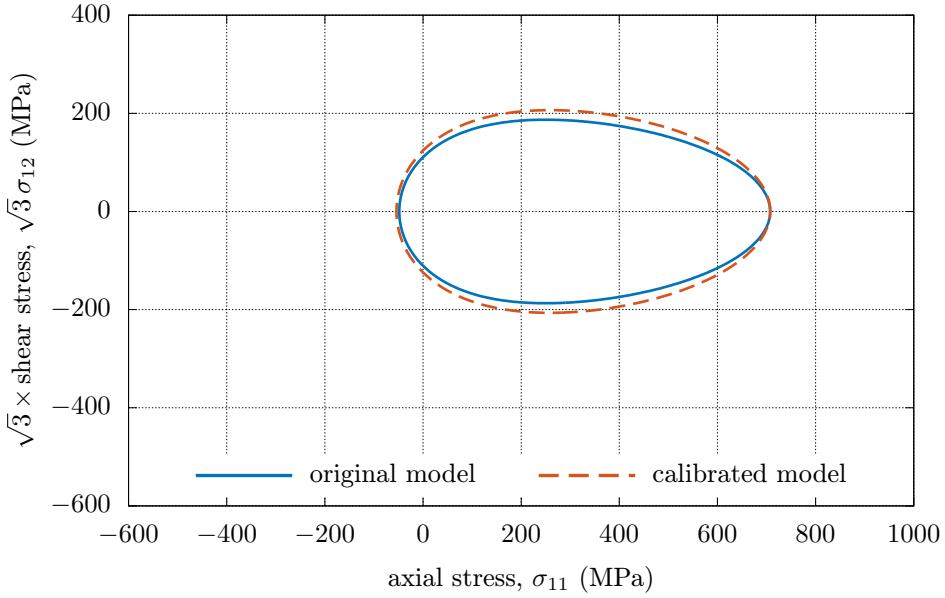

Fig. 5.8: *Comparison of distorted yield surfaces of the original and identified model—set #1.*

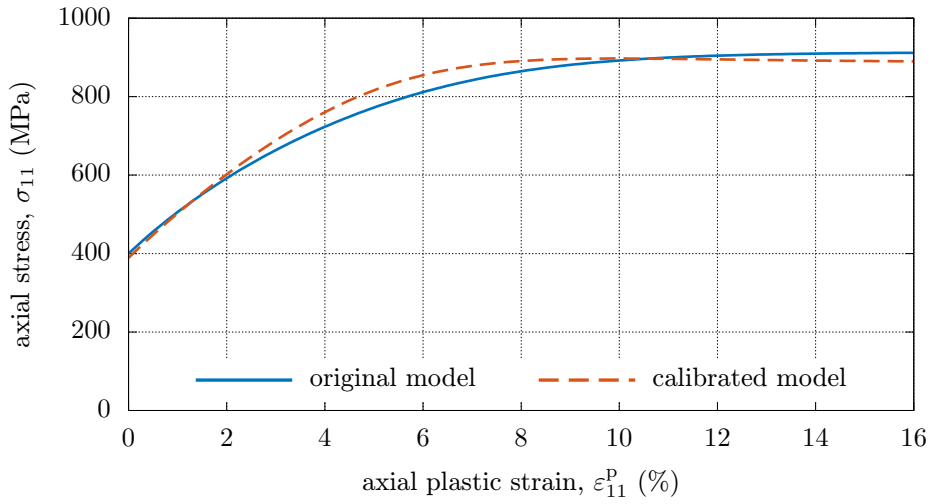

Fig. 5.9: *Original and identified stress–strain curves comparison—set #2.*

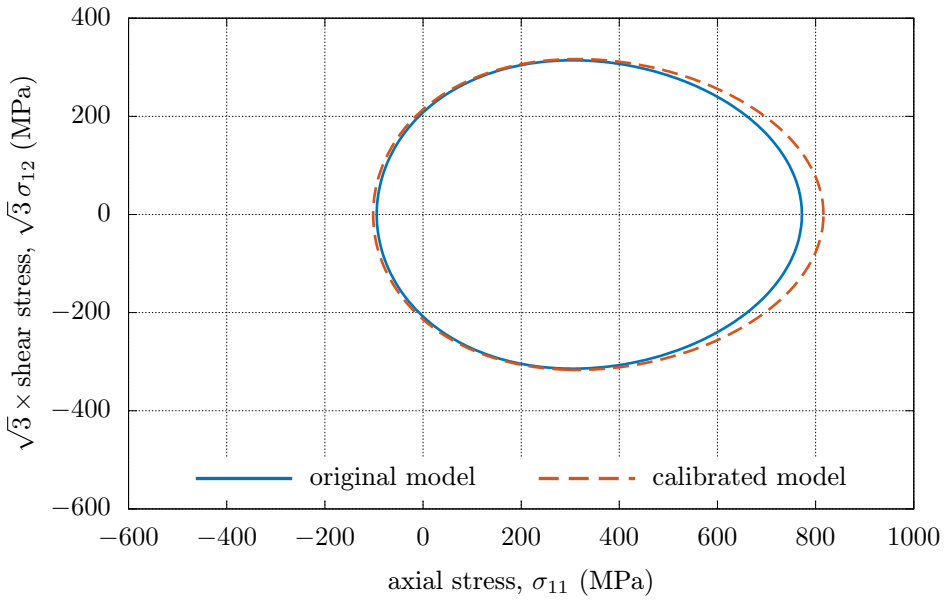

Fig. 5.10: *Comparison of distorted yield surfaces of the original and identified model—set #2.*

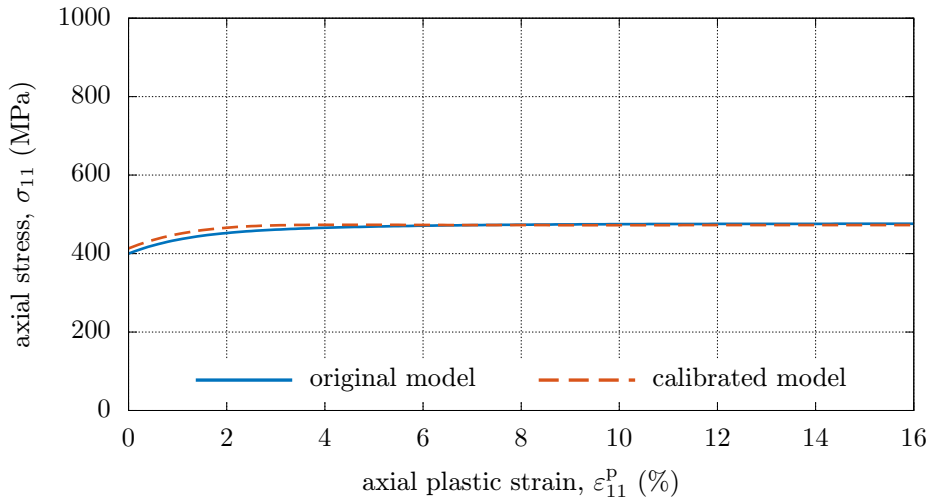

Fig. 5.11: *Original and identified stress–strain curves comparison—set #3.*

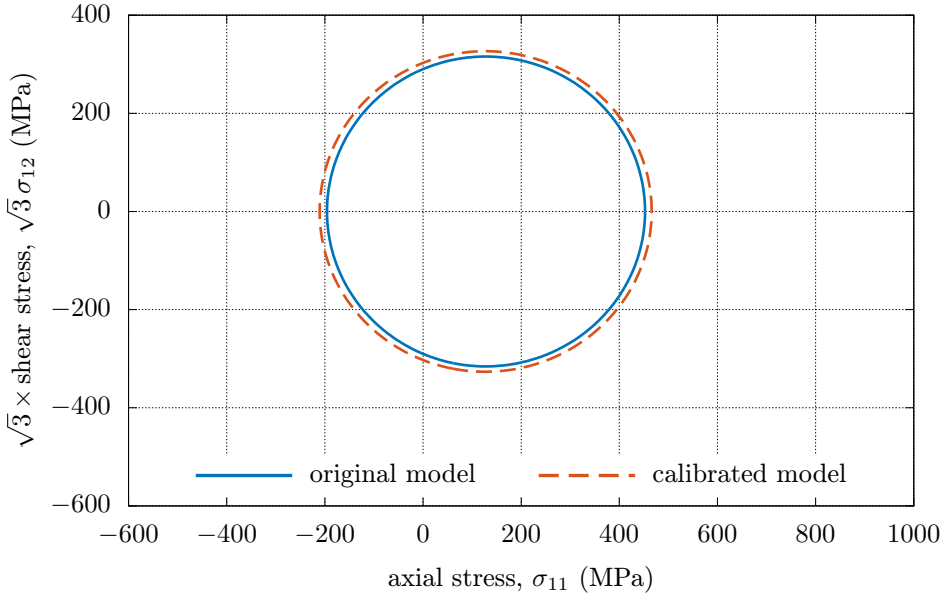

Fig. 5.12: *Comparison of distorted yield surfaces of the original and identified model—set #3.*

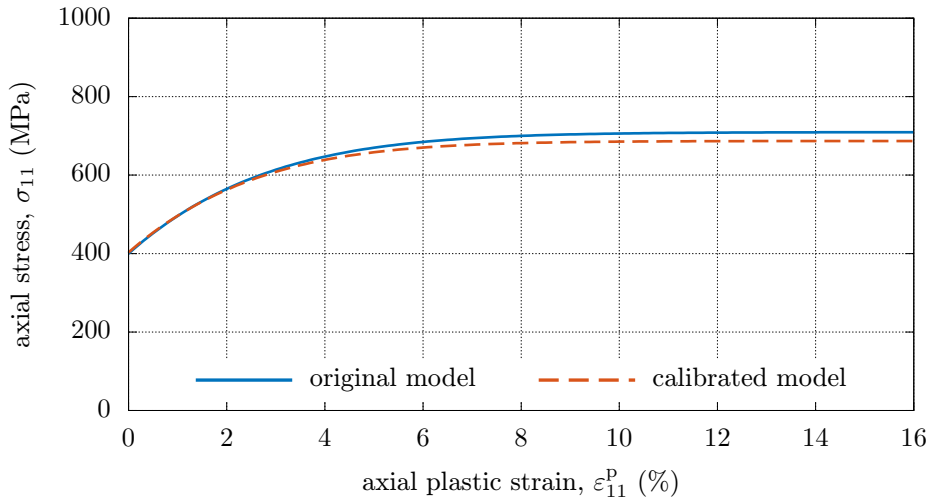

Fig. 5.13: *Original and identified stress–strain curves comparison—set #4.*

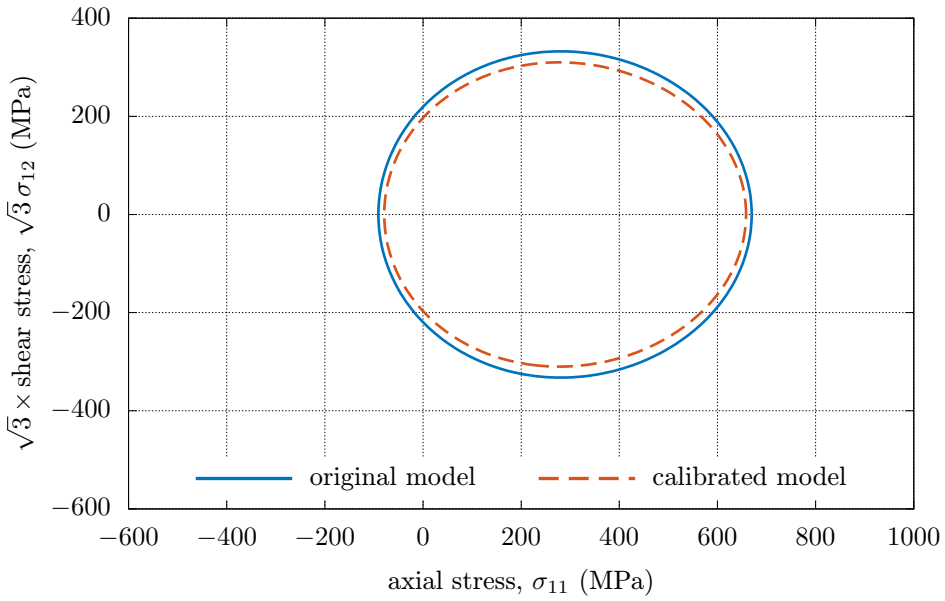

Fig. 5.14: *Comparison of distorted yield surfaces of the original and identified model—set #4.*

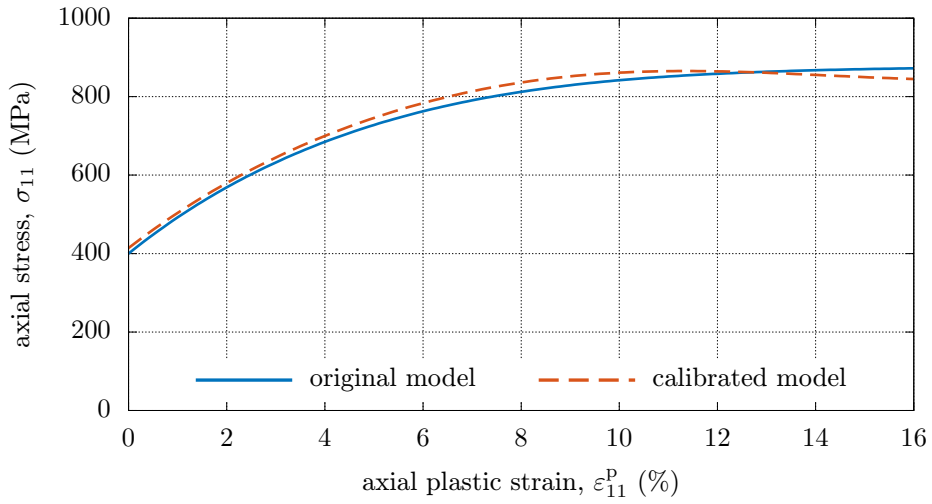

Fig. 5.15: *Original and identified stress–strain curves comparison—set #5.*

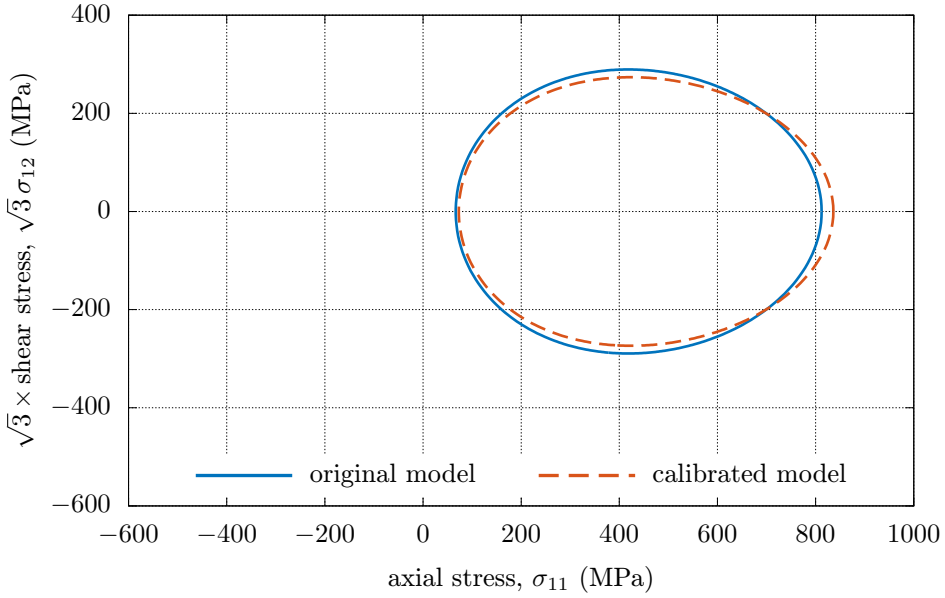

Fig. 5.16: *Comparison of distorted yield surfaces of the original and identified model—set #5.*

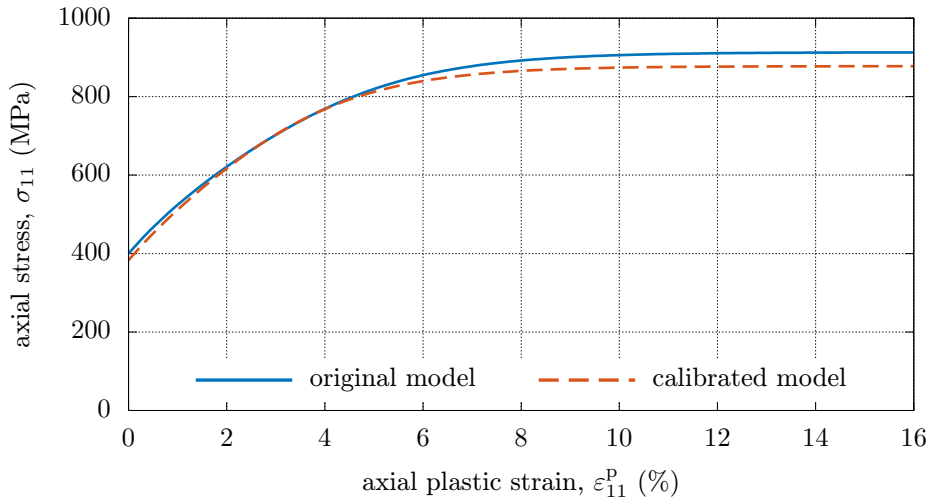

Fig. 5.17: *Original and identified stress–strain curves comparison—set #6.*

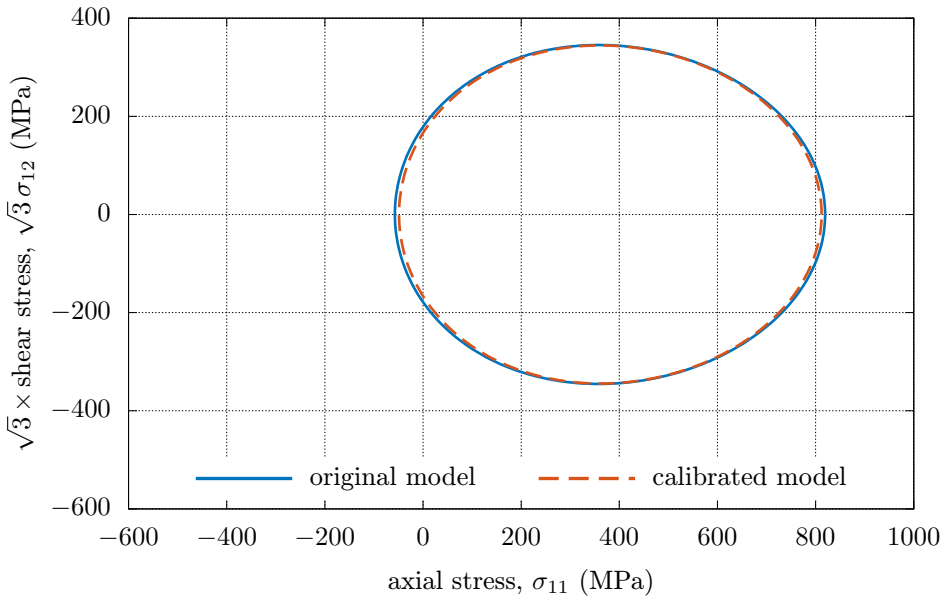

Fig. 5.18: *Comparison of distorted yield surfaces of the original and identified model—set #6.*

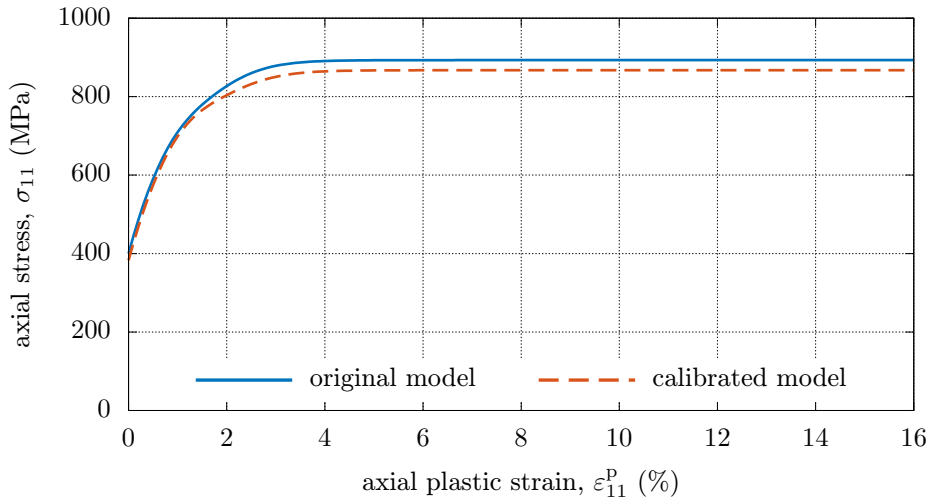

Fig. 5.19: *Original and identified stress–strain curves comparison—set #7.*

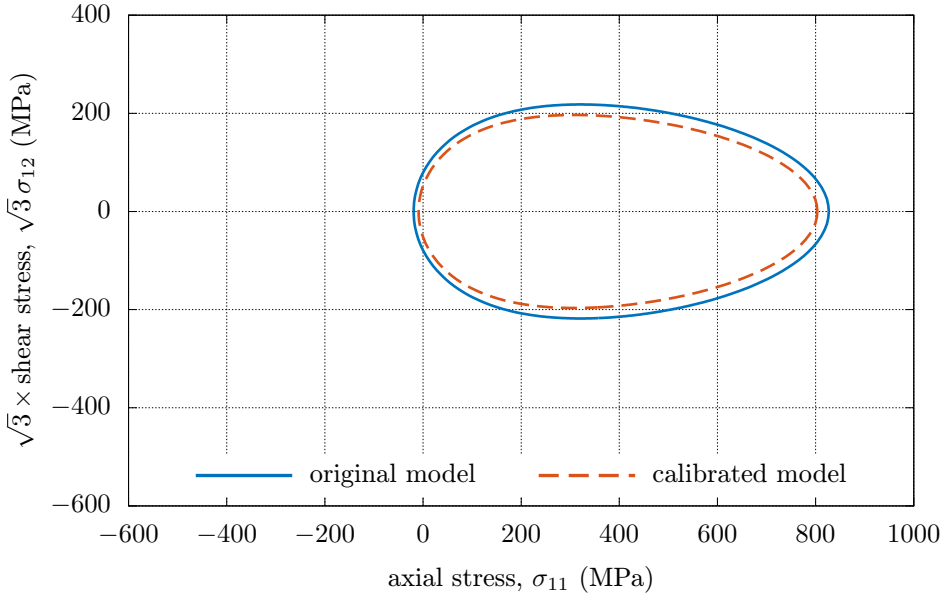

Fig. 5.20: *Comparison of distorted yield surfaces of the original and identified model—set #7.*

$$
\begin{pmatrix}
\frac{A_1}{k_0}\frac{\partial k_0}{\partial A_1} & \frac{A_2}{k_0}\frac{\partial k_0}{\partial A_2} & \frac{A_3}{k_0}\frac{\partial k_0}{\partial A_3} & \frac{B_1}{k_0}\frac{\partial k_0}{\partial B_1} & \frac{B_2}{k_0}\frac{\partial k_0}{\partial B_2} & \frac{C_1}{k_0}\frac{\partial k_0}{\partial C_1} & \frac{C_2}{k_0}\frac{\partial k_0}{\partial C_2} & \frac{D_1}{k_0}\frac{\partial k_0}{\partial D_1} & \frac{D_2}{k_0}\frac{\partial k_0}{\partial D_2} & \frac{D_3}{k_0}\frac{\partial k_0}{\partial D_3} \\
\frac{A_1}{\kappa_1}\frac{\partial \kappa_1}{\partial A_1} & \frac{A_2}{\kappa_1}\frac{\partial \kappa_1}{\partial A_2} & \frac{A_3}{\kappa_1}\frac{\partial \kappa_1}{\partial A_3} & \frac{B_1}{\kappa_1}\frac{\partial \kappa_1}{\partial B_1} & \frac{B_2}{\kappa_1}\frac{\partial \kappa_1}{\partial B_2} & \frac{C_1}{\kappa_1}\frac{\partial \kappa_1}{\partial C_1} & \frac{C_2}{\kappa_1}\frac{\partial \kappa_1}{\partial C_2} & \frac{D_1}{\kappa_1}\frac{\partial \kappa_1}{\partial D_1} & \frac{D_2}{\kappa_1}\frac{\partial \kappa_1}{\partial D_2} & \frac{D_3}{\kappa_1}\frac{\partial \kappa_1}{\partial D_3} \\
\frac{A_1}{\kappa_2}\frac{\partial \kappa_2}{\partial A_1} & \frac{A_2}{\kappa_2}\frac{\partial \kappa_2}{\partial A_2} & \frac{A_3}{\kappa_2}\frac{\partial \kappa_2}{\partial A_3} & \frac{B_1}{\kappa_2}\frac{\partial \kappa_2}{\partial B_1} & \frac{B_2}{\kappa_2}\frac{\partial \kappa_2}{\partial B_2} & \frac{C_1}{\kappa_2}\frac{\partial \kappa_2}{\partial C_1} & \frac{C_2}{\kappa_2}\frac{\partial \kappa_2}{\partial C_2} & \frac{D_1}{\kappa_2}\frac{\partial \kappa_2}{\partial D_1} & \frac{D_2}{\kappa_2}\frac{\partial \kappa_2}{\partial D_2} & \frac{D_3}{\kappa_2}\frac{\partial \kappa_2}{\partial D_3} \\
\frac{A_1}{a_1}\frac{\partial a_1}{\partial A_1} & \frac{A_2}{a_1}\frac{\partial a_1}{\partial A_2} & \frac{A_3}{a_1}\frac{\partial a_1}{\partial A_3} & \frac{B_1}{a_1}\frac{\partial a_1}{\partial B_1} & \frac{B_2}{a_1}\frac{\partial a_1}{\partial B_2} & \frac{C_1}{a_1}\frac{\partial a_1}{\partial C_1} & \frac{C_2}{a_1}\frac{\partial a_1}{\partial C_2} & \frac{D_1}{a_1}\frac{\partial a_1}{\partial D_1} & \frac{D_2}{a_1}\frac{\partial a_1}{\partial D_2} & \frac{D_3}{a_1}\frac{\partial a_1}{\partial D_3} \\
\frac{A_1}{a_2}\frac{\partial a_2}{\partial A_1} & \frac{A_2}{a_2}\frac{\partial a_2}{\partial A_2} & \frac{A_3}{a_2}\frac{\partial a_2}{\partial A_3} & \frac{B_1}{a_2}\frac{\partial a_2}{\partial B_1} & \frac{B_2}{a_2}\frac{\partial a_2}{\partial B_2} & \frac{C_1}{a_2}\frac{\partial a_2}{\partial C_1} & \frac{C_2}{a_2}\frac{\partial a_2}{\partial C_2} & \frac{D_1}{a_2}\frac{\partial a_2}{\partial D_1} & \frac{D_2}{a_2}\frac{\partial a_2}{\partial D_2} & \frac{D_3}{a_2}\frac{\partial a_2}{\partial D_3} \\
\frac{A_1}{c}\frac{\partial c}{\partial A_1} & \frac{A_2}{c}\frac{\partial c}{\partial A_2} & \frac{A_3}{c}\frac{\partial c}{\partial A_3} & \frac{B_1}{c}\frac{\partial c}{\partial B_1} & \frac{B_2}{c}\frac{\partial c}{\partial B_2} & \frac{C_1}{c}\frac{\partial c}{\partial C_1} & \frac{C_2}{c}\frac{\partial c}{\partial C_2} & \frac{D_1}{c}\frac{\partial c}{\partial D_1} & \frac{D_2}{c}\frac{\partial c}{\partial D_2} & \frac{D_3}{c}\frac{\partial c}{\partial D_3}
\end{pmatrix}
=
$$

$$
\begin{pmatrix}
1.00000 & 0 & 0 & 0 & 0 & 0 & 0 & 0 & 0 & 0 \\
-53.059 & 107.01 & -4.3008 & -137.86 & 60.738 & 55.864 & -25.794 & 2.2324 & 1.6481 & -5.4739 \\
0 & 0 & -1.0685 & -0.34747 & 0.15309 & 1.2597 & -0.58165 & 0.58165 & 0.42939 & -1.4262 \\
0 & 0 & 0 & 1.2873 & -0.56716 & -0.47916 & 0.22124 & -0.75347 & -0.55624 & 1.8475 \\
0 & 0 & 0 & 0.031483 & -0.013871 & -0.11414 & 0.052701 & 1.3397 & 0.98901 & -3.2849 \\
0 & 0 & 0 & 0 & 0 & 0 & 0 & 1.4011 & 1.0343 & -3.4354
\end{pmatrix}
. \tag{5.60}
$$

Chapter 6

Results for Cyclic Loading

The closed form solution for the general monotonic uniaxial loading was derived in previous chapter. In this chapter, the solution is used to model the plastic behavior of materials that are subjected to more complex cyclic loading modes, which are also quite common in engineering application. Although the plastic behavior of materials under cyclic loading modes might be considered too complex and beyond the possibility of analytical description, the opposite is true. In particular, many plasticity models involve internal variables that saturate due to cyclic loading [93, A1]. Then, as the limit state of a particular variable is reached, the system of equations may even simplify therefore allowing closed form analytical solution.

There are two well known characteristics of the plastic behavior of materials under the cyclic loading—the *hysteresis loop* and the *cyclic stress–strain curve* (CSSC). In this chapter, an equation of the stabilized hysteresis loop is derived from the equation of the general uniaxial stress–strain curve given in the previous chapter. Next, from the equation of the hysteresis loop, an equation of the cyclic stress–strain curve is derived. Both relations are analyzed and their properties are discussed, including the convergence rates and geometrical properties. Note that due to the saturation of isotropic hardening variable under the cyclic loading, the number of parameters of the α-model with fixed distortional parameter reduces from 6 to 4.

As the monotonic loading curves are useful in developing the calibration algorithms, so are the cyclic curves. Thus, the equation of CSSC is used to develop a calibration algorithm. By comparing the experimental data with the parametrized model of CSSC, a system of nonlinear equations for unknown model's parameters is obtained. Although the analytical solution of the system was not found, the system was reduced to a single nonlinear equation in a single variable. This equation can be effectively solved by numerical methods, *e.g.*, the *bisection method*. Besides, the existence and uniqness of the solution is discussed, and the proposed calibration algorithm is compared to the calibration based on the *nonlinear least squares method*.

Next, in order to test the robustness of the algorithm, some calibration examples are given, making use of the two sets of experimental data of carbon and stainless steels [111, 130]. Finally, the sensitivity analysis of the calibration algorithm is carried out, which helps understand the relation between the experimental data and model's parameters. Note that, besides the calibration algorithm development, the analytical solutions obtained in this chapter may be used to verify and analyze FE implementation of α-model with fixed distortional parameter [A10, A13, A15, A16, A21].

6.1 Solution for Cyclic Loading

The cyclic stress–strain curve is a locus of vertices of the stabilized stress–strain hysteresis loops generated by strain controlled cyclic loading and obtained for different amplitudes of strain, as shown in Fig. 6.3. Henceforth, without loss of generality, just uniaxial cyclic loading mode is addressed. The reason for this is that the uniaxial stress–strain loading is the most widely used in experiments, and the experimental data used later in this chapter to give a calibration example are also obtained from uniaxial testing. To derive an equation of the cyclic stress–strain curve, the same technique as in [93, A1] is used. Note, however, before an equation of the CSSC can be derived, it must be first shown that the back-stress forms a closed symmetric hysteresis loop due to cyclic loading [133, A11, A18, A28].

Let us suppose that a uniaxial symmetric cyclic strain loading with the plastic strain amplitude $\varepsilon^{\mathrm{p}}_{11,\mathrm{a}}$ occurs. A back-stress response to such a loading can be seen in Fig. 6.1. Eq. (5.21) implies that after the k-th loading step—let us suppose that this loading step is compressive—the back-stress amplitude is given by

$$\alpha^{k}_{11,\mathrm{a}} = -\sqrt{\frac{2}{3}}\frac{1}{a_2}\left[1 - \left(1 + \sqrt{\frac{3}{2}}a_2\alpha^{k-1}_{11,\mathrm{a}}\right)\cdot\exp\left(-\sqrt{\frac{3}{2}}a_1a_2\left(2\varepsilon^{\mathrm{p}}_{11,\mathrm{a}}\right)\right)\right], \tag{6.1}$$

where $\alpha^{k-1}_{11,\mathrm{a}}$ is an initial condition from the previous loading step. After the subsequent $(k+1)$ step—which is tensile—the back-stress amplitude is given by

$$\alpha^{k+1}_{11,\mathrm{a}} = \sqrt{\frac{2}{3}}\frac{1}{a_2}\left[1 - \left(1 - \sqrt{\frac{3}{2}}a_2\alpha^{k}_{11,\mathrm{a}}\right)\cdot\exp\left(-\sqrt{\frac{3}{2}}a_1a_2\left(2\varepsilon^{\mathrm{p}}_{11,\mathrm{a}}\right)\right)\right], \tag{6.2}$$

where $\alpha^{k}_{11,\mathrm{a}}$ is an initial condition from the previous loading step. Denoting $\Delta_{k+1} = \alpha^{k+1}_{11,\mathrm{a}} + \alpha^{k}_{11,\mathrm{a}}$, one obtains

$$\begin{aligned}\Delta_{k+1} &= \exp\left(-\sqrt{\frac{3}{2}}a_1a_2\left(2\varepsilon^{\mathrm{p}}_{11,\mathrm{a}}\right)\right)\left(\alpha^{k}_{11,\mathrm{a}} + \alpha^{k-1}_{11,\mathrm{a}}\right)\\ &= \exp\left(-\sqrt{\frac{3}{2}}a_1a_2\left(2\varepsilon^{\mathrm{p}}_{11,\mathrm{a}}\right)\right)\Delta_k\ .\end{aligned} \tag{6.3}$$

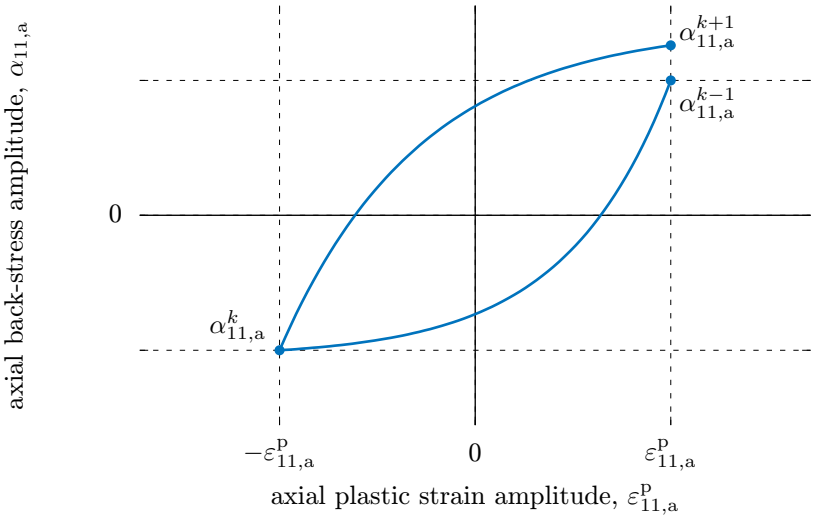

Fig. 6.1: *A sequence of loading steps for back-stress.*

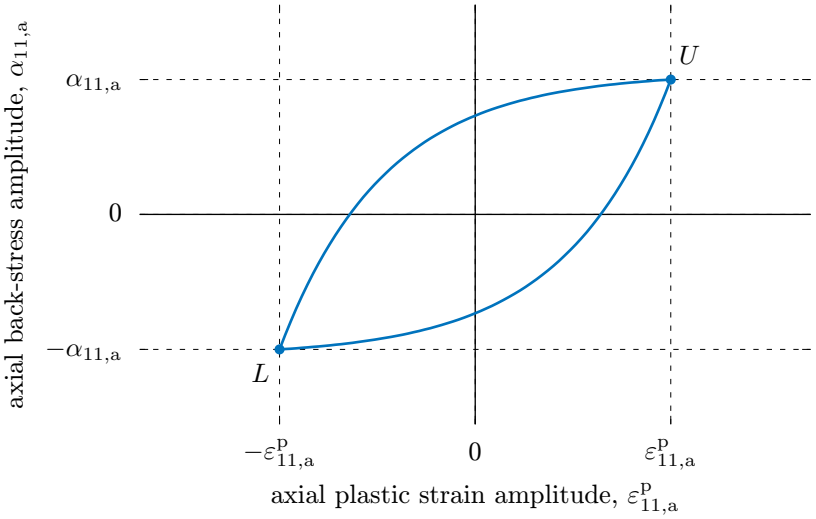

Fig. 6.2: *Symmetric hysteresis loop for back-stress.*

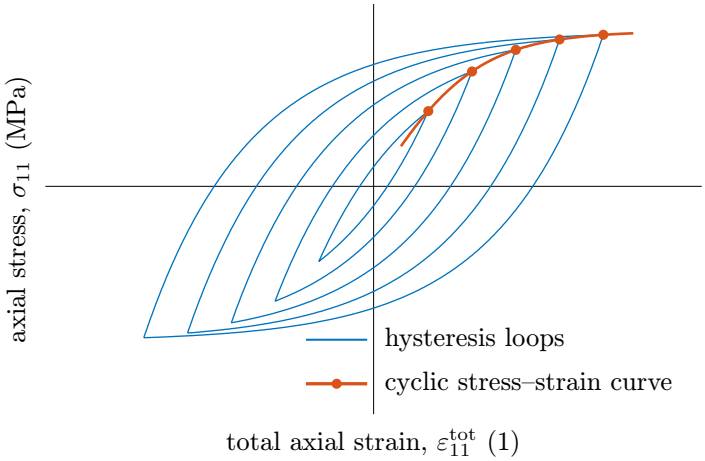

Fig. 6.3: *Example of how a particular cyclic stress–strain curve (CSSC) is constructed from subsequent stabilized hysteresis loops.*

Since $\exp\left(-\sqrt{\frac{3}{2}}a_1 a_2 \left(2\varepsilon_{11,\mathrm{a}}^{\mathrm{p}}\right)\right) < 1$, the sequence Δ_k is a convergent geometric sequence and $\lim_{k\to+\infty}\Delta_k = 0$. Thus, limit value $\alpha_{11,\mathrm{a}}^{k-1} + \alpha_{11,\mathrm{a}}^{k} \overset{k\to+\infty}{=} 0$ implies that $\alpha_{11,\mathrm{a}}^{k-1} \overset{k\to+\infty}{=} -\alpha_{11,\mathrm{a}}^{k}$ and therefore the vertices of hysteresis loop are symmetric. Moreover, it can be easily shown that relation $\alpha_{11,\mathrm{a}}^{k-1} \overset{k\to+\infty}{=} \alpha_{11,\mathrm{a}}^{k+1}$ also holds and therefore the hysteresis loop is closed, eventually as shown in Fig. 6.2 [A28].

It follows from Eq. (5.23) that the isotropic hardening variable k monotonically evolves along any plastic straining path and approaches its saturation value $k_{\mathrm{lim}} = 1/\kappa_2$. Therefore, in the case of the uniaxial cyclic loading, the isotropic hardening is saturated after several cycles and does not evolve anymore. Thus, the back-stress $\boldsymbol{\alpha}$ remains the only evolving internal variable of the model, and a closed stabilized stress–strain hysteresis loop is conditioned by a closed stabilized hysteresis loop for the back-stress component α_{11}. Following an approach by [93, 133], it is assumed that the back-stress component α_{11} forms a closed symmetric hysteresis loop, and, therefore, its vertices must meet the conditions

$$L = \left(-\varepsilon_{11,\mathrm{a}}^{\mathrm{p}}, -\alpha_{11,\mathrm{a}}\right), \tag{6.4}$$

$$U = \left(\varepsilon_{11,\mathrm{a}}^{\mathrm{p}}, \alpha_{11,\mathrm{a}}\right), \tag{6.5}$$

where L and U are the lower and upper vertices of the loop, respectively, $\varepsilon_{11,\mathrm{a}}^{\mathrm{p}}$ is the plastic strain amplitude, and $\alpha_{11,\mathrm{a}}$ is the back-stress amplitude, as shown in Fig. 6.2. Since the back-stress evolves from the L vertex to the U vertex, Eq. (5.21)

yields

$$\alpha_{11,\mathrm{a}} = \sqrt{\frac{2}{3}}\frac{1}{a_2}\left[1 - \left(1 + \sqrt{\frac{3}{2}}a_2\alpha_{11,\mathrm{a}}\right)\cdot\exp\left(-\sqrt{\frac{3}{2}}a_1a_2 2\varepsilon^{\mathrm{p}}_{11,\mathrm{a}}\right)\right]. \tag{6.6}$$

From this equation, the back-stress amplitute $\alpha_{11,\mathrm{a}}$ can be easily expressed as

$$\alpha_{11,\mathrm{a}} = \sqrt{\frac{2}{3}}\frac{1}{a_2}\tanh\left(\sqrt{\frac{3}{2}}a_1a_2\varepsilon^{\mathrm{p}}_{11,\mathrm{a}}\right), \tag{6.7}$$

where $\varepsilon^{\mathrm{p}}_{11,\mathrm{a}}$ is the plastic strain amplitude [A28]. Thus, Eqs. (5.21) and (6.7) describe the closed symmetric hysteresis loops for the back-stress α_{11}. The cyclic stress–strain curve then can be obtained from Eqs. (5.25) and (6.7) in the form

$$\sigma_{11,\mathrm{a}} = \frac{1/\kappa_2}{\sqrt{1 - \dfrac{c}{a_2}\tanh\left(\sqrt{\dfrac{3}{2}}a_1a_2\varepsilon^{\mathrm{p}}_{11,\mathrm{a}}\right)}} + \sqrt{\frac{3}{2}}\frac{1}{a_2}\tanh\left(\sqrt{\frac{3}{2}}a_1a_2\varepsilon^{\mathrm{p}}_{11,\mathrm{a}}\right), \tag{6.8}$$

where $\sigma_{11,\mathrm{a}}$ is the axial stress amplitude evoked by the axial plastic strain amplitude $\varepsilon^{\mathrm{p}}_{11,\mathrm{a}}$. Specifically how CSSC is found from stabilized stress–strain hysteresis loops is shown Fig. 6.3. Since the isotropic hardening variable k is saturated, the initial parameter k_0 and the rate parameter κ_1 do not figure in Eq. (6.8), and the set of model's parameters describing the CSSC is reduced to 4 independent considerable parameters κ_2, a_1, a_2, and c [A28]. Note the stabilized stress–strain hysteresis loop is given by Eqs. (5.21), (5.25), and (6.7).

6.2 Calibration for Cyclic Loading

In previous chapter, the calibration algorithm for model's parameters was proposed. The algorithm was based on experimental data of monotonic loading curves. In this section, the second calibration algorithm is developed. This algorithm employs the equation of cyclic stress–strain curve and appropriate experimental data.

Several experimental parameters can be determined from experimental cyclic stress–strain curve (CSSC) [A11,A18,A28]. Referring to Fig. 6.4, the P parameter denotes an initial size of the elastic domain. The R parameter denotes the limit size of the elastic domain. Finally, the Q parameter denotes the stress amplitude for arbitrary plastic strain amplitude $\varepsilon^{\mathrm{p}}_{11,\mathrm{a},Q}$. As can be seen from Eq. (6.8), the stress amplitude increases as the strain amplitude increases, and therefore $P < Q < R$. For practical application, the experimental parameter P can be determined as the minimal stress amplitude of the experimental CSSC, the parameter R can be determined as the maximum stress amplitude of the experimental CSSC, and the

parameter Q can be determined as the stress amplitude at plastic strain amplitude $\varepsilon^{\mathrm{p}}_{11,\mathrm{a},Q}$, where $\varepsilon^{\mathrm{p}}_{11,\mathrm{a},Q}$ is any plastic strain amplitude of the experimental CSSC. Note better results are obtained if Q is selected near the middle between P and R in terms of stress. Using Eq. (6.8), parameters P, Q, and R can be related to the model's parameters. The P parameter can be expressed by setting $\varepsilon^{\mathrm{p}}_{11,\mathrm{a}} = 0$ in Eq. (6.8) as

$$P = \sigma_{11,\mathrm{a}}\left(\varepsilon^{\mathrm{p}}_{11,\mathrm{a}} \to 0_{+}\right) = \frac{1}{\kappa_2}. \tag{6.9}$$

The stress amplitude Q at some level of plastic strain amplitude $\varepsilon^{\mathrm{p}}_{11,\mathrm{a},Q}$ can be expressed as

$$Q = \sigma_{11,\mathrm{a}}\left(\varepsilon^{\mathrm{p}}_{11,\mathrm{a},Q}\right) = \frac{1/\kappa_2}{\sqrt{1 - \frac{c}{a_2}\tanh\left(\sqrt{\frac{3}{2}}a_1 a_2 \varepsilon^{\mathrm{p}}_{11,\mathrm{a},Q}\right)}} + \\ + \sqrt{\frac{3}{2}}\frac{1}{a_2}\tanh\left(\sqrt{\frac{3}{2}}a_1 a_2 \varepsilon^{\mathrm{p}}_{11,\mathrm{a},Q}\right). \tag{6.10}$$

Further, the limit value R of function (6.8) can be expressed by setting $\varepsilon^{\mathrm{p}}_{11,\mathrm{a}} \to +\infty$ in Eq. (6.8) as

$$R = \sigma_{11,\mathrm{a}}\left(\varepsilon^{\mathrm{p}}_{11,\mathrm{a}} \to +\infty\right) = \frac{1}{\kappa_2}\frac{1}{\sqrt{1 - \frac{c}{a_2}}} + \sqrt{\frac{3}{2}}\frac{1}{a_2}. \tag{6.11}$$

The ratio of the c and the a_2 parameters can be denoted r, *i.e.*,

$$r = \frac{c}{a_2}. \tag{6.12}$$

In Eqs. (6.9)–(6.12), parameters P, Q and R can be determined from experimental data. Due to the restrictions $0 \leq c < a_2$, which can be seen in [121,122], Eqs. (6.9), (6.11), and (6.12) yield

$$R = P\frac{1}{\sqrt{1-r}} + \sqrt{\frac{3}{2}}\frac{1}{a_2} > P\frac{1}{\sqrt{1-r}}. \tag{6.13}$$

The inequality (6.13) imposes an restriction on the r parameter which reads

$$0 \leq r < 1 - \left(\frac{P}{R}\right)^2. \tag{6.14}$$

Sensitivity analysis of the DDH model with respect to the c parameter shows that higher values of the r parameter are necessary to make the c parameter significant

in terms of CSSC influence. Different CSSCs for different values of the r parameter and fixed parameters P, Q and R can bee seen in Fig. 6.5. In this figure, the fixed parameters P, Q and R cause that all depicted curves have a common original point, a cross point and a limit value, respectively. Note that influence of r is small. Thus, the r parameter can be estimated, and in this work it is assumed that Thus, the r parameter can be estimated as 90 % of the upper limit value given by Eq. (6.14). This estimation yields

$$r = 0.9\left(1 - (P/R)^2\right). \tag{6.15}$$

Once the left hand sides of Eqs. (6.9)–(6.12) are determined, a system of four nonlinear equations for four parameters is formulated. The solution of this system gives the initial estimation for material parameters a_1, a_2, κ_2, and c [A18, A28].

Although the system of Eqs. (6.9)–(6.12) is nonlinear, some equations can be solved in analytical way. Thus, Eq. (6.9) yields

$$\kappa_2 = \frac{1}{P}, \tag{6.16}$$

Eq. (6.11) yields

$$a_2 = \frac{\sqrt{\frac{3}{2}}}{R - \frac{P}{\sqrt{1-r}}} \tag{6.17}$$

and Eq. (6.12) yields

$$c = r a_2. \tag{6.18}$$

Further, substituting solutions (6.16), (6.17), and (6.18) into Eq. (6.10), one obtains relation

$$f(a_1) = 0, \tag{6.19}$$

where

$$f(a_1) = \frac{P}{\sqrt{1 - r\tanh\left(\frac{\frac{3}{2}\varepsilon^{\mathrm{p}}_{11,\mathrm{a},Q}}{R - \frac{P}{\sqrt{1-r}}}a_1\right)}} + \left(R - \frac{P}{\sqrt{1-r}}\right)\tanh\left(\frac{\frac{3}{2}\varepsilon^{\mathrm{p}}_{11,\mathrm{a},Q}}{R - \frac{P}{\sqrt{1-r}}}a_1\right) - Q. \tag{6.20}$$

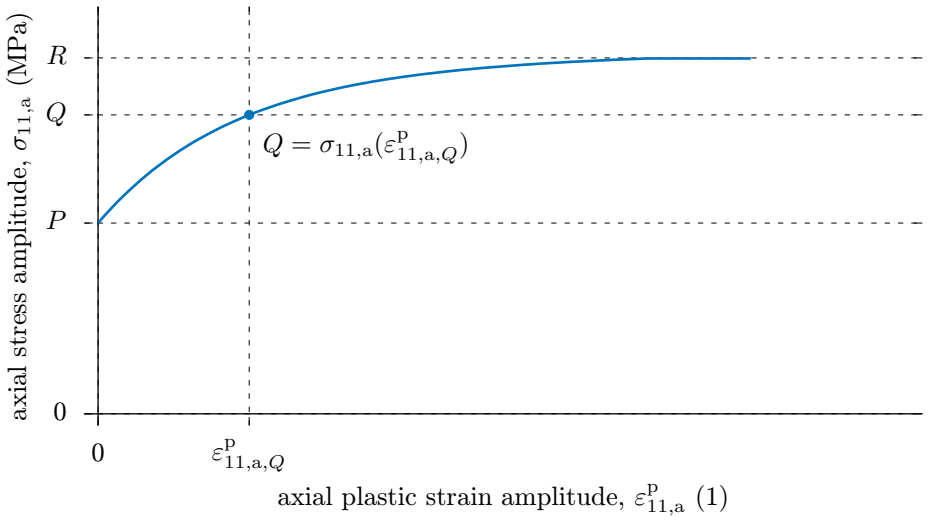

Fig. 6.4: *Geometrical representation of experimental parameters P, Q and R.*

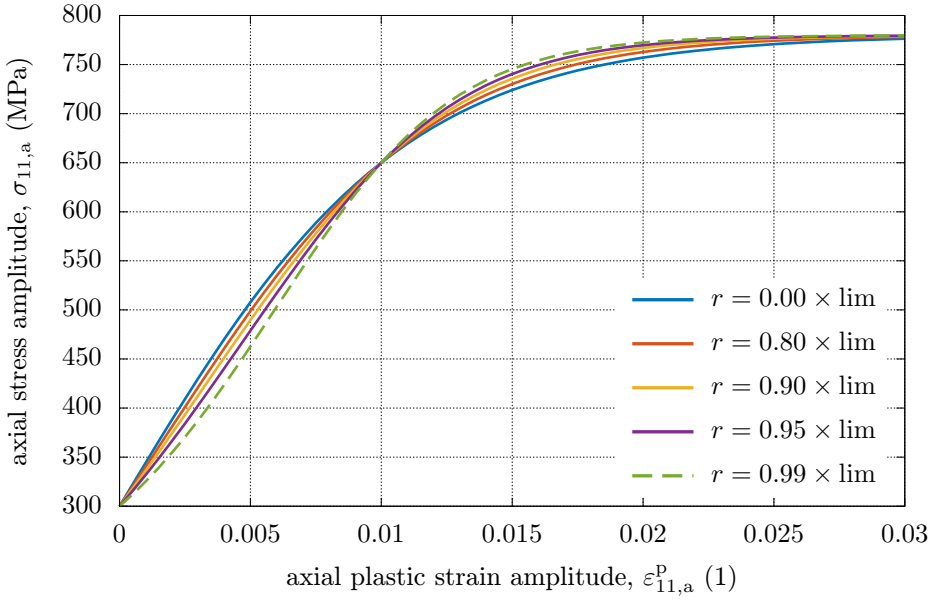

Fig. 6.5: *Different CSSC for different values of the parameter r and fixed values of parameters P, Q and R.*

Eq. (6.19) involves only one unknown variable a_1 and can be solved very effectively by numerical means.

In order to show the existence and uniquness of the solution, the function in Eq. (6.20) has been analyzed. The only restriction for the a_1 parameter is $a_1 \geq 0$, as can be seen in [121, 122]. It can be easily shown that

$$f(a_1)\big|_0 = P - Q < 0, \tag{6.21}$$

and

$$\lim_{a_1 \to +\infty} f(a_1) = R - Q > 0, \tag{6.22}$$

that guaranties the existence of solution in $[0, +\infty)$. Because for $a_1 \geq 0$,

$$f'(a_1) > 0, \tag{6.23}$$

uniqueness of solution in $[0, +\infty)$ is guarenteed as well. To solve Eq. (6.19) the bisection method was used. The left endpoint for the first iteration of the bisection method can be choosen as $a_1 = 0$, the right one can be determined by trivial algorithm based on Eq. (6.22) [A18, A28].

Parameters calibrated by the algorithm developed are suitable to model the cyclic loading cases. Moreover, since the explicit equation of CSSC was derived, this equation can be exploited for an alternative approach based on fitting by the nonlinear least squares method. Since such a formulation may be considered highly nonlinear, it requires a good initial estimation of parameters to achive the convergence of the algorithm. The solution given by Eqs. (6.16)–(6.19) may be used for this purpose.

6.3 Examples for Cyclic Loading

In previous section, two methods of calibrating the model's parameters from CSSC were developed. The first method is based on the solution of the system of equations (6.16)–(6.19). The second method is based on CSSC fitting to appropriate experimental data points. Here, these methods are combined and used in two steps to calibrate model's parameters from experimental data. In the first step, the experimental parameters P, Q, and R are determined from experimental data, and the system of Eqs. (6.16)–(6.19) is solved. This yields four model's parameters a_1, a_2, κ_2, and c. In the second step, these parameters are used as an initial estimation for the nonlinear least squares method, and the calibration is finished [A12].

In order to present a calibration example, an experimental data of CSSC after [111] and [130] was taken. Data is summarized in Tab. 6.1 and depicted in Figs. 6.6 and 6.7. Because no elastic moduli of materials in [111] and [130] were given, Young's modulus of both materials was estimated to be $E = 2 \times 10^5$ MPa.

Tab. 6.1: *Experimental data of cyclic stress–strain curves for steels 304LN [130] and AISI 1018 HR [111].*

304LN		AISI 1018 HR	
total strain amplitude $\varepsilon^{\mathrm{tot}}_{11,\mathrm{a}}$ (%)	stress amplitude $\sigma_{11,\mathrm{a}}$ (MPa)	total strain amplitude $\varepsilon^{\mathrm{tot}}_{11,\mathrm{a}}$ (%)	stress amplitude $\sigma_{11,\mathrm{a}}$ (MPa)
0.20	256	0.13	207
0.50	312	0.26	253
0.77	354	0.39	272
1.00	403	0.52	287
1.20	458	0.65	299
1.40	491	0.78	312
1.60	531	0.91	323
1.80	563	1.04	334
2.00	583	1.17	345
		1.30	355

Tab. 6.2: *Parameters estimated from the experimental data in Tab. 6.1.*

material	P (MPa)	Q (MPa)	R (MPa)	r (1)	$\varepsilon^{\mathrm{p}}_{11,\mathrm{a},Q}$ (%)
304LN	256	430.5	583	0.726 47	0.884 75
AISI 1018 HR	207	305.5	355	0.594 00	0.562 25

Tab. 6.3: *Parameters calibrated from the experimental data in Tab. 6.1.*

material	κ_2 (MPa^{-1})	a_1 (MPa)	a_2 (MPa^{-1})	c (MPa^{-1})	$\varepsilon^{\mathrm{p}}_{11,\mathrm{a},Q}$ (%)
304LN	0.004 019 9	2.879 5	0.335 86	2.841 1e−1	0.884 75
AISI 1018 HR	0.004 663 8	135.30	0.008 331 3	1.776 3e−9	0.562 25

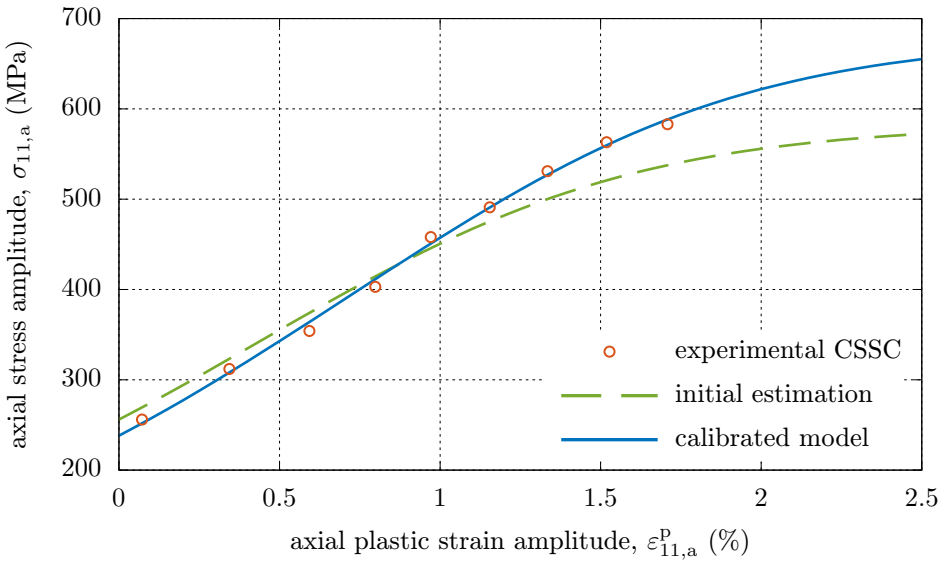

Fig. 6.6: *Model calibrated on 304LN experimental data [130].*

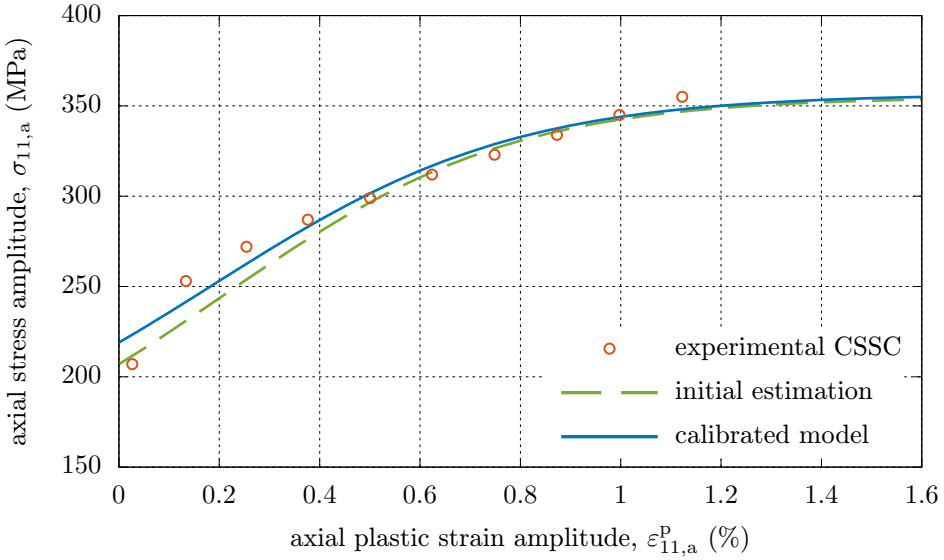

Fig. 6.7: *Model calibrated on AISI 1018 HR experimental data [111].*

Two examples from model performance after initial estimation and final calibration are shown in Figs. 6.6 and 6.7. The experimental parameters P, Q, and R determined from Tab. 6.1 are given in Tab. 6.2, and the calibrated model's parameters are summarized in Tab. 6.3.

As can be seen from Figs. 6.6 and 6.7, the estimated and calibrated CSSCs show quite good agreement, which confirms the accuracy of the estimation given by Eqs. (6.16)–(6.19). Moreover, the bisection method used to solve Eq. (6.19) is very robust, especially in combination with Eqs. (6.21), (6.22), and (6.23). Note the α-model can capture inflection in experimental data, as it can be seen in Fig. 6.6.

6.4 Sensitivity Analysis for Cyclic Loading

In order to understand relations between inputs and outputs of the calibration procedure given by Eqs. (6.16)–(6.19) and to test robustness of the procedure, its sensitivity analysis was carried out. The approach is to consider the derivative $\partial p_{\text{int}}/\partial P_{\text{inp}}$ of a model interal parameter p_{int} with respect to an input data P_{inp}, and pre-multiply it by $P_{\text{inp}}/p_{\text{int}}$ for normalization.

For the sensitivity analysis of cyclic calibration algorithm given by Eqs. (6.16)–(6.19), parameters from Tab. 6.2 of the 304LN grade steel were used. The sensitivity matrix is given by

$$\begin{pmatrix} \frac{P}{\kappa_2}\frac{\partial \kappa_2}{\partial P} & \frac{Q}{\kappa_2}\frac{\partial \kappa_2}{\partial Q} & \frac{R}{\kappa_2}\frac{\partial \kappa_2}{\partial R} & \frac{r}{\kappa_2}\frac{\partial \kappa_2}{\partial r} \\ \frac{P}{a_1}\frac{\partial a_1}{\partial P} & \frac{Q}{a_1}\frac{\partial a_1}{\partial Q} & \frac{R}{a_1}\frac{\partial a_1}{\partial R} & \frac{r}{a_1}\frac{\partial a_1}{\partial r} \\ \frac{P}{a_2}\frac{\partial a_2}{\partial P} & \frac{Q}{a_2}\frac{\partial a_2}{\partial Q} & \frac{R}{a_2}\frac{\partial a_2}{\partial R} & \frac{r}{a_2}\frac{\partial a_2}{\partial r} \\ \frac{P}{c}\frac{\partial c}{\partial P} & \frac{Q}{c}\frac{\partial c}{\partial Q} & \frac{R}{c}\frac{\partial c}{\partial R} & \frac{r}{c}\frac{\partial c}{\partial r} \end{pmatrix} = \begin{pmatrix} -1.00000 & 0 & 0 & 0 \\ -5.3719 & 2.6687 & 3.6820 & -5.2944 \\ 5.2342 & 0 & -6.2342 & 6.9507 \\ 5.2342 & 0 & -6.2342 & 7.9507 \end{pmatrix}. \tag{6.24}$$

This analysis reveals low sensitivity of all internal model's parameters to experimental parameters P, Q, R, and r, suggesting that the calibration procedure is rather robust, and slight changes to the selected experimental parameters yield only small changes to calibrated parameters [A28].

Chapter 7

Conclusions

The origins of phenomenological theories of plasticity can be traced back to 1871 when Saint-Venant published his three postulates, initiating systematic research into the topic [8]. After almost one hundred and fifty years of evolution, continuum models of plasticity have become some of the most successful phenomenological constitutive models of solids [123]. While Saint-Venant's original interest was purely scientific, the plasticity theories rapidly expanded into engineering design, mainly during the 1940s. Nowadays, numerical simulations employing plasticity models are common in industrial applications.

The most advanced of current plasticity models implement a combined isotropic, kinematic, and *directional distortional hardening* (DDH). All these phenomena have been proved by numerous experiments and are characterized by expansion, translation, and distortion of subsequent yield surfaces, respectively. Despite proved by experiments and modeled by many researchers, DDH is not routinely recognized by engineering community. There might be several reasons why, including a lack of DDH implementation in FE codes, a higher number of parameters to be calibrated when compared with the combined isotropic and kinematic hardening models, and a requirement of sophisticated experimental procedures for calibration of parameters, among others. Thus, DDH models might be considered to occupy a *death valley* from an engineering application point of view.

The general aim of this thesis—set up in Chapter 3—was to identify problems applying DDH models and to bring answers, solutions, and explanations of these problems so that the death valley mentioned would be abridged. Thus, there have been several problems identified, and they may be divided into two groups—experimental and theoretical ones. Although the experimental difficulties were mentioned and described in Chapters 2 and 3, the thesis focused on the theoretical problems with using DDH models. The experimental part is mentioned in Chapters 2 and 3 because model calibration requires experimental data and thus one

should always consider possibilities and limitations of the experimental techniques available.

Regarding the theoretical aspects, there have been two main theoretical issues identified why DDH models are not routinely employed—the lack of the analysis and understanding of DDH models, and the lack of effective calibration procedures. Although the development of DDH models often include advanced theoretical frameworks, *e.g.*, the thermodynamical consistency and the yield surface convexity, the analysis of basic properties of models is usually missing. This situation is typical for DDH models, while some other models, *e.g.*, the kinematic hardening models, have been successfully studied from this point of view [93, 119]. Without this analysis, it is difficult to connect model's parameters with particular phenomena or experimental data. In turn, it is a challenge to understand the behavior of the model and use it for engineering applications. In this work, such an analysis was addressed by aims #1 and #2 defined in Chapter 3.

Another challenge preventing use of DDH in engineering applications is the lack of the effective calibration algorithms. There have been a few rather general attempts to calibrate DDH models [122, 133]. Although these attempts are of a high importance, they are usually based on the nonlinear least squares method. Since the DDH models are highly nonlinear, and the method requires an initial estimation of parameters, because of the complexity of these models, a general initial estimation of parameters may be insufficient and the numerical algorithm may not converge. This, of course, decreases an attractivity and applicability of models. Therefore, in this work, advanced calibration algorithms for both the calibration and estimation of initial parameters were addressed by aims #3 and #4 defined in Chapter 3.

7.1 Conclusions of Aim #1—Finding Closed Form Solutions for Monotonic Loading

In Section 5.1, the general stress tensor and backstress in Feigenbaum–Dafalias α-model with fixed distorional parameter [121, 122] were expressed by a product of fixed second-order tensor and a linear parameter. This restricted the stress state to a one-dimensional linear subspace, which corresponds to arbitrary monotonic proportional loading trajectories in stress space. Subsequently, the stress was expressed from the yield condition in terms of hardening variables. Next the differential equations for the isotropic and kinematic hardening variables were analytically integrated, and isotropic and kinematic parameters were expressed in terms of plastic strains. The third internal variable—a scalar-valued distortional parameter c—is fixed in this model by the definition, so no integration was necessary. As the stress was expressed in terms of the internal variables, and the internal variables were expressed in terms of the plastic strain, this transitive relation formed an explicit relation between the stress and the plastic strain—see Eq. (5.25).

With an explicit expression of the stress field in terms of the plastic strain, specific initial conditions, and an elastic model, the stress–strain curve of the material loaded along the linear multiaxial stress trajectory is completely described. In general, this formula reveals how the stress–strain curve shape is influenced by model's parameters. In addition, this formula can be used to verify model implementation in numerical codes, as was done in [A15].

7.2 Conclusions of Aim #2—Locating Limit Envelope for Cyclic Loading

In Section 5.1, an equation of multiaxial stress–strain curve was derived. In Section 6.1, this equation was exploited to derive an equation of the stabilized hysteresis loop inherent to Feigenbaum–Dafalias α-model with fixed distortional parameter. Following the work of Lemaitre and Chaboche [93], the stabilized hysteresis loop was derived from two monotonic stress–strain curves—one for the loading towards tension and another for the loading towards compression. Both curves were dislocated from the origin of the coordinate system and were joined by their ends—see Fig. 6.1. Subsequently, a condition that would close the curves into a loop and make the loop symmetric was found—see Fig. 6.2 and Eq. (6.7). Details of this procedure can be found in [93, A1]. Note, the hysteresis loop was searched just for the backstress. That was possible because the isotropic hardening variable saturates in case of cyclic loading and stress can be simply expressed from the yield condition in terms of backstress—see Eq. (6.8). During the derivation of the equations for the stabilized hysteresis loop for the back-stress, a convergence of the model to a symmetric hysteresis loop was studied. It was shown that a system of concatenated curves matches a geometrical series, which implies quite "fast" convergence—see Eq. (6.3). Since the cyclic stress–strain curve is given by vertices of stabilized hysteresis loops—see Fig. 6.3—it was quite straight-forward to write down its equation from the equation of stabilized stabilized hysteresis stress—see Eq. (6.8).

An analytical expression for the stabilized hysteresis loop and the cyclic stress–strain curve under multiaxial loading has several benefits. It provides a clear explanation for the behavior of the model and the influence of the parameters under cyclic loading, and allows one to study how the shapes of the curves are influenced by internal model's parameters. Moreover, both of these curves may be used to calibrate model's parameters, as reported in [93, 119, A1].

7.3 Conclusions of Aim #3—Developement of Analytical Calibration Algorithms

Two calibration algorithms have been developed—one suitable for calibration from experimental data of monotonic loading and another for calibration from experimental data of cyclic loading.

In Section 5.1, an equation of multiaxial stress–strain curve inherent to Feigenbaum–Dafalias α-model with fixed distortional parameter was derived. In Section 5.2, this equation together with that one for distorted yield surface was used to develop an algorithm for calibration from experimental data of monotonic loading. This algorithm is based on four particular experimental loading cases: an axial stress–strain curve denoted A, a reverse loading denoted B, a second reverse loading denoted C, and, finally, a shape of the yield surface denoted as experiment D. All the experiments are shown in Figs. 5.3–5.6. For each loading case, several experimental parameters need to be determined. In total, there are 10 such parameters denoted $A_1, \ldots, D_3$ that represent characteristics of particular loading cases, *e.g.*, yield strength, tensile strength, stress–strain curve slope at yield strength. These 10 experimental inputs are given by 10 nonlinear equations (5.27)–(5.36). From this system, the final six equations for model's internal parameters are derived and the system is solved. Thus, all six model's parameters are calibrated completely analytically, *i.e.*, no numerical procedures are needed.

In Section 6.1, an equation of the cyclic stress–strain curve inherent to Feigenbaum–Dafalias α-model with fixed distortional parameter was derived. In Section 6.2, this equation was used to develop an algorithm for calibration from experimental data of cyclic loading, namely from the points of the cyclic stress–strain curve. There have been chosen four parameters that represent characteristic features of the cyclic stress–strain curve, *e.g.*, initial stress amplitude, limit stress amplitude. These parameters are given by equations (6.9)–(6.12) and depend on model's parameters. Inverting this system allows the model's parameters to be expressed in terms of feature of the cyclic stress–strain curve. Further, the nonlinear least squares method with initial guess based on the analytical equations (6.9)–(6.12) may be used to obtain more precise calibration from a cyclic stress–strain curve, as the example in Section 6.3 shows.

The calibration algorithm from monotonic experiments given in Section 5.2 and that from the cyclic stress–strain curve given in Section 6.2 make use of several discrete experimental parameters that are expressed in terms of model's parameters. In both cases, the calibration is done via inversion of these expressions, *i.e.*, model's parameters are expressed in terms of experimental parameters. Although the both systems of equations are nonlinear, it was possible to find explicit closed-form relations for inversions. Parameters calibrated by these methods may be directly used for modeling or may be used as an initial estimation for advanced calibration procedures, *e.g.*, the nonlinear least squares method, as was shown in Section 6.3.

The algorithms proposed have several benefits. First, they do not require any initial estimation of parameters. Next, the conditions that guarantee the existence of solution are known, and if the solution exists, it is unique. In Sections 5.3 and 6.3, some examples of calibration procedures were given. Since no experimental data were available in case of calibration from monotonic loading, an exemplary sets of data were generated and used. A similar calibration method as developed here was used to calibrate a fatigue model in [A12].

7.4 Conclusions of Aim #4—Sensitivity Analysis of Calibration Algorithms

In order to understand better relations between inputs and outputs of both calibration procedures, a sensitivity analysis was done in Sections 5.4 and 6.4. For both algorithms, the sensitivity was determined at particular points given by a set of parameters. In order to suppress an influence of magnitudes of input and output parameters, sensitivities were normalized. The results are given by Eqs. (5.60) and (6.24) and revealed that sensitivities of calibration algorithms for the monotonic and cyclic loading varies in about 2 and 1 order orders of magnitude, respectively. The variation of 2 orders of magnitude means that particular model parameter may increase or decrease in a range of 0.01–100 % due to 1 % change in the experimental data. This difference in parameters will not necessarily translate to different overall predictions of stress–strain behavior, and high sensitivity of parameters is not expected affect the overall accuracy of the method.

7.5 Future Work

This thesis includes analysis, algorithms, and calibration techniques that support an application of DDH models, namely of that one by Feigenbaum and Dafalias [121, 122]. It gives answers to numerous questions, *e.g.*, *What is the equation of the stress–strain curve, the hysteresis loop, and the cyclic stress–strain curve under multiaxial loading?*, *How to calibrate the model's parameters?*, *What is a sensitivity of particular model's parameters to experimental data?*, *What is a saturation rate of model's internal variables under cyclic loading?* Due to this, and with respect to the conclusions given in Sections 7.1–7.4, the author believes that all four aims of the thesis might be considered fulfilled. However, as is always the case with research, there are still questions left unanswered and new questions arise from these results.

Most importantly, this thesis offers a theoretical support for the application of DDH models, the development of autonomous—and therefore effective—experimental techniques is required as well. In particular, yield surface distortion can be rather

difficult to detect experimentally. Usually yield surfaces are detected via probes in the stress space. This process can be streamlined and effectivity can be substantially increased through suitable control.

Moreover, there are numerous other topics in metal plasticity, where answers, models, or scientific consensus are still missing. These topics include *finite strains*, *consistent tangent operators for DDH models*, *the exact shape of distorted yield surfaces*, *advanced hardening phenomena*, *etc.*

Also, the work presented in this thesis or closely related to this topic has been published in several conferences and papers, references of which are listed in *Author's Publications*. Some details on the topic might be seen in these references as well.

Notation

Notation	*Unit*	*Description*
A_1, A_2, A_3	MPa	parameters determined from the experiment A
a_1	MPa	internal parameter of kinematic hardening
a_2	MPa^{-1}	internal parameter of kinematic hardening
$\boldsymbol{\alpha}$	MPa	kinematic hardening tensor—back-stress
α	MPa	Euclidean norm of the back-stress tensor $\boldsymbol{\alpha}$
α_{ij}	MPa	back-stress tensor component ij
$\alpha_{11,0}$	MPa	initial condition for the back-stress component 11
$\alpha_{11,\mathrm{a}}$	MPa	amplitude of the back-stress component 11
B_1, B_2	MPa	parameters determined from the experiment B
C_1, C_2	MPa	parameters determined from the experiment C
c	MPa^{-1}	internal parameter of distortional hardening
D_1, D_2, D_3	MPa	parameters determined from the experiment D
$\boldsymbol{d}$	1	unit norm loading direction in stress space
$\boldsymbol{d}^{\mathrm{d}}$	1	unit norm loading direction in deviatoric stress space
$\boldsymbol{\varepsilon}^{\mathrm{p}}$	1	infinitesimal plastic strain tensor
ε^{p}	1	plastic strain tensor norm
$\varepsilon^{\mathrm{p}}_{\mathrm{ef}}$	1	von Mises effective strain
$\varepsilon^{\mathrm{p}}_{ij}$	1	infinitesimal plastic strain tensor component ij
$\varepsilon^{\mathrm{p}}_{0}$	1	norm of the initial plastic strain tensor
$\varepsilon^{\mathrm{p}}_{11,0}$	1	initial plastic strain component 11
$\varepsilon^{\mathrm{p}}_{11,\mathrm{a}}$	1	amplitude of the plastic strain component 11
f	MPa	yield function
k	MPa	isotropic hardening variable
k_0	MPa	initial yield stress given by initial condition for k
κ_1	MPa	internal parameter of isotropic hardening
κ_2	MPa^{-1}	internal parameter of isotropic hardening
λ	s^{-1}	loading index, plastic multiplier
m	1	loading direction sign with respect to $\boldsymbol{d}$ and $\boldsymbol{d}^{\mathrm{d}}$
$\boldsymbol{n}$	1	unit norm tensor normal to the yield surface
$\boldsymbol{n}_{\mathrm{r}}$	1	unit norm tensor along the $(\boldsymbol{s}-\boldsymbol{\alpha})$ direction
P, Q, R	MPa	parameters determined from experiment
r	MPa	estimated parameter
$\boldsymbol{s}$	MPa	deviatoric stress tensor
s	MPa	Euclidean norm of the deviatoric stress tensor $\boldsymbol{s}$
s_{ij}	MPa	deviatoric stress tensor component ij
$\boldsymbol{\sigma}$	MPa	stress tensor
σ	MPa	Euclidean norm of the stress tensor $\boldsymbol{\sigma}$
σ	MPa	axial stress in biaxial testing
σ_{ef}	MPa	von Mises effective stress

Notation	*Unit*	*Description*
σ_{y}	MPa	yield stress
σ_{ij}	MPa	stress tensor component ij
$\sigma_{11,\mathrm{a}}$	MPa	amplitude of the stress tensor component 11
σ_{11}	MPa	axial stress
σ_{12}	MPa	shear stress
τ	MPa	shear stress in biaxial testing

List of Figures

List of Tables

Author's Publications

[A1] S. Parma, Chaboche Hardening Model Identification and Its Application for Experimental Steam Turbine Blade Joint Loading Simulation (Identifikace Chabocheova modelu zpevnění a jeho použití při simulaci zatěžování zkušebního zámku lopatky parní turbíny), Master's thesis, Faculty of Mechanical Engineering, CTU in Prague, Technicka 4, 166 07 Prague 6, Czech Republic, [in Czech language] (2010).

[A2] Z. Hrubý, R. Marek, S. Parma, J. Plešek, H. P. Feigenbaum, Y. F. Dafalias, Calibration of parameters and FE-code implementations of directional distortional hardening models, in: *6th European Congress on Computational Methods in Applied Sciences and Engineering, September 10–14, 2012*, Vienna University of Technology, Vienna, Austria, 2012 pp. 1–2, ISBN 978-3-9502481-9-7.

[A3] R. Marek, J. Plešek, Z. Hrubý, S. Parma, H. P. Feigenbaum, Y. F. Dafalias, Numerical implementation of a simple model for directional distortional hardening in metal plasticity, in: *Výpočty konstrukcí metodou konečných prvků 2012, November 20, 2012*, FME BUT, Brno, 2012.

[A4] R. Marek, J. Plešek, Z. Hrubý, S. Parma, H. P. Feigenbaum, Y. F. Dafalias, Numerical implementation of a simple model for directional distortional hardening, in: *16th Workshop of Applied Mechanics, December 7, 2012*, FME CTU in Prague, Prague, 2012, pp. 5.

[A5] J. Plešek, Z. Hrubý, S. Parma, H. P. Feigenbaum, Y. F. Dafalias, Calibration of a distornional hardening model of plasticity, in: *11th International Conference on Computational Structures Technology, September 4–7, 2012*, Vol. 99, Civil-Comp Press, Dubrovnik, Croatia, 2012, pp. 11, ISBN 978-1-905088-54-6.

[A6] S. Parma, J. Plešek, Z. Hrubý, R. Marek, H. P. Feigenbaum, Y. F. Dafalias, Identification of parameters of the Feigenbaum–Dafalias directional distortional hardening model, in: I. Zolotarev (Ed.), *Engineering Mechanics 2013, May 13–16, 2013*, Institute of Thermomechanics of the CAS, Prague, Svratka, Czech Republic, 2013 pp. 426–437, ISBN 978-80-87012-47-5.

[A7] J. Plešek, Z. Hrubý, S. Parma, R. Marek, H. P. Feigenbaum, Y. F. Dafalias, Calibration and implementation of a simple model with directional distortional hardening, in: *12th International Conference on Computational Plasticity–Fundamentals and Applications, September 3–5, 2013*, International Center for Numerical Methods in Engineering, Barcelona, Spain, 2013, pp. 1.

[A8] R. Marek, J. Plešek, Z. Hrubý, S. Parma, H. P. Feigenbaum, Y. F. Dafalias, Numerical implementation of a simple model for directional distortional hardening in metal plasticity, in: *11th Congress on Computational Mechanics and 5th European Conference on Computational Mechanics and 6th European Conference on Computational Fluid Dynamics, July 20–25, 2014*, International Center for Numerical Methods in Engineering, Barcelona, Spain, 2014, pp. 2, ISBN 978-84-942844-7-2.

[A9] R. Marek, J. Plešek, Z. Hrubý, S. Parma, FE implementation of directional distortional hardening model for metal plasticity, in: V. Adámek, M. Zajíček, A. Jonášová (Eds.), *Computational Mechanics 2014, November 3–5, 2014*, University of West Bohemia, Pilsen, 2014 pp. 81–82, ISBN 978-80-261-0429-2.

[A10] R. Marek, J. Plešek, Z. Hrubý, S. Parma, H. P. Feigenbaum, Y. F. Dafalias, Numerical implementation of plasticity models with directional distortional hardening, in: *17th Workshop of Applied Mechanics, December 18, 2014*, FME CTU in Prague, Prague, 2014.

[A11] S. Parma, Z. Hrubý, R. Marek, J. Plešek, Identification of the directional distortional hardening model on the basis of hysteresis loop, in: V. Adámek, M. Zajíček, A. Jonášová (Eds.), *Computational Mechanics 2014, November 3–5, 2014*, University of West Bohemia, Pilsen, 2014 pp. 103–104, ISBN 978-80-261-0429-2.

[A12] S. Parma, J. Papuga, Identifying parameters of Kohout-Věchet fatigue curve model, in: V. Adámek, M. Zajíček, A. Jonášová (Eds.), *Computational Mechanics 2014, November 3–5, 2014*, University of West Bohemia, Pilsen, 2014 pp. 105–106, ISBN 978-80-261-0429-2.

[A13] Z. Hrubý, J. Plešek, S. Parma, R. Marek, I. Štěpánek, Z. Převorovský, L. Korec, H. P. Feigenbaum, Y. F. Dafalias, Influence of the yield offset definition on calibration and numerical implementation of directional distortional hardening model, in: *4th International Conference on Material Modeling, May 27–29, 2015*, Berkeley, CA, USA, 2015, pp. 1.

[A14] Z. Hrubý, J. Plešek, S. Parma, R. Marek, H. P. Feigenbaum, Y. F. Dafalias, Numerical calibration of material parameters of selected directional distortional hardening models with combined approach using both distorted yield surfaces and stress–strain curves, in: J. Plešek, D. Gabriel, R. Kolman, J. Masák (Eds.), *Výpočty konstrukcí metodou konečných prvků 2015, November 26, 2015*, Institute of Thermomechanics of the CAS, Prague, 2015 pp. 25–26, ISBN 978-80-87012-56-7.

[A15] R. Marek, J. Plešek, Z. Hrubý, S. Parma, H. P. Feigenbaum, Y. F. Dafalias, Numerical implementation of a model with directional distortional hardening, *Journal of Engineering Mechanics (ASCE)* **141** (12) (2015) pp. 04015048-1–04015048-10. doi:10.1061/(ASCE)EM.1943-7889.0000954. URL https://ascelibrary.org/doi/abs/10.1061/\%28ASCE%29EM.1943-7889.0000954

[A16] R. Marek, J. Plešek, Z. Hrubý, S. Parma, H. P. Feigenbaum, Y. F. Dafalias, Study of benefits and limitations linked to implementation of directional distortional hardening models, in: *4th International Conference on Material Modeling, May 27–29, 2015*, Berkeley, CA, USA, 2015, pp. 1.

[A17] S. Parma, C. Ciocanel, H. Seiner, Z. Hrubý, Experiments in directional distortional hardening—Determination of mechanical properties of the S355J0 grade structural steel, Technical Report Z-1527/15, Institute of Thermomechanics of the CAS, Prague (2015).

[A18] S. Parma, Z. Hrubý, R. Marek, J. Plešek, H. P. Feigenbaum, Y. F. Dafalias, Identification of parameters of a directional distortional hardening model, in: *4th International Conference on Material Modeling, May 27–29, 2015*, Berkeley, CA, USA, 2015, pp. 1.

[A19] S. Parma, Z. Hrubý, R. Marek, J. Plešek, Identification and integration of directional distortional hardening model in case of monotonic proportional loading, in: *13th International Conference on Computational Plasticity–Fundamentals and*

Applications, September 1–3, 2015, International Center for Numerical Methods in Engineering, Barcelona, Spain, 2015, pp. 1, ISBN 978-84-944244-6-5.

[A20] S. Parma, J. Plešek, Z. Hrubý, R. Marek, Integration, analysis, and identification of a directional distortional hardening model in metal plasticity, in: A. Berezovski, K. Tamm, T. Peets (Eds.), *28th Nordic Seminar on Computational Mechanics, October 22–23, 2015*, Institute of Cybernetics at Tallinn University of Technology, Tallinn, Estonia, 2015 pp. 137–140, ISBN 978-9949-430-96-3.

[A21] J. Plešek, R. Marek, Z. Hrubý, S. Parma, H. P. Feigenbaum, Y. F. Dafalias, Implementation of directional distortional hardening models for metal plasticity, in: *4th International Conference on Material Modeling, May 27–29, 2015*, Berkeley, CA, USA, 2015, pp. 1.

[A22] J. Plešek, R. Marek, Z. Hrubý, S. Parma, Numerical implementation of directional distortional hardening models for metal plasticity, in: *13th International Conference on Computational Plasticity–Fundamentals and Applications, September 1–3, 2015*, International Center for Numerical Methods in Engineering, Barcelona, Spain, 2015, pp. 1.

[A23] R. Marek, S. Parma, J. Plešek, Pokročilý model směrového zpevnění a jeho numerická kalibrace, in: *Výpočty konstrukcí metodou konečných prvků 2016, November 24, 2016*, FME BUT, Brno, 2016, pp. 2.

[A24] J. Plešek, R. Marek, S. Parma, Directional distortional hardening—convexity, integration and calibration, in: *National Taiwan University, September 22, 2016*, Taipei, Taiwan, 2016, pp. 1, [invited lecture].

[A25] R. Marek, S. Parma, J. Plešek, H. P. Feigenbaum, Y. F. Dafalias, A model for multiaxial ratcheting employing directional distortional hardening, in: *14th International Conference on Computational Plasticity–Fundamentals and Applications, September 5–7, 2017*, Barcelona, Spain, 2017, pp. 1.

[A26] J. Plešek, R. Marek, S. Parma, H. P. Feigenbaum, Y. F. Dafalias, Convexity conditions for a bounding surface model with directional distortional hardening, in: *14th International Conference on Computational Plasticity–Fundamentals and Application, September 5–7, 2017*, International Center for Numerical Methods in Engineering, Barcelona, Spain, 2017, pp. 1.

[A27] C. A. Welling, R. Marek, H. P. Feigenbaum, Y. F. Dafalias, J. Plesek, Z. Hruby, S. Parma, Numerical convergence in simulations of multiaxial ratcheting with directional distortional hardening, *International Journal of Solids and Structures* **126-127** (2017) pp. 105–121. doi:https://doi.org/10.1016/j.ijsolstr.2017.07.032. URL http://www.sciencedirect.com/science/article/pii/S0020768317303499

[A28] S. Parma, J. Plešek, R. Marek, Z. Hrubý, H. P. Feigenbaum, Y. F. Dafalias, Calibration of a simple directional distortional hardening model for metal plasticity, *International Journal of Solids and Structures* **143** (2018) pp. 113–124. doi:https://doi.org/10.1016/j.ijsolstr.2018.02.037. URL http://www.sciencedirect.com/science/article/pii/S0020768318300817

References

[1] C.-A. de Coulomb, Recherches théoriques et expérimentales sur la force de torsion et sur l'élasticité des fils de metal, *Histoire de l'Académie Royale des Sciences* (1784) pp. 229–269.

[2] F. J. R. von Gerstner, Handbuch der Mechanik—Mechanik fester Körper, Johann Spurny, Prague, 1831.

[3] F. A. R. von Gerstner, Handbuch der Mechanik, *Allgemeine Literatur-Zeitung* **1** (77) (1832) pp. 609–615, [book review].

[4] J. C. Maxwell, Maxwell's letter to Thompson from 18 Dec. 1856, [in: The origins of Clerk Maxwell's electric ideas, as described in familiar letters to W. Thomson, Proceedings of the Cambridge Philosophical Society, Vol. 32, Part 5, 1936].

[5] H. E. Tresca, Mémoire sur l'écoulement des corps solides soumis à de fortes pressions, *Comptes rendus de l'Académie des Sciences* **59** (1864) pp. 754–758.

[6] M. Lévy, Mémoire sur les équations générales des mouvements intérieurs des corps solides ductiles au delà des limites où l'élasticité pourrait les ramener à leur premier état, *Comptes rendus de l'Académie des Sciences* **70** (1870) pp. 1323–1325.

[7] M. Lévy, Extrait du mémoire sur les équations générales des mouvements intérieurs des corps solides ductiles au delà des limites où l'élasticité pourrait les ramener à leur premier état, *Journal de Mathématiques Pures et Appliquées. 2. Série* **16** (1871) pp. 396–372.

[8] A. J. C. B. de Saint-Venant, Mémoire sur l'établissement des équations différentielles des mouvements intérieurs opérés dans les corps solides ductiles au delà des limites où l'élasticité pourrait les ramener à leur premier état, *Journal de Mathématiques Pures et Appliquées. 2. Série* **16** (1871) pp. 308–316.

[9] J. Bauschinger, Ueber die Quercontraction und -Dilatation bei der Längenausdehnung und -Zusammendrückung prismatischer Körper, *Der Civilengenieur* **25** (1879) pp. 81–124.

[10] C. O. Mohr, Ueber die Darstellung des Spannungszustandes und des Deformationszustandes eines Körperelementes und über die Anwendung derselben in der Festigkeitslehre, *Der Civilengenieur* **28** (1882) pp. 113–156.

[11] J. Bauschinger, Ueber die Veränderung der Elasticitätsgrenze und der Festigkeit des Eisens und Stahls durch Strecken und Quetschen, durch Erwärmen und Abkühlen und durch oftmal wiederholte Beanspruchung, *Mitteilungen aus dem Mechanisch-Technischen Laboratorium der K. Technischen Hochschule in Munchen* **13** (1886) pp. 1–119. URL `http://mediatum.ub.tum.de/993273`

[12] J. J. Guest, On the strength of ductile materials under combined stress, *The London, Edinburgh, and Dublin Philosophical Magazine and Journal of Science* **50** (302) (1900) pp. 69–132. `doi:10.1080/14786440009463892`. URL `https://doi.org/10.1080/14786440009463892`

[13] M. T. Huber, O podstawach teoryi wytrzymałości, *Czasopismo Techniczne* **12** (1904) pp. 47–59, [in Polish language].

[14] M. T. Huber, Właściwa praca odkształcenia jako miara wytężenia materiału. Przyczynek do podstaw teoryi wytrzymałości, *Czasopismo Techniczne* **22** (1904) pp. 38–81, [Lwow, 1904; Pisma, 2, PWN, Warsaw, 1956; in Polish language].

[15] E. L. Hancock, Results of tests of materials subjected to combined stresses, *Philosophical Magazine Series 6* **16** (95) (1908) pp. 720–725. doi:10.1080/14786441108636551.

[16] C. A. M. Smith, Compound stress experiments, *Proceedings of the Institution of Mechanical Engineers* **77** (1) (1909) pp. 1237–1316. arXiv:https://doi.org/10.1243/PIME_PROC_1909_077_022_02, doi:10.1243/PIME_PROC_1909_077_022_02. URL https://doi.org/10.1243/PIME_PROC_1909_077_022_02

[17] R. E. von Mises, Mechanik der festen Körper im plastisch deformablen Zustand, *Nachrichten von der Gesellschaft der Wissenschaften zu Göttingen, Mathematisch-Physikalische Klasse* **1** (1913) pp. 582–592.

[18] B. P. Haigh, Strain-energy function and the elastic-limit, *Report of the Eighty-Seventh Meeting of the British Association for the Advancement of Science, 9–13 September 1919, Bournemouth* (1920) pp. 486–495.

[19] B. P. Haigh, Strain-energy function and the elastic limit, *Engineering* **109** (1920) pp. 158–160.

[20] H. Hencky, Zur theorie plastischer deformationen und der hierdurch im material hervorgerufenen nachspannungen, *ZAMM - Journal of Applied Mathematics and Mechanics / Zeitschrift für Angewandte Mathematik und Mechanik* **4** (4) (1924) pp. 323–334. arXiv:https://onlinelibrary.wiley.com/doi/pdf/10.1002/zamm.19240040405, doi:10.1002/zamm.19240040405. URL https://onlinelibrary.wiley.com/doi/abs/10.1002/zamm.19240040405

[21] W. Lode, Versuche über den Einfluß der mittleren Hauptspannung auf das Fließen der Metalle Eisen, Kupfer und Nickel, *Zeitschrift für Physik* **36** (11) (1926) pp. 913–939. doi:10.1007/BF01400222. URL https://doi.org/10.1007/BF01400222"

[22] E. Schmid, Über die Schubverfestigung von Einkristallen bei plastischer Deformation, *Zeitschrift für Physik* **40** (1) (1926) pp. 54–74. doi:10.1007/BF01390836. URL https://doi.org/10.1007/BF01390836

[23] G. I. Taylor, H. Quinney, The plastic distortion of metals, *Philosophical Transactions of the Royal Society of London A: Mathematical, Physical and Engineering Sciences* **230** (681–693) (1931) pp. 323–362. arXiv:http://rsta.royalsocietypublishing.org/content/230/681-693/323.full.pdf, doi:10.1098/rsta.1932.0009. URL http://rsta.royalsocietypublishing.org/content/230/681-693/323

[24] A. L. Nádai, Theories of strength, *Transactions of ASME* **55** (1933) pp. A111–A129.

[25] E. Orowan, Zur Kristallplastizität. i – Tieftemperaturplastizität und Beckersche Formel, *Zeitschrift für Physik* **89** (9) (1934) pp. 605–613. doi:10.1007/BF01341478. URL https://doi.org/10.1007/BF01341478

[26] M. Polanyi, Über eine Art Gitterstörung, die einen Kristall plastisch machen könnte, *Zeitschrift für Physik* **89** (9) (1934) pp. 660–664. doi:10.1007/BF01341481. URL https://doi.org/10.1007/BF01341481

[27] G. I. Taylor, The mechanism of plastic deformation of crystals. part i.—theoretical, *Proceedings of the Royal Society of London A: Mathematical, Physical and Engineering Sciences* **145** (855) (1934) pp. 362–387. arXiv:http://rspa.royalsocietypublishing.org/content/145/855/362.full.pdf, doi:10.1098/rspa.1934.0106. URL http://rspa.royalsocietypublishing.org/content/145/855/362

[28] M. Cook, *Journal of the Institute of Metals* **60** (1937) pp. 159.

[29] A. L. Nádai, Plastic behavior of metals in the strain-hardening range. Part I, *Journal of Applied Physics* **8** (3) (1937) pp. 205–213. arXiv:https://doi.org/10.1063/1.1710282, doi:10.1063/1.1710282. URL https://doi.org/10.1063/1.1710282

[30] W. Prager, Mécanique des solides isotropes au delà du domaine élastique, *Mémorial des sciences mathématiques* **87** (1937) pp. 1–66. URL http://www.numdam.org/item/MSM_1937__87__1_0

[31] E. Melan, Zur Plastizität des räumlichen Kontinuums, *Ingenieur-Archiv* **9** (2) (1938) pp. 116–126. doi:10.1007/BF02084409. URL https://doi.org/10.1007/BF02084409

[32] K. Levenberg, A method for the solution of certain non-linear problems in least squares, *Quarterly of Applied Mathematics* **2** (1944) pp. 164–168.

[33] R. Hill, A theory of the yielding and plastic flow of anisotropic metals, *Proceedings of the Royal Society of London A: Mathematical, Physical and Engineering Sciences* **193** (1033) (1948) pp. 281–297. arXiv:http://rspa.royalsocietypublishing.org/content/193/1033/281.full.pdf, doi:10.1098/rspa.1948.0045. URL http://rspa.royalsocietypublishing.org/content/193/1033/281

[34] L. J. Klinglert, G. Sachs, Plastic flow characteristics of aluminum-alloy plate, *Journal of the Aeronautical Sciences* **15** (10) (1948) pp. 599–604. doi:10.2514/8.11662. URL https://doi.org/10.2514/8.11662

[35] R. Hill, The Mathematical Theory of Plasticity, Oxford University Press, 1950.

[36] E. Landau, Differential and Integral Calculus, Chelsea Publishing Company, New York, 1951.

[37] D. C. Drucker, W. Prager, Soil mechanics and plastic analysis or limit design, *Quarterly of Applied Mathematics* **10** (1952) pp. 157–165. doi:https://doi.org/10.1090/qam/48291.

[38] S. P. Timoshenko, History of Strength of Materials, Maple Press Company, York, PA, 1952.

[39] A. Y. Ishlinskii, General theory of plasticity with linear strain hardening, *Ukraïns'kyĭ Matematychnyĭ Zhurnal* **201** (25) (1954) pp. 314–325, [in Russian language].

[40] W. Prager, The theory of plasticity: A survey of recent achievements, *Proceedings of the Institution of Mechanical Engineers* **169** (1) (1955) pp. 41–57. doi:10.1243/PIME_PROC_1955_169_015_02.

[41] W. Prager, A new method of analysing stresses and strains in work-hardening plastic solids, *Journal of Applied Mechanics* **23** (1956) pp. 493–496.

[42] P. M. Naghdi, F. Essenburg, W. Koff, Experimental study of initial and subsequent yield surface in plasticity, *Journal of Applied Mechanics* **201** (25) (1958) pp. 201.

[43] H. Ziegler, A modification of Prager's hardening rule, *Quarterly of Applied Mathematics* **17** (1) (1959) pp. 55–65. doi:http://www.jstor.org/stable/43634629.

[44] H. G. McComb, Some experiments concerning subsequent yield surfaces in plasticity, Tech. Rep. D-396, National Aeronautics and Space Adminstration (1960).

[45] H. J. Ivey, Plastic stress–strain relations and yield surfaces for aluminum alloys, *Journal of Mechanical Engineering and Sciences* **3** (1) (1961) pp. 15–31. arXiv:https://doi.org/10.1243/JMES_JOUR_1961_003_005_02, doi:10.1243/JMES_JOUR_1961_003_005_02. URL https://doi.org/10.1243/JMES_JOUR_1961_003_005_02

[46] D. Marquardt, An algorithm for least-squares estimation of nonlinear parameters, *Journal of the Society for Industrial and Applied Mathematics* **11** (2) (1963) pp. 431–441. arXiv:https://doi.org/10.1137/0111030, doi:10.1137/0111030. URL https://doi.org/10.1137/0111030

[47] W. A. Szczepiński, On the effect of plastic deformation on yield criterion, *Archives of Mechanics* **15** (2) (1963) pp. 275–296.

[48] W. M. Mair, H. L. D. Pugh, Effect of pre-strain on yield surfaces in copper, *Journal of Mechanical Engineering Science* **6** (2) (1964) pp. 150–163. doi:10.1243/JMES_JOUR_1964_006_025_02. URL http://jms.sagepub.com/content/6/2/150.full.pdf+html

[49] J. Parker, M. B. Bassett, Plastic stress–strain relationships—some experiments to derive a subsequent yield surface, *Journal of Applied Mechanics* **31** (4) (1964) pp. 676–682. doi:10.1115/1.3629730. URL http://dx.doi.org/10.1115/1.3629730

[50] A. Baltov, A. Sawczuk, A rule of anisotropic hardening, *Acta Mechanica* **1** (2) (1965) pp. 81–92. doi:10.1007/BF01174305. URL http://dx.doi.org/10.1007/BF01174305

[51] P. Theocaris, C. Hazell, Experimental investigation of subsequent yield surfaces using the moiré method, *Journal of the Mechanics and Physics of Solids* **13** (5) (1965) pp. 281–294. doi:http://dx.doi.org/10.1016/0022-5096(65)90032-3. URL http://www.sciencedirect.com/science/article/pii/0022509665900323

[52] P. J. Armstrong, C. O. Frederick, A mathematical representation of the multiaxial Baushinger effect, Tech. Rep. CEGB RD/B/N/731, Berkeley nuclear laboratories, R&D department, CA. (1966).

[53] A. K. Mālmeisters, Геометрия теорий прочности, *Механика полимеров (Mechanics of Polymers)* **4** (1966) pp. 519–526, [in Russian language].

[54] Z. Mróz, On the description of anisotropic workhardening, *Journal of the Mechanics and Physics of Solids* **15** (3) (1967) pp. 163–175. doi:https://doi.org/10.1016/0022-5096(67)90030-0. URL http://www.sciencedirect.com/science/article/pii/0022509667900300

[55] I. I. Goľdenblat, V. A. Kopnov, Criteria of Strength and Plasticity in Construction Materials, Mashinostroenie, Moscow, 1968, [in Russian language].

[56] Š. Schwarz, The theory of solutions of equations (Základy náuky o riešení rovníc), 2nd Edition, Vydavateľstvo SAV, Bratislava, 1968, [in Slovak language].

[57] F. Rotvel, Biaxial fatigue tests with zero mean stresses using tubular specimens, *International Journal of Mechanical Sciences* **12** (7) (1970) pp. 597–613. doi:https://doi.org/10.1016/0020-7403(70)90091-3. URL http://www.sciencedirect.com/science/article/pii/0020740370900913

[58] V. I. Danilov, К формулировке закона деформационного упрочнения (On the formulation of the law of distortional hardening), *Механика твердого тела (Mechanics of Solids)* **6** (1971) pp. 146–150, [in Russian language].

[59] K. C. Valanis, A theory of viscoplasticity without a yield surface–Part I. General theory, *Archives of Mechanics* **23** (4) (1971) pp. 517–534.

[60] K. C. Valanis, A theory of viscoplasticity without a yield surface–Part II. Application to mechanical behavior of metals, *Archives of Mechanics* **23** (4) (1971) pp. 535–551.

[61] J. F. Williams, N. L. Svensson, A rationally based yield criterion for work hardening materials, *Meccanica* **6** (2) (1971) pp. 104–114. doi:10.1007/BF02151650. URL https://doi.org/10.1007/BF02151650

[62] S. Hecker, Experimental investigation of corners in the yield surface, *Acta Mechanica* **13** (1-2) (1972) pp. 69–86. doi:10.1007/BF01179659. URL http://dx.doi.org/10.1007/BF01179659

[63] A. Phillips, C. Liu, J. Justusson, An experimental investigation of yield surfaces at elevated temperatures, *Acta Mechanica* **14** (2-3) (1972) pp. 119–146. doi:10.1007/BF01184853. URL http://dx.doi.org/10.1007/BF01184853

[64] A. Phillips, J.-L. Tang, The effect of loading path on the yield surface at elevated temperatures, *International Journal of Solids and Structures* **8** (1972) pp. 463–474.

[65] E. Shiratori, K. Ikegami, K. Kaneko, The influence of the bauschinger effect on the subsequent yield condition, *Bulletin of JSME* **16** (100) (1973) pp. 1482–1493. doi:10.1299/jsme1958.16.1482. URL http://ci.nii.ac.jp/naid/110002362076/en/

[66] M. Michno, W. Findley, Subsequent yield surface for annealed mild steel under dead-weight loading – Aging, normality, convexity, corners, Bauschinger, and cross effect, *Journal of Engineering Materials and Technology* **96** (1) (1974) pp. 56–64.

[67] A. Phillips, J.-L. Tang, M. Ricciuti, Some new observations on yield surfaces, *Acta Mechanica* **20** (1–2) (1974) pp. 23–39. doi:10.1007/BF01374960. URL http://dx.doi.org/10.1007/BF01374960

[68] Y. F. Dafalias, E. P. Popov, A model of nonlinearly hardening materials for complex loading, *Acta Mechanica* **21** (3) (1975) pp. 173–192. doi:10.1007/BF01181053. URL https://doi.org/10.1007/BF01181053

[69] R. D. Krieg, A practical two surface plasticity theory, *Journal of Applied Mechanics* **42** (3) (1975) pp. 641–646. doi:10.1115/1.3423656. URL http://dx.doi.org/10.1115/1.3423656

[70] Y. F. Dafalias, E. P. Popov, Plastic internal variables formalism of cyclic plasticity, *Journal of Applied Mechanics* **43** (4) (1976) pp. 645–651. doi:10.1115/1.3423948. URL http://dx.doi.org/10.1115/1.3423948

[71] S. S. Hecker, Experimental studies of yield phenomena in biaxially loaded metals, *American Society of Mechanical Engineers* (1976) pp. 1–33. URL http://www.osti.gov/scitech/servlets/purl/7128705

[72] M. Michno, W. Findley, An historical perspective of yield surface investigations for metals, *International Journal of Non-Linear Mechanics* **11** (1) (1976) pp. 59–82. doi:http://dx.doi.org/10.1016/0020-7462(76)90039-1. URL http://www.sciencedirect.com/science/article/pii/0020746276900391

[73] Y. F. Dafalias, E. P. Popov, Cyclic loading for materials with a vanishing elastic region, *Nuclear Engineering and Design* **41** (2) (1977) pp. 293–302. doi:https://doi.org/10.1016/0029-5493(77)90117-0. URL http://www.sciencedirect.com/science/article/pii/0029549377901170

[74] D. Lee, F. Zaverl, A generalized strain rate dependent constitutive equation for anisotropic metals, *Acta Metallurgica* **26** (11) (1978) pp. 1771–1780. doi:https://doi.org/10.1016/0001-6160(78)90088-3. URL http://www.sciencedirect.com/science/article/pii/0001616078900883

[75] D. Lee, F. Zaverl, A description of history dependent plastic flow behavior of anisotropic metals, *Journal of Engineering Materials and Technology* **101** (1) (1979) pp. 59–67. doi:10.1115/1.3443652. URL http://dx.doi.org/10.1115/1.3443652

[76] L. Ascione, R. S. Olivito, G. Spadea, An experimental study on subsequent yield surfaces for metals, *Matériaux et Construction* **15** (1) (1982) pp. 21–26. doi:10.1007/BF02473555. URL http://dx.doi.org/10.1007/BF02473555

[77] K. Ikegami, Experimental Plasticity on the Anisotropy of Metals, Springer Netherlands, Dordrecht, 1982 pp. pp. 201–242. doi:10.1007/978-94-009-6827-1_14. URL http://dx.doi.org/10.1007/978-94-009-6827-1_14

[78] N. Gupta, H. Lauert, A study of yield surface upon reversal of loading under biaxial stress, *ZAMM - Journal of Applied Mathematics and Mechanics / Zeitschrift für Angewandte Mathematik und Mechanik* **63** (10) (1983) pp. 497–504. doi:10.1002/zamm.19830631005. URL http://dx.doi.org/10.1002/zamm.19830631005

[79] M. Ortiz, E. P. Popov, Distortional hardening rules for metal plasticity, *Journal of Engineering Mechanics* **109** (4) (1983) pp. 1042–1057.

[80] A. Troshchenko, N. Kul'chitskii, An experimental investigation of the initial and subsequent yield surfaces of 40kh steel, *Strength of Materials* **15** (11) (1983) pp. 1590–1595. doi:10.1007/BF01523566. URL http://dx.doi.org/10.1007/BF01523566

[81] M. A. Eisenberg, C.-F. Yen, The anisotropic deformation of yield surfaces, *Journal of Engineering Materials and Technology* **106** (4) (1984) pp. 355–360. doi:10.1115/1.3225730. URL http://dx.doi.org/10.1115/1.3225730

[82] A. Phillips, W. Lu, An experimental investigation of yield surfaces and loading surfaces of pure aluminum with stress-controlled and strain-controlled paths of loading, *Journal of Engineering Materials and Technology* **106** (4) (1984) pp. 349–354. doi:10.1115/1.3225729. URL http://dx.doi.org/10.1115/1.3225729

[83] D. W. A. Rees, An examination of yield surface distortion and translation, *Acta Mechanica* **52** (1) (1984) pp. 15–40. doi:10.1007/BF01175962. URL https://doi.org/10.1007/BF01175962

[84] A. Phillips, P. K. Das, Yield surfaces and loading surfaces of aluminum and brass: An experimental investigation at room and elevated temperatures, *International*

Journal of Plasticity **1** (1) (1985) pp. 89–109. doi:http://dx.doi.org/10.1016/0749-6419(85)90015-4. URL http://www.sciencedirect.com/science/article/pii/0749641985900154

[85] J. C. Simo, R. L. Taylor, Consistent tangent operators for rate-independent elastoplasticity, *Computer Methods in Applied Mechanics and Engineering* **48** (1) (1985) pp. 101–118. doi:https://doi.org/10.1016/0045-7825(85)90070-2. URL http://www.sciencedirect.com/science/article/pii/0045782585900702

[86] M. G. Stout, P. L. Martin, D. E. Helling, G. R. Canova, Multiaxial yield behavior of 1100 aluminum following various magnitudes of prestrain, *International Journal of Plasticity* **1** (2) (1985) pp. 163–174. doi:http://dx.doi.org/10.1016/0749-6419(85)90027-0. URL http://www.sciencedirect.com/science/article/pii/0749641985900270

[87] D. Helling, A. Miller, M. Stout, An experimental investigation of the yield loci of 1100-0 aluminum, 70:30 brass, and an overaged 2024 aluminum alloy after various prestrains, *Journal of Engineering Materials and Technology* **108** (4) (1986) pp. 313–320. doi:10.1115/1.3225888. URL http://dx.doi.org/10.1115/1.3225888

[88] K. Runesson, A. Samuelsson, L. Bernspång, Numerical technique in plasticity including solution advancement control, *International Journal for Numerical Methods in Engineering* **22** (3) (1986) pp. 769–788. doi:10.1002/nme.1620220315. URL https://onlinelibrary.wiley.com/doi/abs/10.1002/nme.1620220315

[89] D. E. Helling, A. K. Miller, The incorporation of yield surface distortion into a unified constitutive model, Part I: Equation development, *Acta Mechanica* **69** (1–4) (1987) pp. 9–23. doi:10.1007/BF01175711. URL http://dx.doi.org/10.1007/BF01175711

[90] C. F. Yen, M. A. Eisenberg, The role of a loading surface in viscoplasticity theory, *Acta Mechanica* **69** (1–4) (1987) pp. 77–96. doi:10.1007/BF01175715. URL http://dx.doi.org/10.1007/BF01175715

[91] P. Bogacki, L. F. Shampine, A 3(2) pair of Runge - Kutta formulas, *Applied Mathematics Letters* **2** (4) (1989) pp. 321–325. doi:https://doi.org/10.1016/0893-9659(89)90079-7. URL http://www.sciencedirect.com/science/article/pii/0893965989900797

[92] P. Cayla, M. Boucher, A theoretical and experimental approach of strain induced anisotropy, *International Deep Drawing Research Group* (1990) Gothenburg.

[93] J. Lemaitre, J.-L. Chaboche, Mechanics of Solid Materials, Cambridge University Press, 1990.

[94] G. Z. Voyiadjis, M. Foroozesh, Anisotropic distortional yield model, *Computer Methods in Applied Mechanics and Engineering* **57** (3) (1990) pp. 537–547. doi:10.1115/1.2897056. URL http://dx.doi.org/10.1115/1.2897056

[95] S. Cheng, E. Krempl, Experimental determination of strain-induced anisotropy during nonproportional straining of an Al/Mg alloy at room temperature, *International Journal of Plasticity* **7** (8) (1991) pp. 827–846. doi:http://dx.doi.org/10.1016/0749-6419(91)90020-Y. URL http://www.sciencedirect.com/science/article/pii/074964199190020Y

[96] H. C. Wu, W. C. Yeh, On the experimental determination of yield surfaces and some results on annealed 304 stainless steel, *International Journal of Plasticity* **7** (8) (1991) pp. 803–826. doi:http://dx.doi.org/10.1016/0749-6419(91)90019-U. URL http://www.sciencedirect.com/science/article/pii/074964199190019U

[97] A. S. Khan, X. Wang, An experimental study on subsequent yield surface after finite shear prestraining, *International Journal of Plasticity* **9** (8) (1993) pp. 889–905. doi:http://dx.doi.org/10.1016/0749-6419(93)90056-V. URL http://www.sciencedirect.com/science/article/pii/074964199390056V

[98] M. Boucher, P. Cayla, J. P. Cordebois, Experimental studies of yield surfaces of aluminium alloy and low carbon steel under complex biaxial loading, *European Journal of Mechanics – A/Solids* **14** (1) (1995) pp. 1–17.

[99] H.-C. Wu, H.-K. Hong, J.-K. Lu, An endochronic theory accounted for deformation induced anisotropy, *International Journal of Plasticity* **11** (2) (1995) pp. 145–162. doi:https://doi.org/10.1016/0749-6419(94)00042-5. URL http://www.sciencedirect.com/science/article/pii/0749641994000425

[100] H. Wu, J. Lu, W. Pan, Some observations on yield surfaces for 304 stainless steel at large prestrain, *Journal of Applied Mechanics* **62** (3) (1995) pp. 626–632. doi:10.1115/1.2895992. URL http://dx.doi.org/10.1115/1.2895992

[101] T. Kurtyka, M. Życzkowski, Evolution equations for distortional plastic hardening, *International Journal of Plasticity* **12** (2) (1996) pp. 191–213. doi:http://dx.doi.org/10.1016/S0749-6419(96)00003-4. URL http://www.sciencedirect.com/science/article/pii/S0749641996000034

[102] W.-C. Yeh, C.-D. Ho, W.-F. Pan, An endochronic theory accounting for deformation induced anisotropy of metals under biaxial load, *International Journal of Plasticity* **12** (8) (1996) pp. 987–1004. doi:https://doi.org/10.1016/S0749-6419(96)00038-1. URL http://www.sciencedirect.com/science/article/pii/S0749641996000381

[103] L. Dietrich, Z. L. Kowalewski, Experimental investigation of an anisotropy in copper subjected to predeformation due to constant and monotonic loadings, *International Journal of Plasticity* **13** (1–2) (1997) pp. 87–109. doi:http://dx.doi.org/10.1016/S0749-6419(97)00002-8. URL http://www.sciencedirect.com/science/article/pii/S0749641997000028

[104] H. Ishikawa, Subsequent yield surface probed from its current center, *International Journal of Plasticity* **13** (6–7) (1997) pp. 533–549. doi:http://dx.doi.org/10.1016/S0749-6419(97)00024-7. URL http://www.sciencedirect.com/science/article/pii/S0749641997000247

[105] C. Lissenden, B. Lerch, J. Ellis, D. Robinson, Experimental determination of yield and flow surfaces under axial-torsional loading, in: S. Kalluri, P. Bonacuse (Eds.), *Multiaxial fatigue and deformation testing techniques*, Vol. 1280 of American society for testing and materials special technical publication, American Society for Testing and Materials, 1997 pp. pp. 92–112, symposium on Multiaxial Fatigue and Deformation Testing Techniques, Denver, CO, May 15, 1995. doi:10.1520/STP16214S. URL http://www.refdoc.fr/Detailnotice?idarticle=15448531

[106] L. F. Shampine, M. W. Reichelt, The MATLAB ODE Suite, *SIAM Journal on Scientific Computing* **18** (1) (1997) pp. 1–22. arXiv:https://doi.org/10.1137/S1064827594276424, doi:10.1137/S1064827594276424. URL https://doi.org/10.1137/S1064827594276424

[107] C. Gil, C. Lissenden, B. Lerch, Determination of yield in inconel axial-torsional loading at temperatures up to 649 °C, Tech. Rep. NASA/TM—1998-208658 (1998).

[108] J. M. Pestana, A. J. Whittle, Formulation of a unified constitutive model for clays and sands, *International Journal for Numerical and Analytical Methods in Geomechanics* **23** (12) (1999) pp. 1215–1243. doi:10.1002/(SICI)1096-9853(199910)23:12<1215::AID-NAG29>3.0.CO;2-F. URL https://onlinelibrary.wiley.com/doi/abs/10.1002/%28SICI%291096-9853%28199910%2923%3A12%3C1215%3A%3AAID-NAG29%3E3.0.CO%3B2-F

[109] M. François, A plasticity model with yield surface distortion for non proportional loading, *International Journal of Plasticity* **17** (5) (2001) pp. 703–717. doi:http://dx.doi.org/10.1016/S0749-6419(00)00025-5. URL http://www.sciencedirect.com/science/article/pii/S0749641900000255

[110] G. Grewolls, R. Kreißig, Anisotropic hardening – numerical application of a cubic yield theory and consideration of variable r-values for sheet metal, *European Journal of Mechanics - A/Solids* **20** (4) (2001) pp. 585–599. doi:https://doi.org/10.1016/S0997-7538(01)01156-1. URL http://www.sciencedirect.com/science/article/pii/S0997753801011561

[111] A. Plumtree, H. A. Abdel-Raouf, Cyclic stress–strain response and substructure, *International Journal of Fatigue* **23** (9) (2001) pp. 799–805. doi:http://dx.doi.org/10.1016/S0142-1123(01)00037-8. URL http://www.sciencedirect.com/science/article/pii/S0142112301000378

[112] M. Yu, Advances in strength theories for materials under complex stress state in the 20th century, *Applied Mechanics Reviews* **55** (3) (2002) pp. 169–218. doi:10.1115/1.1472455. URL http://dx.doi.org/10.1115/1.1472455

[113] A. A. Brown, J. Casey, D. Nikkel Jr., Experiments conducted in the context of the strain-space formulation of plasticity, *International Journal of Plasticity* **19** (11) (2003) pp. 1965–2005, finite Plasticity and Viscoplasticity - Theoretical, Experimental and Computational Aspects. doi:http://dx.doi.org/10.1016/S0749-6419(03)00046-9. URL http://www.sciencedirect.com/science/article/pii/S0749641903000469

[114] Y. F. Dafalias, D. Schick, C. Tsakmakis, A simple model for describing yield surface evolution during plastic flow, in: K. Hutter, H. Baaser (Eds.), *Deformation and Failure in Metallic Materials*, Lecture Notes in Applied and Computational Mechanics, Springer Berlin Heidelberg, 2003 pp. 169–201. doi:10.1007/978-3-540-36564-8_7. URL http://dx.doi.org/10.1007/978-3-540-36564-8_7

[115] H.-C. Wu, Effect of loading-path on the evolution of yield surface for anisotropic metals subjected to large pre-strain, *International Journal of Plasticity* **19** (10) (2003) pp. 1773–1800. doi:http://dx.doi.org/10.1016/S0749-6419(03)00012-3. URL http://www.sciencedirect.com/science/article/pii/S0749641903000123

[116] M. T. Huber, Specific work of strain as a measure of material effort, *Archives of Mechanics* **56** (3) (2004) pp. 173–190.

[117] S. Kolling, A. Haufe, M. Feucht, P. A. Du Bois, SAMP-1: A semi-analytical model for the simulation of polymers., in: *4. LS-DYNA Anwenderforum*, Bamberg, 2005.

[118] H. P. Feigenbaum, Y. F. Dafalias, Directional distortional hardening in metal plasticity within thermodynamics, *International Journal of Solids and Structures* **44** (22) (2007) pp. 7526–7542. doi:http://dx.doi.org/10.1016/j.ijsolstr.2007.04.025. URL http://www.sciencedirect.com/science/article/pii/S0020768307002077

[119] R. Halama, H. Robovská, L. Volková, T. Skočovský, D. Stacha, M. Švrček, A. Vicherek, Parameter identification of Chaboche nonlinear kinematic hardening model, in: K. Frydrýšek, et al. (Eds.), *Conference of Applied Mechanics 2007, Malenovice, April 16–19, 2007*, Technical University of Ostrava, Ostrava, Czech Republic, 2007 pp. 97–98, [in Czech language].

[120] A. S. Khan, R. Kazmi, B. Farrokh, Multiaxial and non-proportional loading responses, anisotropy and modeling of Ti–6Al–4V titanium alloy over wide ranges of strain rates and temperatures, *International Journal of Plasticity* **23** (6) (2007) pp. 931–950. doi:https://doi.org/10.1016/j.ijplas.2006.08.006. URL http://www.sciencedirect.com/science/article/pii/S0749641906001264

[121] H. P. Feigenbaum, Y. F. Dafalias, Simple model for directional distortional hardening in metal plasticity within thermodynamics, *Journal of Engineering Mechanics* **134** (9) (2008) pp. 730–738. doi:10.1061/(ASCE)0733-9399(2008)134:9(730). URL https://ascelibrary.org/doi/abs/10.1061/%28ASCE%290733-9399%282008%29134%3A9%28730%29

[122] H. P. Feigenbaum, Directional Distortional Hardening in Plasticity Based on Thermodynamics, Ph.D. thesis, University of California, Davis, CA 95616, USA (2008).

[123] E. d. S. Neto, D. Perić, D. Owens, Computational methods for plasticity: Theory and applications, John Wiley & Sons Ltd, 2008.

[124] M. Taiebat, Y. F. Dafalias, SANISAND: Simple anisotropic sand plasticity model, *International Journal for Numerical and Analytical Methods in Geomechanics* **32** (8) (2008) pp. 915–948. arXiv:https://onlinelibrary.wiley.com/doi/pdf/10.1002/nag.651, doi:10.1002/nag.651. URL https://onlinelibrary.wiley.com/doi/abs/10.1002/nag.651

[125] A. S. Khan, R. Kazmi, A. Pandey, T. Stoughton, Evolution of subsequent yield surfaces and elastic constants with finite plastic deformation. Part-I: A very low work hardening aluminum alloy (Al6061-T6511), *International Journal of Plasticity* **25** (9) (2009) pp. 1611–1625, exploring New Horizons of Metal Forming Research. doi:http://dx.doi.org/10.1016/j.ijplas.2008.07.003. URL http://www.sciencedirect.com/science/article/pii/S0749641908001113

[126] A. S. Khan, A. Pandey, T. Stoughton, Evolution of subsequent yield surfaces and elastic constants with finite plastic deformation. Part III: Yield surface in tension–tension stress space (Al 6061–T 6511 and annealed 1100 Al), *International Journal of Plasticity* **26** (10) (2010) pp. 1432–1441. doi:http://dx.doi.org/10.1016/j.ijplas.2009.07.007. URL http://www.sciencedirect.com/science/article/pii/S0749641909000941

[127] M. E. Nixon, O. Cazacu, R. A. Lebensohn, Anisotropic response of high-purity α-titanium: Experimental characterization and constitutive modeling, *International Journal of Plasticity* **26** (4) (2010) pp. 516–532. doi:https://doi.org/10.1016/j.ijplas.2009.08.007. URL http://www.sciencedirect.com/science/article/pii/S0749641909001077

[128] K. Osakada, History of plasticity and metal forming analysis, *Journal of Materials Processing Technology* **210** (11) (2010) pp. 1436–1454. doi:https://doi.org/10.1016/j.jmatprotec.2010.04.001. URL http://www.sciencedirect.com/science/article/pii/S0924013610001111

[129] J. Plesek, H. P. Feigenbaum, Y. F. Dafalias, Convexity of yield surface with directional distortional hardening rules, *Journal of Engineering Mechanics* **136** (4) (2010) pp. 477–484. doi:10.1061/(ASCE)EM.1943-7889.0000077.

[130] S. K. Paul, S. Sivaprasad, S. Dhar, S. Tarafder, Key issues in cyclic plastic deformation: Experimentation, *Mechanics of Materials* **43** (11) (2011) pp. 705–720. doi:http://dx.doi.org/10.1016/j.mechmat.2011.07.011. URL http://www.sciencedirect.com/science/article/pii/S0167663611001347

[131] A. V. Shutov, S. Panhans, R. Kreissig, A phenomenological model of finite strain viscoplasticity with distortional hardening, *ZAMM-ZEITSCHRIFT FUR ANGEWANDTE MATHEMATIK UND MECHANIK* **91** (8) (2011) pp. 653–680. doi:10.1002/zamm.201000150.

[132] S. Sung, L. Liu, H. Hong, H. Wu, Evolution of yield surface in the 2D and 3D stress spaces, *International Journal of Solids and Structures* **48** (6) (2011) pp. 1054–1069. doi:http://dx.doi.org/10.1016/j.ijsolstr.2010.12.011. URL http://www.sciencedirect.com/science/article/pii/S0020768310004476

[133] Z. Hrubý, Directional Distortional Hardening – Models' Parameters Calibration and FE-code Implementation, Ph.D. thesis, Faculty of Mechanical Engineering, CTU in Prague, Technicka 4, 166 07 Prague 6, Czech Republic (2012).

[134] G. Hu, K. Zhang, S. Huang, J.-W. W. Ju, Yield surfaces and plastic flow of 45 steel under tension-torsion loading paths, *Acta Mechanica Solida Sinica* **25** (4) (2012) pp. 348–360. doi:http://dx.doi.org/10.1016/S0894-9166(12)60032-9. URL http://www.sciencedirect.com/science/article/pii/S0894916612600329

[135] A. S. Khan, S. Yu, Deformation induced anisotropic responses of Ti–6Al–4V alloy. Part I: Experiments, *International Journal of Plasticity* **38** (2012) pp. 1–13. doi:https://doi.org/10.1016/j.ijplas.2012.03.015. URL http://www.sciencedirect.com/science/article/pii/S0749641912000551

[136] A. S. Khan, S. Yu, H. Liu, Deformation induced anisotropic responses of Ti–6Al–4V alloy. Part II: A strain rate and temperature dependent anisotropic yield criterion, *International Journal of Plasticity* **38** (2012) pp. 14–26. doi:https://doi.org/10.1016/j.ijplas.2012.03.013. URL http://www.sciencedirect.com/science/article/pii/S0749641912000538

[137] Y.-P. Yao, Y.-X. Kong, Extended UH model: Three-dimensional unified hardening model for anisotropic clays, *Journal of Engineering Mechanics* **138** (7) (2012) pp. 853–866. arXiv:https://ascelibrary.org/doi/pdf/10.1061/\%28ASCE\%29EM.1943-7889.0000397, doi:10.1061/(ASCE)EM.1943-7889.0000397. URL https://ascelibrary.org/doi/abs/10.1061/%28ASCE%29EM.1943-7889.0000397

[138] Z. Mikulášek, Phenomenological modelling of eclipsing system light curves, *Astronomy & Astrophysics* **584** (2015) A8. doi:10.1051/0004-6361/201425244. URL https://www.aanda.org/articles/aa/abs/2015/12/aa25244-14/aa25244-14.html

[139] M. K. Transtrum, P. Qiu, Bridging mechanistic and phenomenological models of complex biological systems, *PLOS Computational Biology* **12** (5) (2016) pp. 1–34. doi:10.1371/journal.pcbi.1004915. URL https://doi.org/10.1371/journal.pcbi.1004915

[140] J. W. Eaton, Gnu octave (2018-Jan-22). URL https://www.gnu.org/software/octave/

[141] K.-C. Chou, Application of phenomenological theory to chemical metallurgy, *ISIJ International* **58** (5) (2018) pp. 785–791. doi:10.1051/0004-6361/201425244.

Appendix A. Computer Program for Parameters Calibration from Quasistatic Loading Data

```
% monotonic_calibration.m file
% calibration algorithm for directional distortional model -- alpha model
% with fixed c parameter -- monotonic loading data
% model published by Feigenbaum & Dafalias (2008)
% written by Slavomir Parma
% Prague, Czech Republic, September 21, 2015
% utf-8 code page, CR line end (linux)
% GNU Octave 4.2.1, Matlab R2012b (8.0.0.783)
% algorithm published in paper
% Slavomír Parma, Jiří Plešek, René Marek, Zbyněk Hrubý,
% Heidi P. Feigenbaum, Yannis F. Dafalias
% International Journal of Solids and Structures (2018)
% Calibration of a simple directional distortional hardening model
% for metal plasticity

%% initialization
clear all; close all; % clc;

%% input file loading
input_dir_name = './input/';
input_file_name = 'input_parameters.dat';
parameters = load([ input_dir_name input_file_name ]);

%% input parameters initialization
A1 = parameters(1);
A2 = parameters(2);
A3 = parameters(3);
B1 = parameters(4);
B2 = parameters(5);
C1 = parameters(6);
C2 = parameters(7);
D1 = parameters(8);
D2 = parameters(9);
D3 = parameters(10);
eps= parameters(11); % eps_pl at the first unloading level

%% calibration
% calibration of the 'k0' parameter
k0 = A1;

% calibration of the 'c' parameter
c = 3* sqrt((D1-D2)*(D1-D2-2*D3)) / ...
( (D1-D2-D3)*(D1+D2-sqrt((D1-D2)*(D1-D2-2*D3))) );
```

```
% calibration of the 'a_2' parameter

% B
q3 = 9/2*sqrt(3/2)*c;
q2 = -3*sqrt(3/2)*c*(B1+B2);
q1 = sqrt(3/2)*c*(B1^2+B2^2)+3*(B1-B2);
q0 = -(B1^2-B2^2);

Discriminant = 18*q3*q2*q1*q0 - 4*q2^3*q0 + q2^2*q1^2 ...
- 4*q3*q1^3 - 27*q3^2*q0^2;

alpha_B = -q2/(3*q3) ...
- 1/(3*q3)* nthroot( 1/2* (2*q2^3 - 9*q3*q2*q1 ...
+ 27*q3^2*q0 + sqrt(-27*q3^2*Discriminant) ) , 3) ...
- 1/(3*q3)* nthroot( 1/2* (2*q2^3 - 9*q3*q2*q1 ...
+ 27*q3^2*q0 - sqrt(-27*q3^2*Discriminant) ) , 3);

% C
q3 = 9/2*sqrt(3/2)*c;
q2 = -3*sqrt(3/2)*c*(C1+C2);
q1 = sqrt(3/2)*c*(C1^2+C2^2)+3*(C1-C2);
q0 = -(C1^2-C2^2);

Discriminant = 18*q3*q2*q1*q0 - 4*q2^3*q0 + q2^2*q1^2 ...
- 4*q3*q1^3 - 27*q3^2*q0^2;

alpha_C = -q2/(3*q3) ...
- 1/(3*q3)* nthroot( 1/2* (2*q2^3 - 9*q3*q2*q1 ...
+ 27*q3^2*q0 + sqrt(-27*q3^2*Discriminant) ) , 3) ...
- 1/(3*q3)* nthroot( 1/2* (2*q2^3 - 9*q3*q2*q1 ...
+ 27*q3^2*q0 - sqrt(-27*q3^2*Discriminant) ) , 3);

a2 = sqrt(2/3)*( 2*alpha_B - alpha_C )/alpha_B^2;

% calibration of the 'a1' parameter
a1 = -sqrt(2/3)/(a2*eps)*log(1-sqrt(3/2)*alpha_B*a2);

% calibration of the 'kappa2' parameter
kappa2 = 1/( sqrt(1-c/a2) * ( A3 - sqrt(3/2)/a2 ) );

% calibration of the 'kappa1' parameter
kappa1 = (2*A2 - sqrt(3/2)*k0*a1*c - 3*a1) / (1-kappa2*k0);

%% file output
output_dir_name = './output/';
output_file_name = 'output_parameters.dat';
```

```
output_file = fopen([ output_dir_name output_file_name ], 'wt');
fprintf ( output_file, ['%% calibrated parameters: k0(MPa) c(MPa^-1) ' ...
'a1(MPa) a2(MPa^-1) kappa1(MPa^2) kappa2(MPa^-1)\n']);
fprintf ( output_file, '%-5.0f\n', k0);
fprintf ( output_file, '%-6.4f\n', c);
fprintf ( output_file, '%-6.0f\n', a1);
fprintf ( output_file, '%-6.4f\n', a2);
fprintf ( output_file, '%-6.0f\n', kappa1);
fprintf ( output_file, '%-6.4f'  , kappa2);
fclose(output_file);
```

Appendix B. Computer Program for Parameters Calibration from Cyclic Loading Data

```
% cyclic_calibration.m file
% calibration algorithm for directional distortional model -- alpha model
% with fixed c parameter -- cyclic loading data
% model published by Feigenbaum & Dafalias (2008)
% written by Slavomir Parma
% Flagstaff, Arizona, USA, December 8, 2014
% utf-8 code page, CR line end (linux)
% GNU Octave 4.2.1, Matlab R2012b (8.0.0.783)
% algorithm published in paper
% Slavomír Parma, Jiří Plešek, René Marek, Zbyněk Hrubý,
% Heidi P. Feigenbaum, Yannis F. Dafalias
% International Journal of Solids and Structures (2018)
% Calibration of a simple directional distortional hardening model
% for metal plasticity

% initialization
clear all; close all; % clc;

addpath(fullfile(cd,'input')); % experimental data folder
addpath(fullfile(cd,'output')); % output files folder

%% experimental data allocation
input_file_names_CSSC = { 'CSSC_a.csv'; 'CSSC_b.csv'};
input_file_names_youngs_modulus = ...
{ 'youngs_modulus_a.txt'; 'youngs_modulus_a.txt'};

for i=1:length(input_file_names_CSSC)

%% experimental data loading

% experimental data of CSSC
CSSC = load(input_file_names_CSSC{i});
% experimental data of Young's modulus
E = load(input_file_names_youngs_modulus{i});

%% computation of plastic strain

CSSC_eps_tot = CSSC(:,1); % total strain amplitude
CSSC_sigma   = CSSC(:,2); % stress amplitude

% plastic strain amplitude - Hooke's law
CSSC_eps = CSSC_eps_tot - CSSC_sigma/E;
```

```
%% initial estimation - determination of parameters A, B, C, eps_B, r

% one possible approach to estimation, different can be applied
A = min(CSSC(:,2));
% one possible approach to estimation, different can be applied
C = max(CSSC(:,2));

data_length = length(CSSC);
middle_position = floor(data_length/2);
% one possible approach to estimation, different can be applied
eps_B = 0.5*(CSSC_eps(middle_position)+CSSC_eps(middle_position+1));
% one possible approach to estimation, different can be applied
B     = 0.5*(CSSC_sigma(middle_position)+CSSC_sigma(middle_position+1));

r = 0.9*(1-(A/C)^2);

%% initial estimation - determination of parameters a1, a2, k2, c

f_k2 = @(pA) 1/pA;
f_a2 = @(pA,pC,pr) sqrt(1.5)/(pC-pA/sqrt(1-pr));
f_c  = @(pa2,pr) pr*pa2;
f_a1_all_parameters = @(pA,pB,pC,peps_B,pa1,pa2,pr) ...
pA/sqrt(1-pr*tanh(sqrt(3/2)*pa1*pa2*peps_B)) ...
+ sqrt(3/2)/pa2*tanh(sqrt(3/2)*pa1*pa2*peps_B)-pB;

k2 = f_k2(A);
a2 = f_a2(A,C,r);
c  = f_c(a2,r);

f_a1 = @(pa1) f_a1_all_parameters(A,B,C,eps_B,pa1,a2,r);
a10 = 0; % initial estimation
a1 = fsolve(f_a1,a10);

%% calibration - Nonlinear Least Squares Method

% reparametrization to preserve restrictions for parameters
% a1 <-- aa1^2           means a1>=0
% a2 <-- cc^2 + aa2^2    means a2>=c
% k2 <-- kk2^2           means k2>=0
% c  <-- cc^2            means c>=0

% transformation from internal to standard parameters

f_internal_to_standard = @(aa1,aa2,kk2,cc) ...
% a1     a2          k2     c
[ aa1^2, cc^2+aa2^2, kk2^2, cc^2 ];
```

```
% transformation from standard to internal parameters
f_standard_to_internal = @(a1,a2,k2,c) ...
% aa1       aa2         kk2       cc
[ sqrt(a1), sqrt(a2-c), sqrt(k2), sqrt(c) ];

initial_estimation_internal = f_standard_to_internal(a1,a2,k2,c);

f_CSSC_all_parameters = @(aa1,aa2,kk2,cc,peps) ...
(1/kk2^2)./sqrt(1-cc^2/(cc^2+aa2^2) ...
*tanh(sqrt(3/2)*aa1^2*(cc^2+aa2^2)*peps)) ...
+ sqrt(3/2)/(cc^2+aa2^2)*tanh(sqrt(3/2)*aa1^2*(cc^2+aa2^2)*peps);

f_least_squares_all_parameters = @(peps,psigma,aa1,aa2,kk2,cc) ...
sum(  (psigma - f_CSSC_all_parameters(aa1,aa2,kk2,cc,peps)).^2  );

f_least_squares = @(X) f_least_squares_all_parameters ...
(CSSC_eps,CSSC_sigma,X(1),X(2),X(3),X(4));

identified_parameters_internal = fminsearch ...
(f_least_squares, initial_estimation_internal);

%% data processing

% internal parameters
initial_estimation_internal = num2cell(initial_estimation_internal);
[ie_aa1, ie_aa2, ie_kk2, ie_cc] = initial_estimation_internal{:};

identified_parameters_internal = num2cell(identified_parameters_internal);
[ip_aa1, ip_aa2, ip_kk2, ip_cc] = identified_parameters_internal{:};

%% data presentation

figure(i)
plot(CSSC_eps,CSSC_sigma,'xr','MarkerSize',7,'Linewidth',1);hold on;

Eps = 0:1e-4:0.1;
plot(Eps,f_CSSC_all_parameters(ie_aa1,ie_aa2,ie_kk2,ie_cc,Eps), ...
'g--','Linewidth',1);hold on;
plot(Eps,f_CSSC_all_parameters(ip_aa1,ip_aa2,ip_kk2,ip_cc,Eps), ...
'b-','Linewidth',1);hold on;

legend('experimental CSSC','initial estimation', ...
'identified model','location','SE');

xlabel('\epsilon^p_{11,a} [1]');
ylabel('\sigma_{11,a} [MPa]');
```

```
if i==1
    axis([0 0.02 0 500]);
elseif i==2
    axis([0 0.07 0 750]);
end

% standard parameters computation
initial_estimation_standard = ...
num2cell(f_internal_to_standard(ie_aa1, ie_aa2, ie_kk2, ie_cc));
[ie_a1, ie_a2, ie_k2, ie_c] = initial_estimation_standard{:};

identified_parameters_standard = ...
num2cell(f_internal_to_standard(ip_aa1, ip_aa2, ip_kk2, ip_cc));
[ip_a1, ip_a2, ip_k2, ip_c] = identified_parameters_standard{:};

% parameters output to graphs
if 1==1 % yes/no

ie_x = 0.4;
ie_y = 0.55;
ie_d = 0.07;

ip_x = ie_x + 0.3;
ip_y = ie_y;
ip_d = ie_d;

set(gcf,'DefaulttextInterpreter','latex','DefaulttextFontSize', 12, ...
'DefaulttextUnits','normalized');

box1 = 4;
box2 = 17;

text(ie_x,ie_y,'estimated');
text(ie_x,ie_y-1*ie_d,[ ' \hbox to' sprintf('%5.2f',box1) ...
'mm{$a_1$} \hbox to' sprintf('%5.2f',box2) ...
'mm{=\hfill$' sprintf('%6.0f',ie_a1) '$}' ]);
text(ie_x,ie_y-2*ie_d,[ ' \hbox to' sprintf('%5.2f',box1) ...
'mm{$a_2$} \hbox to' sprintf('%5.2f',box2) ...
'mm{=\hfill$' sprintf('%6.5f',ie_a2) '$}' ]);
text(ie_x,ie_y-3*ie_d,[ ' \hbox to' sprintf('%5.2f',box1) ...
'mm{$\kappa_2$} \hbox to' sprintf('%5.2f',box2) ...
'mm{=\hfill$' sprintf('%6.5f',ie_k2) '$}' ]);
text(ie_x,ie_y-4*ie_d,[ ' \hbox to' sprintf('%5.2f',box1) ...
'mm{$c$} \hbox to' sprintf('%5.2f',box2) ...
'mm{=\hfill$' sprintf('%6.5f',ie_c ) '$}' ]);

text(ip_x,ip_y,'identified');
```

```
text(ip_x,ip_y-1*ip_d,[ ' \hbox to' sprintf('%5.2f',box1) ...
'mm{$a_1$} \hbox to' sprintf('%5.2f',box2)  ...
'mm{=\hfill$' sprintf('%6.0f',ip_a1) '$}' ]);
text(ip_x,ip_y-2*ip_d,[ ' \hbox to' sprintf('%5.2f',box1) ...
 'mm{$a_2$}      \hbox to' sprintf('%5.2f',box2)  ...
'mm{=\hfill$' sprintf('%6.5f',ip_a2) '$}' ]);
text(ip_x,ip_y-3*ip_d,[ ' \hbox to' sprintf('%5.2f',box1) ...
 'mm{$\kappa_2$} \hbox to' sprintf('%5.2f',box2)  ...
'mm{=\hfill$' sprintf('%6.5f',ip_k2) '$}' ]);
text(ip_x,ip_y-4*ip_d,[ ' \hbox to' sprintf('%5.2f',box1) ...
 'mm{$c$}        \hbox to' sprintf('%5.2f',box2)  ...
'mm{=\hfill$' sprintf('%6.5f',ip_c ) '$}' ]);
end

hold off;

%% data printing

set(gcf, 'PaperUnits', 'centimeters');
set(gcf, 'PaperSize', .5*[29.7 21]);
orient landscape; % graphs corection
orient portrait;
print('-depsc2','-loose','-r2400', ...
sprintf('output\\CSSC_%d.eps',i) );

end
```

Appendix C. Computer Program for Sensitivity Analysis of Monotonic Calibration Procedure

```
% Slavomir Parma
% Institute of Thermomechanics of the CAS, v.v.i.
% Dolejskova 1402/5, 182 00 Prague 8, Czech Republic
% parma@it.cas.cz , origon@seznam.cz
% GNU Octave Version 4.2.1, package "symbolic 2.6.0",
% package "sympy-1.1.1" for symbolic computations in python
% GNU bash version 4.3.30, linux 3.16.0-4-amd64, Debian 3.16.43-2
% LF line end (linux), utf-8 encoding
% September 22, 2017
% sensitivity analysis of the alpha c directional distortional hardening
% model by Feigenbaum and Dafalias, model published in:
% - Feigenbaum, H. P., 2008. Directional distortional hardening in
% plasticity based on thermodynamics. PhD dissertation,
% University of California, Davis.
% - Feigenbaum, H. P., Dafalias, Y. F., 2008. Simple model for
% directional distortional hardening in metal plasticity within
% thermodynamics. Journal of Engineering Mechanics 134 (9),
% pp. 730--738.
%    URL http://ascelibrary.org/doi/abs/10.1061/
% %28ASCE%290733-9399%282008%29134%3A9%28730%29
%
% results of this analysis are reported in a paper "Calibration of
% a simple directional distortional hardening model for metal
% plasticity", IJSS, (2017)

clc; clear all; close all;
more off;
addpath(genpath(pwd));  % add all subdirectories of actual working
% directory to path
output_file_name = 'output/sensitivity_analysis.txt';
system([ 'rm ' output_file_name ] );

pkg load symbolic  % https://octave.sourceforge.io/symbolic/overview.html



%% %% symbolic computation of sensitivity
digits(10);
syms x;  % this line may be erased
disp('Loading symbolic equations of model...');
s_model_setup;
```

```
%% computation of jacobian
disp('Computing symbolic jacobian...');
J_F = sym(NaN(length(F),length(X)));
for i=1:size(J_F)(1)
for j=1:size(J_F)(2)
fprintf(1,'%d,%d\n',i,j);
J_F(i,j) = jacobian(F(i),X(j));
end
end

%% numerical evaluation of jacobian
num_J_F = sym(NaN(length(F),length(X)));

for i=1:size(J_F)(1)
num_J_F(i,:) = subs(J_F(i,:), Par, Val );
end

eval_num_J_F = double(num_J_F);
output_matrix{1} = eval_num_J_F;

break

%% %% numerical computation of sensitivity
disp('Computing numeric jacobian...');
VAL_0 = double(VAL_0);  % VAL represents a point in which jacobian
% is evaluated, VAL is loaded from the script "s_model_setup"
% dv = min(VAL(1,1:6))*1e-4
dv = 1e-6

f_k0 = function_handle(fs_k0, 'vars', X );  % symbolic functions
% converted to standard ones, variables order specified by vector
% X defined in the script "s_model_setup"
f_c  = function_handle(fs_c , 'vars', X );
f_a2 = function_handle(fs_a2, 'vars', X );
f_a1 = function_handle(fs_a1, 'vars', X );
f_k2 = function_handle(fs_k2, 'vars', X );
f_k1 = function_handle(fs_k1, 'vars', X );

% fk = function_handle(k, 'vars', X );

number_of_functions = size(VAL)(1);
number_of_variables = size(VAL)(2);
Z = NaN(number_of_functions,number_of_variables);

 coefficients = [ -1/2 0 1/2 ];  % coefficients for central
% differences
% https://en.wikipedia.org/wiki/Finite_difference_coefficient
```

```
% coefficients = [ 1/12 -2/3 0 2/3 -1/12 ];
% coefficients = [ -1/60 3/20 -3/4 0 3/4 -3/20 1/60 ];
length_coefficients = length(coefficients);
accuracy = length_coefficients-1;

f_expand = @(X) feval(@(x)x{:}, num2cell(X));

for i=1:number_of_variables

sum_Y = zeros(number_of_functions,1);

for j=1:length_coefficients
VAL = VAL_0;
mult = (j-1)-accuracy/2;
VAL(:,i) = VAL(:,i) + mult*dv;

[ A1, A2, A3, B1, B2, C1, C2, D1, D2, D3, eps_pl ] = f_expand(VAL(1,:));

A1 = f_A1(k0, k1, k2, a1, a2, c, sgn, eps_pl, eps_pl_0, alpha_0);
A2 = f_A2(k0, k1, k2, a1, a2, c, sgn, eps_pl, eps_pl_0, alpha_0);
A3 = f_A3(k0, k1, k2, a1, a2, c, sgn, eps_pl, eps_pl_0, alpha_0);

[ k0, k1, k2, a1, a2, c, sgn, eps_pl, eps_pl_0, alpha_0 ] = f_expand(VAL(4,:));
B1 = f_B1(k0, k1, k2, a1, a2, c, sgn, eps_pl, eps_pl_0, alpha_0);
B2 = f_B2(k0, k1, k2, a1, a2, c, sgn, eps_pl, eps_pl_0, alpha_0);

[ k0, k1, k2, a1, a2, c, sgn, eps_pl, eps_pl_0, alpha_0 ] = f_expand(VAL(6,:));
C1 = f_C1(k0, k1, k2, a1, a2, c, sgn, eps_pl, eps_pl_0, alpha_0);
C2 = f_C2(k0, k1, k2, a1, a2, c, sgn, eps_pl, eps_pl_0, alpha_0);

[ k0, k1, k2, a1, a2, c, sgn, eps_pl, eps_pl_0, alpha_0 ] = f_expand(VAL(8,:));
D1 = f_D1(k0, k1, k2, a1, a2, c, sgn, eps_pl, eps_pl_0, alpha_0);
D2 = f_D2(k0, k1, k2, a1, a2, c, sgn, eps_pl, eps_pl_0, alpha_0);
D3 = f_D3(k0, k1, k2, a1, a2, c, sgn, eps_pl, eps_pl_0, alpha_0);

% Y = [ k0, k1, k2, a1, a2, c, sgn, eps_pl, eps_pl_0, alpha_0 ]';
% Y = [ A1, A2, A3, a1, a2, c, sgn, eps_pl, eps_pl_0, alpha_0 ]';
% Y = [ A1, A2, A3, 1, 1, 1, 1, 1, 1, 1 ]';
 Y = [ A1, A2, A3, B1, B2, C1, C2, D1, D2, D3 ]';

sum_Y = sum_Y + coefficients(j)*Y;
end

Z(:,i) = sum_Y/dv;  % central differences
end

output_matrix{2} = Z;
```

```
output_matrix{3} = (output_matrix{2}-output_matrix{1})./ ...
(output_matrix{2}+1e10*realmin)*1e2;

output_matrix{4} = Z;

output_matrix{5} = NaN(size(output_matrix{4}));


%% %% printing results


diary (output_file_name);

disp('Sensitivity matrix for DDH alpha c model');
disp('');
disp('Sensitivity computed for these values of parameters:');
disp('');
disp(output{5});

disp('');
disp('Sensitivity of the model computed by symbolic derivatives:');
disp('');
disp(output{1});

disp('');
disp('Sensitivity of the model computed by numeric derivatives:');
disp('');
disp(output{2});
disp('');

if 1
disp('');
disp('Comparison of both approaches - Error (%):');
disp('');
disp(output{3});
disp('');
end
```

Appendix D. Computer Program for Sensitivity Analysis of Cyclic Calibration Procedure

```
% Slavomir Parma
% Institute of Thermomechanics of the CAS, v.v.i.
% Dolejskova 1402/5, 182 00 Prague 8, Czech Republic
% parma@it.cas.cz , origon@seznam.cz
% GNU Octave Version 4.2.1, package "symbolic 2.6.0",
% package "sympy-1.1.1" for symbolic computations in python
% GNU bash version 4.3.30, linux 3.16.0-4-amd64, Debian 3.16.43-2
% LF line end (linux), utf-8 encoding
% September 22, 2017
% sensitivity analysis of the alpha c directional distortional hardening
% model by Feigenbaum and Dafalias, model published in:
% - Feigenbaum, H. P., 2008. Directional distortional hardening in
% plasticity based on thermodynamics. PhD dissertation,
% University of California, Davis.
% - Feigenbaum, H. P., Dafalias, Y. F., 2008. Simple model for
% directional distortional hardening in metal plasticity within
% thermodynamics. Journal of Engineering Mechanics 134 (9),
% pp. 730--738.
%    URL http://ascelibrary.org/doi/abs/10.1061/
% %28ASCE%290733-9399%282008%29134%3A9%28730%29
%
% results of this analysis are reported in a paper "Calibration of
% a simple directional distortional hardening model for metal
% plasticity", IJSS, (2017)

clc; clear all; close all;
more off;
addpath(genpath(pwd));  % add all subdirectories of actual working
% directory to path
output_file_name = 'output/sensitivity_analysis.txt';
system([ 'rm ' output_file_name ] );

% https://octave.sourceforge.io/symbolic/overview.html
pkg load symbolic



%% %% symbolic computation of sensitivity
digits(10);
syms x;  % this line may be erased
disp('Loading symbolic equations of model...');
s_model_setup;
```

```
%% computation of jacobian
disp('Computing symbolic jacobian...');
J_F = jacobian(F,X);


%% numerical evaluation of jacobian
num_J_F = sym(NaN(size(VAL)));
num_J_F = subs(J_F, Par, VAL );
eval_num_J_F = double(num_J_F);
output_matrix{1} = eval_num_J_F;



%% %% numerical computation of sensitivity
disp('Computing numeric jacobian...');
VAL_0 = double(VAL_0);  % VAL represents a point in which jacobian
% is evaluated, VAL is loaded from the script
% "s_model_setup"
% dv = min(VAL(1,1:6))*1e-4
dv = 1e-6

f_k2 = function_handle(fs_k2, 'vars', X );  % symbolic functions
% converted to standard ones, variables order specified by vector
% X defined in the script "s_model_setup"
f_a1 = function_handle(fs_a1, 'vars', X );
f_a2 = function_handle(fs_a2, 'vars', X );
f_c  = function_handle(fs_c,  'vars', X );

number_of_functions = length(F);
number_of_variables = length(X);
Z = NaN(number_of_functions,number_of_variables);

 coefficients = [ -1/2 0 1/2 ];  % coefficients for central
% differences
% https://en.wikipedia.org/wiki/Finite_difference_coefficient
% coefficients = [ 1/12 -2/3 0 2/3 -1/12 ];
% coefficients = [ -1/60 3/20 -3/4 0 3/4 -3/20 1/60 ];
length_coefficients = length(coefficients);
accuracy = length_coefficients-1;

f_expand = @(X) feval(@(x)x{:}, num2cell(X));  % distribution of
% vector components to variables

for i=1:number_of_variables

sum_Y = zeros(number_of_functions,1);
```

```
for j=1:length_coefficients
VAL = VAL_0;
mult = (j-1)-accuracy/2;
VAL(i) = VAL(i) + mult*dv;

[ P, Q, R, r, eps_Q ] = f_expand(VAL);
k2 = f_k2(P, Q, R, r, eps_Q);
a1 = f_a1(P, Q, R, r, eps_Q);
a2 = f_a2(P, Q, R, r, eps_Q);
c  = f_c(P, Q, R, r, eps_Q);

% Y = [ P, Q, R, r ]';
Y = [ k2, a1, a2, c ]';

sum_Y = sum_Y + coefficients(j)*Y;
end

Z(:,i) = sum_Y/dv;  % central differences
end

output_matrix{2} = Z;

output_matrix{3} = (output_matrix{2}-output_matrix{1})./...
(output_matrix{2}+1e10*realmin)*1e2;

output_matrix{4} = Z;

output_matrix{5} = NaN(size(output_matrix{4}));


% percentual representation
Z = Z(:,1:end-1);

Z(1,:) = Z(1,:)/k2;
Z(2,:) = Z(2,:)/a1;
Z(3,:) = Z(3,:)/a2;
Z(4,:) = Z(4,:)/c;

Z(:,1) = Z(:,1)*P;
Z(:,2) = Z(:,2)*Q;
Z(:,3) = Z(:,3)*R
Z(:,4) = Z(:,4)*r;


output_matrix{6} = Z;
```

```
%% %% printing results

diary (output_file_name);

disp('Sensitivity matrix for DDH alpha c model');
disp('');
disp('Sensitivity computed for these parameters:');
disp('');
disp(output{5});


disp('');
disp('Numeric derivative result:');
disp('');
disp(output{2});
disp('');

if 1
disp('');
disp('Error (%):');
disp('');
disp(output{3});
disp('');
end

if 1
disp('');
disp('Pretty:');
disp('');
disp(output{4});
disp('');
end


disp('');
disp('Sensitivity of the model computed by numeric derivatives (%):');
disp('');
disp(output{6});
disp('');


diary off
```